PARAMETRIC INVESTIGATION OF Ru-BASED CATALYSTS FOR CO_2 REFORMING OF GLYCEROL

by

Mert Özden

B.S., Chemical Engineering, İzmir İnstitute of Technology, 2017

Submitted to the Institute for Graduate Studies in
Science and Engineering in partial fulfillment of
the requirements for the degree of
Master of Science

Graduate Program in Chemical Engineering

Boğaziçi University

2019

ACKNOWLEDGEMENTS

I want to express my gratitude to my thesis supervisor, Prof. Ahmet Kerim Avcı for believing that I could fit into his research group and gave me the shot. His help eased my transition into a new city and a new work environment. He always listened to my concerns and problems, and gave me the time and resources to fix every single of them along the way. Like my father said, graduate research is like a master-apprentice relation. I find myself very lucky to have such great master and mentor.

I would like to thank my thesis committee, Prof. Ayşe Nilgün Akın and Prof. Ahmet Erhan Aksoylu for sparing their time to read and evaluate this thesis. Also, I would like to thank Prof. Aksoylu for his wisdom, his help in or out of the classes are in extreme value. I appreciate that he found time to answer all of my questions even in his very busy schedule.

This thesis would be undone without the help of KB-404. In the lion's share, Selin, thank you for everything. I've learned many things from you, and I won't ever stop appreciating that. Without your tenacity and awareness, this work would be completely different. Also, say hi to Coşkun. Semih, you were and you are my partner in almost every class we took together. We will keep working together, and improve our work for sure. As the old saying goes "erken kalkan çok yol alır". Sinan, thank you for showing me the ropes around the lab and experimental work. Your wisdom and experience is nothing to take lightly. I wish you and your family the best in Bursa. Özge, you were my partner in destiny with similar work we done. Although, you've been in some tough situations, you got up and work tirelessly. Uğurcan, though we were in different labs, thank you for everything. Lastly, you're away but always in our heart and whatsapp group, Furkan, thank you for your help and friendship. A lot's changed since we begin, but our friendship carries on.

To my friends outside of the work, Atakan, Can, Efe, Zafer and Berkay. I would've lost in loneliness without you in İstanbul. Thank you for always cheering me up even though you are in İzmir. Power of technology I guess, because you were never away. BKB stays strong. To Kaan and Raiden, this city is fun with you. In every endeavor we have, we always laughed.

Thanks to CATREL team in both KB-403, KB-405, and KB-411. Time to time, we all need each other, and thanks for not denying that help when I need. I hope that, i contributed you likewise.

I want to appreciate the hard work done to maintain the department by Murat Düzgünoğlu, Yakup Bal, Belgin Balkan, Melike Gürbüz and Dilek Kirkoç.

There are two heroes that played an enormous part in this thesis. I always know that, I'm not thanking them enough. However, thanks Mukadder and Mahir Özden. You are the pillars of my life. Without your support, both material and spiritual, this thesis would not exist. I understand the hard work you endure to raise me, and I will always appreciate that deep in my soul. I love you both. Also, my family in İstanbul, my aunt Nilgün, my uncle Enis, my cousins Ezgi and Seniha. I love you guys.

Everyone that I have mentioned above is special. However, there is one special person that is my beacon of light. My moral compass, my everything. Yağmur, I love you. You are the strongest and most beautiful person that I have met. You motivated me whenever I'm down and I miss you whenever you're not with me. Thank you for everything you did for me.

Financial support provided by TÜBİTAK-117M163 and BAP-13880 are acknowledged.

ABSTRACT

PARAMETRIC INVESTIGATION OF Ru-BASED CATALYSTS FOR CO_2 REFORMING OF GLYCEROL

Glycerol is the major side product of the biodiesel production *via* transesterification. Reforming processes of glycerol has started to draw attention due to increased biodiesel demand in the world. Apart from conventional reforming processes, dry reforming of glycerol is very promising due to its consumption with CO_2, a major greenhouse gas. Literature is very scarce about catalysis of GDR over noble metal catalysts. Therefore, this study aims to develop active and stable Ru based catalysts for glycerol dry reforming process. Ruthenium is selected due to it being cheaper than Rh and other noble metals and showing promise as the active metal of the catalyst. Effects of reaction parameters, namely reaction temperature, molar CO_2 to glycerol feed ratio (CO_2/G), and residence time on reactant conversions and product yields and selectivities were investigated. Single oxide supported Ru catalysts were tested in activity experiments and the promising Ru/La_2O_3 (RuLa) and Ru/ZrO_2 (RuZr) catalysts were tested in stability experiments for 72 hours. Both Ru/La_2O_3 and Ru/ZrO_2 were not stable, where they had deactivated approximately by 20 and 30%, respectively. From literature, positive effect of binary oxide supports on catalytic activity and stability was known. Thus, 5 binary oxide supported Ru catalysts were tested and among them, Ru/La_2O_3-ZrO_2 (RuLZ) was exhibited superior activity and product selectivity. Optimum conditions for RuLZ were, 750 °C, CO_2/G = 3, and residence time of 0.5 mg min NmL^{-1}. Under these conditions RuLZ have exhibited 32.1% CO_2 and 73% glycerol conversion, which are 90% and 100% of the equilibrium conversions, respectively. RuLZ have also exhibited 92 and 96% of the thermodynamic H_2 and CO selectivity, respectively. Produced syngas had H_2/CO ratio of 0.7. RuLZ have shown the most important improvement at catalyst stability; after 72 hours it has deactivated by 13%.

ÖZET

GLİSEROLÜN CO_2 İLE REFORMLANMASI İÇİN GELİŞTİRİLEN Ru TEMELLİ KATALİZÖRLERİN PARAMETRİK İNCELENMESİ

Gliserol, transesterifikasyon reaksiyonu ile üretilen biyodizelin yan ürünüdür. Dünyada artan biyodizel üretiminden dolayı, gliserolün değerli ürünlere reformlanması dikkat çekmektedir. Gliserolün en önemli sera gazlarından birisi olan CO_2 ile reformlanması (kuru reformlama) iki önemli atığın uzakaştırılması dolayısıyla ümit vaadetmektedir. Ancak, literatür gliserolün kıymetli metal bazlı katalizörler ile kuru reformlanması konusunda çok sınırlıdır. Bu çalışmanın hedefi, gliserolün aktif ve stabil Ru bazlı katalizörlerle kuru reformlanmasını incelemektir. Yapısı bu reaksiyonu katalizlemeye müsait olduğu için ve kıymetli metaller arasında ucuz olduğundan dolayı Ru aktif metal olarak seçilmiştir. Reaksiyon sıcaklığı, CO_2 ve gliserolün molar giriş oranları ve alıkonma süresi gibi reaksiyon parametrelerinin aktivite ve ürün dağılımı üzerindeki etkileri incelenmiştir. Çalışmanın ilk kısmında tekil oksit destekli katalizörler denenirken, bu katalizörler arasında Ru/La_2O_3 (RuLa) ve Ru/ZrO_2 (RuZr) umut verici aktiviteler göstermiştir. Fakat bu katalizörler, 72 saatlik dayanım deneyinin sonunda sırasıyla %20 ve %30'a yakın aktivite kaybı göstermişlerdir. Literatürde ikili oksit desteklerin aktivite ve dayanıma olan katkıları bilinmektedir. Bu sebepten ötürü ikili oksit destekli Ru katalizörler sentezlenmiş ve karşılaştırma deneylerinde incelenmiştir. Bu deneyler sonucunda Ru/La_2O_3-ZrO_2 (RuLZ) katalizörü üstün aktivite ve istenen ürün seçilimi göstermiştir. RuLZ belirlenen en uygun çalışma koşulları 750 °C, CO_2/gliserol oranı 3, ve 0.5 mg dk NmL^{-1} alıkonma süresinde, %32.1 CO_2 dönüşümü, %73 gliserol dönüşümü ve sırasıyla termodinamik limitin %92'si ve %96'sı kadar H_2 ve CO seçimliliği göstermiştir. Üretilen sentez gazının H_2/CO oranı 0.7 dir. RuLZ sadece %13'lük bir aktivite kaybına uğrayıp üstün dayanım göstermiştir.

TABLE OF CONTENTS

LIST OF FIGURES

LIST OF TABLES

LIST OF SYMBOLS

F	Total volumetric flow rate (NmL min^{-1})
S_i	Selectivity of species i
T	Temperature (°C)
V	Volume (μL)
W	Catalyst weight (mg)
x_i	Conversion with respect to reactant i
Y_i	Yield of species i
ΔH^o	Standard enthalpy of reaction (kJ mol^{-1})
ν_i	Volumetric flow rate of species i (NmL min^{-1})
τ	Space time (mg min NmL^{-1})

LIST OF ACRONYMS/ABBREVIATIONS

BET	Brauner-Emmett-Teller
DRIFTS	Diffuse reflectance infrared Fourier transform spectroscopy
DRM	Dry reforming of methane
DSC	Differential scanning calorimeter
EDS	Energy dispersive spectroscopy
EDX	Energy-dispersive X-ray spectroscopy
FESEM	Field emission scanning electron microscopy
FTIR	Fourier transform infrared spectroscopy
FTS	Fischer-Tropsch synthesis
G	Glycerol
GC	Gas chromatograph
GDR	Glycerol dry reforming
GHSV	Gas hourly space velocity
GSR	Glycerol steam reforming
HPLC	High performance liquid chromatograph
HRTEM	High-resolution transmission electron microscopy
ID	Inner diameter
IR	Infrared
LRS	Low resolution spectrograph
MFC	Mass flow controller
MW	Molecular weight
PID	Proportional integral derivative
QMS	Quadrupole mass analyzer
RWGS	Reverse water gas shift
SAXS	Small angle x-ray scattering
SEM	Scanning electron microscopy
SRM	Steam reforming of Methane
SMSI	Strong metal support interaction

TEM	Transmission electron microscopy
TGA	Thermogravimetric analysis
ToS	Time on stream
TPD	Temperature programmed desorption
TPR	Temperature programmed reduction
TPO	Temperature programmed oxidation
WAXS	Wide angle x-ray scattering
WGS	Water-gas shift
XANES	X-ray absorption near edge structure
XPS	X-ray photoelectron spectroscopy
XRD	X-ray diffraction
XRF	X-ray fluorescence

1. INTRODUCTION

Energy is one of the most important demand in order to maintain the life. Until 21st century, this demand suppied by non-renewable sources such as coal, petroleum, etc. However, when these suppies started to deplete, the need of a renewable energy source increased to replace non-renewable sources. One of the most researched and prefered solution is biodiesel production. This is due to the fact that biodiesel can be produced from sustainable resources and, it can replace current non-renewable fuels easily [1]. In Europe, awareness of biodiesel production started in early 2000 and production of biodiesel increased significantly. This trend can be seen in Figure 1.1.

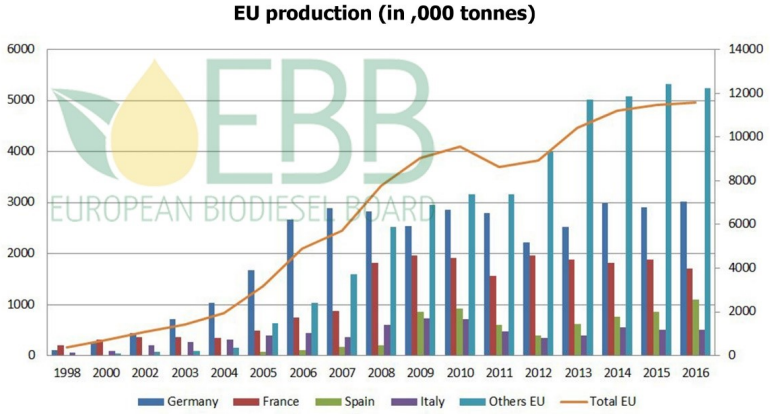

Figure 1.1. Biodiesel production in EU countries in 2016 [2].

When biodiesel produced from biofeedstock with transesterification, for every 3 moles of biodiesel, 1 mol of glycerol is produced. This creates 10 wt.% glycerol in the reaction mixture by weight [3]. Considering 21.1 million tonnes of biodiesel produced in the 2017 in European Union countries, approximately 2.34 million tonnes of glycerol produced during this process [2].

Glycerol (glycerin or propane-1,2,3-triol), is currently used for over 1500 processes worldwide [4]. However, crude glycerol produced from the transesterification processes

contains many impurities, thus requiring expensive purification processes before being suitable for new product technologies. One of the most important uses of glycerol is converting it to syngas using reforming processes. Syngas, can then be used for in many processes such as Fischer-Tropsch synthesis, production of methanol, DME and ammonia. Syngas can be produced from glycerol using various processes. Most common processes are steam reforming, dry reforming and autothermal reforming. In steam reforming, feedstock fed with steam to reform it into syngas which is rich with hydrogen. Whereas in dry reforming steam replaced with carbon dioxide. Autothermal reforming is the mixture of non-catalytic partial oxidation with steam reforming. Although steam reforming is the most widespread process in terms of both usage and research, dry reforming is a very promising process. Since carbon dioxide is a major greenhouse gas, usage of it in reforming makes the process very important in environmental aspect. Moreover, dry reforming delivers syngas composition close to its ideal value of $H_2/CO \sim 1$.

There are very few studies about dry reforming of glycerol in the literature. Available studies generally focuses on Ni-based catalysts [5–8]. There are only a few studies that includes noble metals such as Rh [9–11]. Generally, support materials used in glycerol dry reforming are Al_2O_3, CeO_2, cement clinker, SiO_2 and ZrO_2. Recently, a study which employes mixed oxide supported catalysts, improves the activity and stability of Rh exceptionally [11]. However, most of the investigated catalysts in literature are prone to deactivation due to sintering and coke formation. Although, noble metals are better at preserving their activity, they are not completely invulnerable [12]. Therefore, aim of this study is to develop Ru catalysts that are active and stable under GDR conditions. Ruthenium is selected as the active metal due to it being cheaper than Rh and other noble metals, and having a potential to catalyze this reaction effectively [9, 13]. This study has divided into two parts, which are Ru catalysts supported on single oxides, and Ru catalysts supported on binary oxides. In both of the parts, synthesized catalysts had put into comparison at a default condition in which their activities are compared. Then effect of the reaction parameters are investigated over the promising catalysts in order to find the optimum operating conditions for GDR.

This thesis consists of 5 main parts. Part 1 is the Introduction. Part 2 includes, an extensive literature survey on glycerol dry reforming, catalysts used for this reaction and Ru-based catalysts for glycerol steam reforming and methane dry reforming. In Part 3, catalyst preparation, experimental rig and characterization systems are presented. Part 4 reports the results of catalytic activity and stability tests with catalysts characterizations. Lastly, in Part 5, conclusions from the thesis are listed with recommendations to improve further work.

2. LITERATURE SURVEY

Synthesis gas (syngas) is the mixture of H_2, CO and CO_2 in varying compositions. Synthesis gas is used commonly in energy applications and in Fischer-Tropsch synthesis as the building block for artificial higher hydrocarbon synthesis [14]. In theory, syngas may be produced from any hydrocarbon feedstock. However, in industrial practice, large-scale syngas production is done with natural gas, naphtha, residual oil, petroleum coke and coal [15]. Mainly, reforming processes are used to produce syngas from these non-renewable resources. More specifically, steam reforming, dry reforming, autothermal reforming and partial oxidation are the main reforming types to produce syngas. Amidst these processes, steam reforming of methane (SRM) is the most widely used and researched process [13].

In the last decade, dry reforming of hydrocarbons has started to draw attention from scientific community [16]. Dry reforming is the process where CO_2 is used to convert hydrocarbon feeds into syngas. These hydrocarbon feeds are mainly hydrocarbons such as methane and ethane, alcohols such as methanol and ethanol, and polyols such as glycerol. Dry reforming also shows the importance of being a CO_2 removal process. Therefore, it also carries an important mission towards a greener world.

Similarly to SRM, dry reforming of methane (DRM) is addressed extensively in the literature. In this process, reaction temperature can go up to 1000 °C due to very endothermic nature of the reaction. Commonly, Ni-based catalysts are used for both research and industrial use. However, these catalysts are prone to coking and sintering in these harsh conditions [12]. For these reasons, research of noble metal based catalysts carries importance, where they are resistant to coke formation and provide better activity than Ni. On the other hand, as the name suggests, noble metals are expensive relatively to Ni, requiring a significant advantage beforehand to replace Ni-based catalysts in industrial usage.

2.1. Glycerol Dry Reforming

Glycerol is the major by-product of transesterification reaction of vegetable oils for biodiesel production. Increase in biodiesel production generated an excess of glycerol in the market. Although high purity glycerol finds its value in the food, cosmetics and pharmaceutical applications, it is expensive to purify glycerol up to desired purity. Therefore, converting glycerol into more cost-effective valuable such as syngas is more attractive than high-grade purification [17].

Glycerol dry reforming (GDR) is trending in the scientific community due to breaking down glycerol with CO_2, a greenhouse gas, to make syngas through a carbon negative path. Overall reaction of GDR can be described as follows:

$$C_3H_8O_3 + CO_2 \rightleftharpoons 4CO + 3H_2 + H_2O \qquad \Delta H^0 = 293.2 \text{ kJ mol}^{-1} \tag{2.1}$$

GDR is defined as combination of glycerol decomposition (Equation 2.2) and reverse water gas shift due to CO_2 in the feed (Equation 2.3) by Lin *et al.* [18]:

$$C_3H_8O_3 \rightleftharpoons 3CO + 4H_2 \qquad \Delta H^0 = 251.2 \text{ kJ mol}^{-1} \tag{2.2}$$

$$CO_2 + H_2 \rightleftharpoons CO + H_2O \qquad \Delta H^0 = 41.2 \text{ kJ mol}^{-1} \tag{2.3}$$

Thermal decomposition of glycerol complicates the dry reforming reactions and leads to many side reactions. Besides conversion into CO and H_2 (Equation 2.2), glycerol can decompose into several compounds as can be seen in Figure 2.1 [19]:

$$C_3H_8O_3 \rightleftharpoons C_3H_6O_2 + H_2O \qquad \Delta H^0 = 450 \text{ kJ mol}^{-1} \tag{2.4}$$

$$C_3H_8O_3 \rightleftharpoons C_3H_6O_3 + H_2 \qquad \Delta H^0 = -15 \text{ kJ mol}^{-1} \tag{2.5}$$

$$C_3H_8O_3 \rightleftharpoons C_2H_4 + CO + 2H_2O \tag{2.6}$$

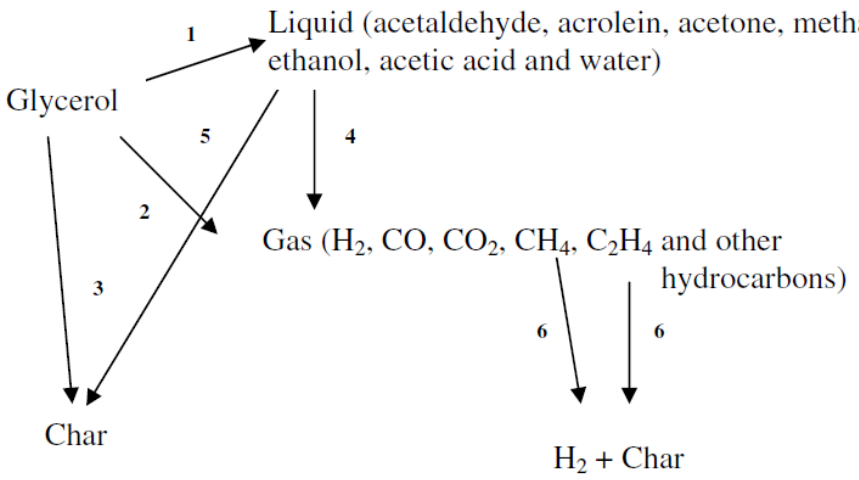

Figure 2.1. Glycerol decomposition scheme (Valliyappan *et al.* [20]).

In first pathway, acetol decomposes into acrolein *via* Equation 2.7 which produces ethane, ethylene, propanal, hydrogen and carbon monoxide at high temperatures [21].

$$C_3H_6O_2 \rightleftharpoons C_3H_4O + H_2O \qquad \Delta H^0 = -36 \text{ kJ mol}^{-1} \tag{2.7}$$

Glyceraldehyde decomposes into 2-oxopropanal *via* Equation 2.8 and then 2-oxopropanal decomposes into acetaldehyde (Equation 2.9). Lastly, acetaldehyde decomposes into methane and CO *via* Equation 2.10.

$$C_3H_6O_3 \rightleftharpoons C_3H_4O_2 + H_2O \tag{2.8}$$

$$C_3H_4O_2 \rightleftharpoons CH_3CHO + CO \tag{2.9}$$

$$CH_3CHO \rightleftharpoons CH_4 + CO \tag{2.10}$$

In GDR, catalyst deactivation occurs due to sintering and coke deposition [22]. Methane is a side product of GDR. SRM (Equation 2.11), DRM (Equation 2.12), and methanation (Equation 2.13) are the major reactions producing or consuming CH_4 [23]:

$$CH_4 + H_2O \rightleftharpoons CO + 3H_2 \qquad \Delta H^0 = 206.1 \text{ kJ mol}^{-1} \tag{2.11}$$

$$CH_4 + CO_2 \rightleftharpoons 2CO + 2H_2 \qquad \Delta H^0 = 247.3 \text{ kJ mol}^{-1} \tag{2.12}$$

$$CO_2 + 4H_2 \rightleftharpoons CH_4 + 2H_2O \qquad \Delta H^0 = -165 \text{ kJ mol}^{-1} \tag{2.13}$$

Elemental carbon can be produced *via* Boudouard reaction (Equation 2.14), coke gasification (Equations 2.15 and 2.16) or methane decomposition (Equation 2.17) [23].

$$2CO \rightleftharpoons C_{(s)} + CO_2 \qquad \Delta H^0 = -172.4 \text{ kJ mol}^{-1} \tag{2.14}$$

$$C_{(s)} + H_2O \rightleftharpoons H_2 + CO \qquad \Delta H^0 = 131 \text{ kJ mol}^{-1} \tag{2.15}$$

$$C_{(s)} + 2H_2O \rightleftharpoons 2H_2 + CO_2 \qquad \Delta H^0 = 90 \text{ kJ mol}^{-1} \tag{2.16}$$

$$CH_4 \rightleftharpoons 2H_2 + C_{(s)} \qquad \Delta H^0 = 74 \text{ kJ mol}^{-1} \tag{2.17}$$

Advantage of glycerol dry reforming to other reforming processes is that GDR produces syngas with H_2/CO ratio close to 1. This ratio makes GDR product syngas more suitable for Fischer-Tropsch synthesis (FTS) [24]:

$$nCO + (2n+1)H_2 \rightleftharpoons C_nH_{2n+2} + nH_2O \tag{2.18}$$

2.1.1. Thermodynamics of Glycerol Dry Reforming

For the thermodynamics analysis of GDR, literature is very scarce. There is only one article about GDR thermodynamics, and remaining related papers are about thermodynamics of autothermal reforming or other reforming processes of glycerol.

Only article about glycerol dry reforming thermodynamics was published by Wang *et al.* [24] in 2009. In this paper, the authors performed a thermodynamic analysis of GDR by the Gibbs free energy minimization method as a function of CO_2 to glycerol ratio, temperature, and pressure. They have utilized Lagrange's undetermined multiplier method and MATLAB to calculate equilibrium compositions. They have found that increasing pressure has a negative effect on product yield, and they have stated that maximum yield can be obtained at atmospheric pressure. Also, they have found that increasing temperature increases H_2 yield. They have stated that increasing CO_2/G above 2 unfavors H_2 generation. However, increasing CO_2/G above 3 increases syngas yield up to 7 moles of syngas per mole glycerol. They have found that optimum condition for syngas production is 727 ^oC and $CO_2/G = 1$, which generates 6.4 mol of syngas with $H_2/CO = 1$ per mole of glycerol with 33% CO_2 conversion. They have stated that, under the optimum conditions for syngas production, carbon deposition can be eliminated *via* sequestration of CO_2 in the form of carbon nanofilaments.

Another article that can help to understand the thermodynamics of GDR, is written by Kale *et al.* [25]. They have done a thermodynamic analysis on dry autothermal reforming of glycerol to investigate the effect of O_2 to glycerol ratio (OCGR) and CO_2 to glycerol ratio (CGR) on product distribution at atmospheric pressure and 327-727 ^oC temperature range. They have shown the thermodynamic feasibility of the process in the parameter range mentioned above and found that process is favorable for syngas production at H_2/CO ratio of 1. The authors alo reported that higher OCGR and higher CGR are good for syngas production at H_2/CO ratio of 1, lower carbon and methane formation, while lower OCGR and CGR gives good H_2 and total H_2 yields, low water and CO_2 production. They have found that process temperature around 580 ^oC is good for minimizing methane, steam and carbon formation and the thermoneutral temperature of 653 ^oC at atmospheric pressure, OCGR = 0.3 and CGR = 1 gave 2.67 mol of H_2, 4.8 mol of total H_2 with negligible methane and carbon formation. Therefore, they identified that these parameters are the best thermoneutral conditions for dry autothermal reforming of glycerol.

Freitas and Guirardello [17] have performed a thermodynamic analysis for H_2 and syngas production from glycerol. In this study, steam reforming, partial oxidation, autothermal reforming, dry reforming and supercritical water gasification were evaluated. They have calculated the composition of the products using Gibbs energy minimization approach combined with virial equation of state. They have validated their model with simulated and experimental data obtained in literature. The authors have found that, H_2 yields increase directly with temperature in all reforming processes analyzed. For the partial oxidation and dry reforming processes, increase of operating pressure results in carbon formation in the product stream. For the dry reforming, they have found that best conditions are, 600 °C, atmospheric pressure, $CO_2/G = 1$. These parameters gave, molar fractions of 0.417 H_2 and 0.625 syngas, with $H_2/CO = 2$. However, they have found 1.16 moles of solid carbon in the product stream.

Wang *et al.* [23] investigated the thermodynamics of dry autothermal reforming of glycerol with *in-situ* H_2 separation in 2017. They have investigated the effect of H_2 separation on product distributions and reaction heat by employing Gibbs free energy minimization method. They have found that separation of H_2 promotes its yield and decreases methane formation, and at high CO_2/G, carbon formation is restricted. Additionally, H_2 removal is beneficial to the autothermal process achievement at high temperature. They have also investigated the effect of impurities that may come from the crude glycerol coming from biodiesel production. Specifically, methanol impurity impacts the autothermal process and hinders syngas production. However, they found that at high temperatures, H_2 separation and glycerol impurities have a positive effect on the attainment of thermoneutral condition.

Additionally, there are several studies that implement the mixtures of glycerol could improve syngas production and therefore reducing the cost of biodiesel production [26]. Zakaria *et al.* [27] have analyzed the thermodynamics of the ethanol-glycerol mixture dry reforming. They have employed Gibbs free energy minimization method to investigate the thermodynamics of this process. They have determined the equilibrium compositions as a function of CO_2 to glycerol-ethanol mixture ratio (CEG) ranging

from 1 to 12, where ethanol to glycerol ratio is kept constant at 1, temperature ranging between 300-1000 °C and, operating pressure range of 1 to 50 bar. The optimum conditions for H_2 production are temperatures between 800 and 1000 °C and CEG of 1 at atmospheric pressure. For the syngas production, the optimum conditions are determined as temperatures above 800 °C, CEG of 1 and atmospheric pressure. High pressure and high CEG do not favor H_2 formation. Under given optimum conditions, carbon formation can be thermodynamically inhibited.

Finally, Saimon *et al.* [28] have studied thermodynamic properties of dry reforming of methanol-ethanol-glycerol mixture employing Gibbs free energy minimization method in 2017. They have investigated product yields while changing CO_2 to methanol-ethanol-glycerol mixture ratio (CMEG) from 1/6 to 6/1 while keeping mixture ratio constant at 1:1:1 and temperature from 300 to 1000 °C. Optimum parameters for H_2 yield were found as CMEG of 1/6 at 1000 °C and atmospheric pressure. They have found that, H_2 yield improves at high temperatures and low pressures and low CMEG. Aditionally, they have compared methanol-ethanol-glycerol mixture to ethanol-glycerol and found that ethanol-glycerol mixture has higher H_2 yield due to higher H_2 availability.

2.1.2. Catalysis of Glycerol Dry Reforming

Similar to thermodynamics of GDR, literature is limited about the catalysis of GDR. However, there are several articles that can be investigated for the catalysis of glycerol dry reforming.

In this field, the first catalysis article was published by Fernandez *et al.* [29] in 2010. They have compared pyrolysis, steam reforming and dry reforming using a commercial activated carbon as catalyst. They have found that, reforming processes promote higher glycerol conversions than sole thermal decomposition. The authors reported that, steam reforming generates the lowest gas fraction and highest amounts of H_2 and syngas, whereas in dry reforming this occurrence is reversed. They have

found that, microwave heating produced higher gas yields with large syngas content than conventional heating processes. Finally, they have stated that use of carbon-based catalysts are suitable for producing syngas with H_2/CO ratio close to 1.

In 2013, Lee *et al.* [30] investigated the application of cement clinker (CC) as Ni-catalyst support for glycerol dry reforming. They have addressed on the coking and therefore deactivation of Ni-based catalysts in reforming processes. To solved this issue, they have used cement clinker comprised of 62% calcium oxide and 17% silica supported nickel catalyst for GDR. They have experimented with Ni-CC catalysts with different metal loadings and various CO_2 partial pressures at 750 °C. They have characterized their catalysts using XRD, XRF, BET, TGA and FESEM-EDS techniques. They have found that, addition of Ni has improved BET surface area with at least 32-folds increment. Also, XRD examination showed that formation of complex oxide phases depends on Ni loading. Their experimental results showed that, GDR reaction yield syngas with H_2/CO ratio below 2 which is suitable for FTS. They have stated that, side reactions such as methanation and hydrogenation of CO_2 had majorly affected syngas production. Following up on this work, Lee *et al.* [31] obtained glycerol conversions ranging from 46% to 75% over 4 h on stream test. With the help of XRD, they have found that different types of Ni oxide formed with varying Ni loading. Screening of the catalysts has determined that 20% Ni is the best loading, as 20% Ni/CC has the highest activity and stability regardless of coking. This catalyst yielded syngas with the H_2/CO ratio of 1.5 at 750 °C. They have characterized their spent catalysts in FESEM and found whisker-type carbon in the surface of the catalyst. Using TPO, they have found that spent catalyst can be recycled completely with O_2. Also in 2014, Lee *et al.* [5] have employed NH_3- and CO_2-TPD to exhibit the presence of strong pair of acidic and basic sites on the catalysts. They have identified bunsenite species with crystallite size of 15-18 nm and calcium silicate using XRD. From the reaction tests, they have confirmed the absence of a direct interaction between CO_2 and glycerol compound during GDR and H_2 is primarily produced from glycerol decomposition. They have revised the optimum reaction condition as CO_2/G = 1 and 700 °C. Therefore, they have stated their glycerol conversion as 70 to 80% at CO_2/G = 1-1.67.

Siew *et al.* [6, 32–34] studied GDR on La-promoted Ni/Al_2O_3 catalyst. In their studies, 3% La-promotion over 20% Ni/Al_2O_3 yielded best results for GDR reaction. The authors [32] reported that this catalyst can be used for GDR reaction and experimental results yielded syngas with H_2/CO ratio between 0.8 and 2. They have found that, glycerol decomposition and glycerol dehydrogenation as the most likely competing route in a parallel pathway to produce syngas, while CH_4 produced from glycerol dehydrogenation. Furthermore, they have stated that, the role of CO_2 is mostly as partner in RWGS reaction. This results in, CO-rich syngas when CO_2 amount increased. Addition of La showed a higher carbon resistance compared with non-promoted catalyst due to redox property of La to remove carbon. Siew *et al.* [33] also worked on characterization of La-promoted Ni/Al_2O_3 catalyst. Physicochemical characterization showed that La promotion can enhance the metal dispersion on alumina support by decreasing crystallite site. However, smaller crystallite size led to smaller BET surface area due to pore blockage. In 2015, Siew *et al.* [34] extended their reaction parameters to, 650 to 850 °C and CO_2 to glycerol ratio 0 to 5. Experimental results have yielded 96% glycerol conversion at CO_2 to glycerol ratio 1.67 with syngas H_2/CO below 2. Changing from their previous work, ratio scan showed CO_2 has also taken part in other reaction pathways, such as carbon gasification. Lastly in 2015, Siew *et al.* [6] worked on a longevity study on La-Ni/Al_2O_3. In this study, they have found that, above 3% La doping, BET specific surface area reduces significantly due to pore blockage. Also, increased La doping reduces the catalyst acidity, leading to rapid carbon deactivation. This characterizations was done with TPO, FESEM and TEM imagery.

In 2016, Arif *et al.* [7] investigated Ni/ZrO_2 and Ni/CaO as catalysts for GDR. They have carried out the reaction in a fixed bed batch reactor at 700 °C under atmospheric pressure for 3 hours. They have synthesized the catalysts by wet impregnation and characterized them using BET, SEM, XRD, TGA, and TPR techniques. Experimental results showed that 15% Ni/CaO gives the highest H_2 yield and glycerol conversion of 24.59% and 30.32%, respectively. They have verified their results by XRD, where catalyst shows low crystallinity and good dispersion of Ni which results

in high specific surface area, validated by BET. In [35] the authors have added La_2O_3 as the support. However, 15% Ni/CaO showed best performance again. They have analyzed the effect of temperature and CO_2/G for 15% Ni/CaO. From their analysis, optimum conditions are determined as 800 °C and CO_2/G = 1. Experiment done with these determined reaction parameters gave glycerol conversion of 37.66% and H_2 yield 32.45%.

Harun *et al.* [36] investigated Ag-promoted Ni/SiO_2 catalysts for GDR. They have carried out GDR using Ag promoted Ni-based catalysts supported on SiO_2, prepared the catalyts using wet impregnation method and characterized them by BET, SEM, XRD, and TGA techniques. In experiments, they have used a tubular reactor at 700 °C, atmospheric pressure and CO_2/G = 1. They have reported syngas with H_2/CO ratio below 1. From their reaction study, 5% Ag doped Ni/SiO_2 results in highest glycerol conversion and hydrogen yield, reported as 32.6% and 27.4%, respectively. Following up on that work, Harun *et al.* [37] published another article about characterization of Ni catalyst supported on α-Al_2O_3 and SiO_2 for GDR. Their synthesis method and reaction conditions remained the same. Ni/Al_2O_3 gave higher glycerol conversion and H_2 yield than Ni/SiO_2. They have reported that, this was due to smaller crystallite size and higher specific surface area of Ni/Al_2O_3 compared to Ni/SiO_2. Adding to that, structure of Al_2O_3 improved the activity and stability of the catalyst, by providing uniform metal dispersion and inhibiting carbon deposition. They have observed encapsulating carbon and filamentous carbon deposits on the Ni/Al_2O_3 and Ni/SiO_2, respectively. Recently, Harun *et al.* [8] studied Ag-promoted Ni/Al_2O_3 catalysts. In this work, they have investigated temperature as a parameter also, which ranged from 600 °C to 900 °C. CO_2/G was 0.5. From the experimental results, 3% Ag doped Ni/Al_2O_3 gave highest glycerol conversion and H_2 yield of 40.7% and 32%, respectively. They have found that, optimum conditions for highest H_2 production, minimum CH_4 production and carbon deposition were 800 °C and CO_2/G = 1. They have explained the activity of 3% Ag doped Ni/Al_2O_3 to the small metal crystallite size which enhances metal dispersion in catalyst matrix.

In 2018, Tavanarad *et al.* [38] published an article about GDR on Ni catalysts supported on mesoporous nanocrystalline Al_2O_3. In this article, they have synthesized mesoporous Ni/γ-Al_2O_3 with various Ni contents. Their results showed that increasing the Ni content from 5 to 20 wt.% decreased BET areas of the samples from 180 to 143 m^2/g and increased Ni crystalline size from 6.6 to 19 nm. From their experimental results, 15 wt.% Ni/Al_2O_3 showed the best activity. However, catalyst showed a significant decrease during the first 5 h of reaction followed by a stable activity for 15 h time on stream. Tavanarad *et al.* [9] also investigated synthesis and application of noble metal nanocatalysts suported on $MgAl_2O_4$ in GDR. In this article, they have prepared Rh, Ru, Ir, Pd and Pt catalysts supported on $MgAl_2O_4$. They have determined the physiochemical properties of the fresh and spent catalysts using BET, TPR, TPO, TEM and H_2S chemisorption techniques. BET analysis showed higher surface area for the Rh, Ru and Pd catalysts compared to other catalysts. TEM images showed the sizes of active metals are smaller than 5 nm with high dispersion on the surface of catalyst. From H_2S chemisorption results, crystallite sizes of the metals was in range of 1.28 to 4.2 nm. Their experimental results showed that, Rh catalyst gives the highest catalytic activity, which they attribute to its high BET and active metal areas. However, catalytic activity of Rh catalyst declined with time on stream due to carbon formation. They have seen that, increasing CO_2/G ratio from 0 to 3 improved the catalytic activity and decreased deposited carbon on the catalyst surface.

In 2018, Bulutoğlu *et al.* [10] published an article about GDR over Rh-based ceria and zirconia catalysts. In this article, effects of temperature and feed composition on conversion, product distribution and stability were investigated. They have characterized both fresh and spent catalysts by *in-situ* FTIR, Raman spectroscopy, TEM and EDX techniques in order to determine molecular-level origins of deactivation and aging. Both Rh/CeO_2 and Rh/ZrO_2 showed increased glycerol conversions with increasing temperature, where significant increase were seen above 650 and 700 °C. They have obtained syngas with H_2/CO ratio of 0.8, and carbon formation was minimized with increasing temperature. They have found an inversely proportional relation between glycerol and CO_2 conversions, where CO_2 conversion remained constant upon

increasing CO_2/G. from 1 to 4. Rh/ZrO_2 exhibited higher conversion than Rh/CeO_2, which is in alignment with the slightly higher specific surface area and smaller Rh-particle size on ZrO_2. Characterization studies showed that, Rh and CeO_2 showed strong metal-support interaction, which explained by encapsulated Rh nanoparticles by CeO_2 and partially supressed the activity of Rh sites. However, they state that this enacapsulation seems to improve the stability of Rh/CeO_2, which showed better stability compared to Rh/ZrO_2 after 72 h time on stream experiments at 750 °C and CO_2/G = 4. This stability of Rh/CeO_2 was associated with the inhibition of coke formation on the catalyst surface by the mobile oxygen species and creation of oxygen vacancies on CeO_2 domains. They have explained the deactivation of Rh/ZrO_2 by the sintering of Rh nanoparticles and carbon formation.

Recently, Bac *et al.* [11] have published about exceptionally acitve and stable catalysts for GDR. In this article, Al_2O_3-ZrO_2-TiO_2 (AZT) supported Rh, Ni and Co catalysts was investigated for GDR, within 600-750 °C and CO_2 to glycerol ratio 1 to 4. Rh/AZT was found the most active catalyst, where reactant conversions on this catalyst exceeded 90% of other thermodynamic equivalents at 750 °C and CO_2/G = 2-4. In these reaction parameters, activity of Ni/AZT was increased to 95% of thermodynamic CO_2 conversion by increasing the residence time. Stability-wise, loss of CO_2 conversion was 13% during 72 h time on stream experiments, which confirms the exceptional stability of Rh/AZT and Ni/AZT. When spent catalysts was characterized by TEM-EDX, XPS, XANES and *in-situ* FTIR, Co/AZT suffered from sintering, carbon deposition and oxidation of Co sites. When stable catalysts was characterized, Rh/AZT showed no significant deactivation, and Ni/AZT preserved most of its original metallic pattern and gasified carbonaceous deposits during early stages of the reaction.

2.2. Ruthenium-based Catalysts in Reforming

Since early 1990's, transition metals were actively researched in literature for dry reforming processes [13]. From the reaction thermodynamics of DRM, we know that carbon formation is very likely (see Section 2.1). Rostrup-Nielsen and Bak Hansen

found that, on Ni-based catalysts, this leads to formation of carbon whiskers *via* dissolution of adsorbed carbon atoms in the nickel crystal and therefore nucleation of the whisker from Ni-surfaces [12]. However, carbon formation rate was found to be far less on noble metals, which explained by a smaller dissolution of carbon into these metals. More specifically, Rh and Ru was found more active than Ni, for both steam reforming and dry reforming of methane.

In Section 2.1.2, there are several studies that proves the superior activity of Rh-based catalysts for GDR [10, 11]. However, industrialization of Rh-based catalysts is very hard due to its cost, which is 50 to 100 fold of Ruthenium [12]. Therefore, articles about the performance of Ru-based catalysts in reforming reactions is investigated in this section. First, articles about Ru-based catalysts in dry reforming of methane, then articles about Ru-based catalysts in glycerol steam reforming (GSR) are reviewed.

2.2.1. Ru-based Catalysts in Dry Reforming of Methane

First article specifically about Ru-based catalysts in dry reforming of methane was written by Ferreira-Aparicio *et al.* [39]. The authors have done a transient kinetic study of DRM over Ru supported on silica, γ-alumina, and graphite catalysts. They have used transient kinetic analysis and temporal analysis of products (TAP) to unravel the reaction mechanism and identify the uniqueness of each support. In experiments done with Ru/SiO_2, reforming process occurs only on the ruthenium phase and rapid deactivation of the catalyst is related to large residence time of surface carbon intermediates which favors polymerisation and graphitisation. Over graphite, support functions as CH_x species collector, which reduces the residence time of carbonaceous species on the metal phase leading to a very stable catalyst. Reaction network gets complex over alumina support, which alumina hydroxyl groups feed continuously the active Ru phase in H and O adspecies. Although, this complex network limits the catalyst deactivation, accumulation of CO_x adspecies still occur on this support. Following this study, in 2000 Ferreira-Aparicio *et al.* [40] investigated mechanistic aspects of DRM over Ru/Al_2O_3 and Ru/SiO_2 catalysts. Adding to their previous work, infrared spectroscopy revealed

adsorbed intermediate species (ie. formate, bicarbonate and carbonate) on Ru/Al_2O_3, where these intermediates constitutes a key step in reaction development. By isotopic tracing, they have found that hydroxyl groups on the oxide supports participate in the reaction mechanism. They have proposed a Langmuir-Hinshelwood type mechanism for Ru/SiO_2 where a bifunctional mechanism for Ru/Al_2O_3.

In 2000, Schuurman *et al.* [41] studied on bifunctional pathways in DRM over MgO-promoted Ru/C catalysts. In this article, they have carried out steady-state and isotopic transient kinetic experiments in a TAP reactor at 550 °C. Activated carbon is inert under CO_2 atmosphere; however, in the ruthenium presence, gasification of support takes place which indicates the ability of metal to catalyze CO_2 into CO, and spillover oxygen can react with the support. They have found addition of MgO to ruthenium dispersed on activated carbon limits WGS reaction and the gasification of the support, which improves the catalyst selectivity and stability in DRM. Also, decomposition of CO_2 as $MgCO_3$ provides a constant oxygen source near Ru particles, which favors the oxidation of carbon which promotes dehydrogenation of CH_4 to CO. However, this oxygen source is not enough to promote the secondary oxidation of adsorbed hydrogen. They have found that, hydroxyl groups at the metal and promoter interface could also help limit catalyst deactivation. Therefore, promoted catalyst revealed a cooperative interaction amidst the metal and the basic oxide *via* bifunctional mechanism.

Carrara *et al.* [42] carried out kinetic and stability studies of DRM over Ru/La_2O_3. From their stability experiments, catalyst remained stable over 80 hours in 550 to 630 °C temperature range and P_{CO_2}/P_{CH_4} ratio equal to 1. However, when this ratio increased above 1, significant deactivation was observed at 550 °C. To understand this response, they have studied ruthenium reactivity in reductive and CO_2 rich atmosphere by *in-situ* LRS and XPS. They have proposed that, partial re-oxidation of Ru could one of the factors leading to deactivation. At the stable parameters, kinetics of DRM over Ru/La_2O_3 was investigated. They have found that, the metal and the oxide plays key roles in paraffin decomposition and CO_2 activation, respectively.

Safariamin *et al.* [43] studied DRM over 5 wt% Ru loaded alumina, ceria, ceria-alumina with different amounts of ceria (nCe10Al, n = 1, 3, 5; n = atomic ratio) with CH_4/CO_2 ratio 1 and in the temperature range of 400-800 °C. They have evaluated coke deposited on catalysts and found carbon deposition on Ru/CeO_2, Ru/1Ce10Al and Ru/3Ce10Al. On Ru/Al_2O_3 and Ru/5Ce10Al they couldn't find any carbon deposition. They have found that, addition of CeO_2 on Al_2O_3 can enable Ru-Ce interaction and due to alumina, well dispersed Ru species can reduce easily. Therefore, Ru/5Ce10Al was found the most active and stable catalyst among they have tested.

Chen *et al.* [44] studied syngas production from DRM over ruthenium supported on $Ce_{0.75}Zr_{0.25}O_2$. In this article, they have investigated the effect of Ru content on $Ru/Ce_{0.75}Zr_{0.25}O_2$ catalysts. When they have increased Ru content in catalyst above 1.5 wt%, surface area and pore volume of catalysts decreased drastically. They have found the interaction between Ru and support increases with the decrease of Ru crystallites *via* H_2-TPR and XRD. Using CO chemisorption, they have proved that strong interaction between support and metal decreases available Ru atoms. However, they have stated this strong interaction may favor TOF of CH_4 and CO_2. From H_2-TPR and XPS, they have shown that Ru species promote the reduction of the support at high temperatures. Their H_2-TPD results showed that, reduced CZ support can store H_2, which they relate to formed anionic vacancy. From their experimental results, 1.5 wt% Ru/CZ exhibits good stability through excellent resistance to carbon deposition during the reaction. They have stated a mechanism involving hydrides participating in carbon elimination, which was based on the cerium and zirconium hydrides detected on the spent catalysts. Finally, they have explained the good catalyst stability with the resistance of metallic Ru to carbon deposition, redox role of the support and hydrogen storage of reduced CZ.

In 2012, Kehres *et al.* [45] researched the dynamical properties of $Ru/MgAl_2O_4$ catalyst during reduction and DRM. They have perfomed combined in situ small and wide-angle X-ray scattering (SAXS/WAXS) studies to investigate the dynamical properties of 4 wt.% $Ru/MgAl_2O_4$ (ruthenium on spinel) during both reduction and re-

action. Reduction in pure H_2 occurs at a temperature between 100 to 120 °C. DRM experiments were done at temperatures between 450 to 750 °C and CO_2 to CH_4 ratio of 3. They have found that, particle diameter remained stable during repeated DRM experiments, which indicates preserved nanostructure. They have seen no sintering of Ru nanoparticles and no deactivation at any time and temperature in experiments. They have determined the apparent activation energy for DRM at experimental conditions to be 75 ± 1 kJ mol^{-1}.

In 2014, Derk *et al.* [46] studied catalytic DRM over ruthenium-doped ceria and ruthenium supported on ceria. They have investigated two types of Ru-ceria catalysts, in which doped catalyst synthesized by combustion to create atomically doped metal oxide, and supported catalyst was synthesized by impregnation. Using XRD, Ru-XPS, and IR spectrum of CO on them, they have found that two catalysts has different physical properties; but deliver the same catalytic activity, which is 48% CH_4 conversion at 600 °C. Using transient oxygen reaction spectroscopy the authors showed the necessity of reduction to the activity.

In 2016, Gennequin *et al.* [47] have investigated the influence of the ruthenium on the activity and stability of Co-Mg-Al-based catalysts in DRM. In this article, they have synthesized $Co_xMg_{6-x}Al_2$ (with x=2 and 6) mixed oxide catalysts by impregnation on the dried hydrotalcite and by memory effect on hydrotalcite calcined at 500 °C. From their experiments, they have seen that addition of ruthenium increases CO_2 and CH_4 conversions and decreases water formed on the support. They have found that, using hydrotalcite memory effect to impregnate ruthenium provides better dispersed and more accessible Ru particles and helps oxidizing carbon deposited on catalyst. In stability experiments, after 24h at 700 °C, they have seen lower cobalt content inhibits carbon deposition. They correlated this coke inhibition with the strength of the basic sites in CO_2-TPD. They have stated that, formation of carbon species is dependent to temperature. However, formation of carbon species does not affect catalyst performance during reaction.

Whang *et al.* [48] worked on enhanced activity and durability of Ru catalyst dispersed on zirconia for DRM in 2017. In this article, they have prepared Ru/SiO_2, ZrO_2-SiO_2, Ru/ZrO_2-SiO_2, and Co-Ru/ZrO_2-SiO_2 catalysts and tested in DRM at 800 °C and different space velocities. Their activity tests showed that, Ru/ZrO_2-SiO_2, and Co-Ru/ZrO_2-SiO_2 catalysts showed high CH_4 and CO_2 conversions, whereas other catalysts showed poor results. When they characterized the catalysts, Ru/SiO_2 had large Ru nanoparticles of 6.3 nm, whereas Ru/ZrO_2-SiO_2 had smaller Ru nanoparticles of 1.4 nm. From TPR and XANES results, they have determined that Ru and ZrO_2 exhibits strong-metal support interaction. Also, Ru/ZrO_2-SiO_2 catalyst showed high activity at higher GHSV. After 20h, CH_4 turnover number reduced only 0.13 $mol_{CH_4}/g_{cat}.h$ from 0.92 to 0.79 $mol_{CH_4}/g_{cat}.h$. They have found that, 0.13 wt% Ru immobilized at ZrO_2 was active and stable for DRM at harsh condition, even without the aid of Co.

2.2.2. Ru-based catalysts in Glycerol Steam Reforming

Gallo *et al.* [49] studied Sn doping on Ru-based catalysts on Mg(Al)O mixed oxides, which will provide high activity and selectivity in GSR. They have studied the effect of Sn loading, and characterized catalysts with HRTEM, DRIFTS and QMS of adsorbed CO. Ru-Sn catalysts prepared by chemical vapor deposition showed glycerol conversions over 87.5% and high H_2/CO_2 selectivity. These catalysts preserved their activity over 20 hours. They have found that, effect of Sn doping changes according to the Sn/Ru ratios. At low Sn/Ru ratios, Sn coated Ru faces selectively, and only active unsaturated Ru sites are exposed. However, increasing Sn/Ru ratios results in active catalysts with higher CO selectivity. Following this work, Gallo *et al.* [50] published another article about influence of reaction parameters for GSR over Ru supported on Mg(Al)O catalysts in 2012. They have tested these catalysts in GDR reaction at 450-650 °C, glycerol concentration range 10-40 wt.% in water. Using HRTEM, they have seen no significant sintering of Ru-particles in 20 hours reaction tests. Activity-wise, catalysts show 96% glycerol conversion, 96% H_2 yield and 91% CO_2 selectivity. They have found trace amounts of CH_4, CO selectivity lower than 3.5% and coke deposition of 1.1 $mg_C g_{cat}^{-1} h^{-1}$. They couldn't find any advantage of increasing temperature since

it only increased glycerol conversion and H_2 yield by 2%. When they have increased glycerol concentration to 40 wt.%, conversion and H_2 yield decreased to 60% and 50%, respectively. Catalysts remained stable although coke formation increased 10-fold. CO_2 selectivity decreased to 82% while both CO and CH_4 selectivity increased smoothly. They have suggested that, reaction temperature of 650 °C can allow working with glycerol concentration of 40% and also increasing space velocity results in 97% glycerol conversion and 85 mol.% without increasing coke formation on catalysts significantly.

In 2012, Sundari and Vaidya investigated reaction kinetics of GSR over Ru/Al_2O_3 [51]. They have investigated the kinetics in the range of 350-500 °C and W/F_{AO} ratio 0.4-1.98 g h/mol. Increase in temperature, steam/glycerol ratio and space time resulted an increase in the H_2 yield. They have found that, reaction system belongs to kinetically controlled reaction regime systems. By employing integral method of analysis, they have found that the reaction order with respect to glycerol is equal to one. They have evaluated the activation energy as 21.2 kJ/mol based on the temperature dependence of the reaction rate constant. They have found a heterogeneous first-order kinetic model which is in alignment with literature.

Kim and Lee studied GSR on Ru and Ru-M (M = Fe, Ni, Co, and Mo) catalysts supported on yttria, ceria-zirconia, and γ-alumina [52]. They have found that, nature of the support leads to improvement of the H_2 production turnover rate and product selectivity on yttria and ceria-zirconia supported catalysts *via* promotion of WGS reaction. $Ru/\gamma\text{-}Al_2O_3$ demonstrates low H_2 production turnover rate with high CO selectivity and favors C_1-C_2 hydrocarbons formation. They have found that, metal promotion on bimetallic Ru-M catalysts (excluding Mo) is not effective which only increases glycerol conversion very little. In time on stream experiments, $Ru/\gamma\text{-}Al_2O_3$ deactivated significantly due to coke formation. Coke formation is not significant on yttria and ceria-zirconia supported catalysts. However, these catalysts deactivate due to sintering of Ni-particles. In Ru-Mo catalysts, sintering is reduced due to MoO_x species on the surface. $Ru\text{-}Mo/Y_2O_3$ catalysts exhibit extensive stability due to sintering blockage of Mo, and coke formation reduction of yttria.

Gallegos-Suarez *et al.* [53] studied H_2 production from GSR with carbon supported ruthenium catalysts. They have used activated carbon (AC), two commercial carbon nanofibers (PS, and HHT), high surface area graphite (HSAG), and multiwall carbon nanotubes (CNT) to support Ru-catalysts for GSR. From their experimental results, they have found that GSR over Ru/C catalysts is a structure sensitive reaction. Thus, activity for H_2 production decreased with decreasing Ru particle size. They have found that, stability of catalyst is affected by the reactivity to gasification of the carbon support. Therefore, the more graphitized the carbon, the less reactive but more stable the catalyst. When they compared the catalysts, Ru-HHT and Ru-CNT exhibited the best results. However, activity of Ru-HSAG was close for consideration due to much cheaper manufacture of the support. For this reason, they have selected Ru-HSAG catalyst for being tested in the Pd membrane reactor at 500 °C. Implementing a membrane reactor increased glycerol conversion by 11.1%, H_2 yield by 11.3%, CO_2 selectivity by 9.6% in 5 hour experiments. This difference increases significantly over 40 hour experiments. They have explained this stability by the enhancement of the WGS reaction and reduction of C_2 olefins which are the precursors of coke deposits.

In 2017, Kousi *et al.* [54] have studied GSR over modified Ru/Al_2O_3 catalysts. They have investigated Ru/Al_2O_3, Ru/B_2O_3-Al_2O_3 and Ru/MgO-Al_2O_3 for their physiochemical and catalytic properties in GSR. They have employed N_2 adsorption desorption, powder XRD, CO Adsorption, NH_3-TPD, CO_2-TPD, TPR, TEM and SEM-EDS to analyze the textural and structural properties of the catalysts. From their experiments, they have found that at low reaction temperatures, support affects the activity, where at high temperatures metal activity dominates. They have found that the nature of support plays a key role in selectivity. However, they have found that catalytic performance can still be effected by the metal-support interface, where metal phase converts intermediates into syngas. They have found that, selectivity of these intermediates depends on the acidity of the support. Modified catalysts did not improve activity and stability, where best catalyst among tested is Ru/Al_2O_3 with 92% conversion to gas-phase products and 68% H_2 yield at 500 °C. Ru/B_2O_3-Al_2O_3 could only provided similar results at 100 °C higher, at 600 °C. Ru/MgO-Al_2O_3 was the worst

among tested catalysts, which couldn't reach any significant conversion or H_2 yield. They have found that, all of these 3 catalysts are not stable, which they explained by graphitic carbon accumulated on the catalyst. They have determined the carbon shape as platelet-like with encapsulating properties. Ru/Al_2O_3 was more carbon resistant than Ru/B_2O_3-Al_2O_3, due to more acidic nature of Ru/B_2O_3-Al_2O_3.

Finally, Dahdah *et al.* [55] have studied GSR over Ru-Mg-Al hydrotalcite-derived mixed oxide. More specifically, they have investigated the role of preparation method in catalyctic activity. They have synthesized the catalysts using two different methods. First, the grafted catalyst was synthesized by co-precipitation of Ru-Mg-Al precursors at constant pH. Second, impregnated catalyst was synthesized by wet impregnation of calcined Mg-Al support and ruthenium nitrosyl nitrate. They have calcined both catalysts at 600 °C and then characterized by XRD, CO_2-TPD, and H_2-TPR. They have compared catalyst activity in GSR at 400 to 700 °C, steam to glycerol ratio of 9, and flow rate of 0.075 ml/min. From their XRD analysis, they have verified the presence of Ru in the hydrotalcite structure of grafted catalyst. Yet, this catalyst exhibited lower catalytic activity above 600 °C in GSR. They have attributed this result to the trapped Ru particles in the bulk of support, which lowers accessibility to active phase in the grafted catalyst. They have verified this in TPR, which reveals the high metal-support interaction by higher temperature reduction peaks, but overall hydrogen consumption is lower. Both catalysts showed deactivation during activity test due to coke formation, which they associate with liquid product formation. They have found that different synthesis techniques differ Ru particle size on catalyst, therefore generating significant difference in catalyst activity.

2.3. Lanthana-Zirconia Supported Catalysts in Reforming

Throughout the literature survey, supports plays a critical role in reforming reaction. Some supports disperse the active metal very good, but fails to remove carbon species, thus leading to a active catalyst with very rapid deactivation [9, 32, 54, 55]. And there are several supports that removes carbon species efficiently, but does not

exhibit very good activity [30, 40, 52, 53]. Goal of this work is to find the support that combines both of activity and stability properties for the Ru-based catalysis of GDR. For different reforming reactions and different active metals, there are several studies that accomplished this feat [11]. From the study of Whang *et al.* [48], the strong metal-support interaction between Ru and ZrO_2 is known. Thus, zirconia based supports drew attention for finding the right support for ruthenium, also from the work of Carrara *et al.* [42] stability of Ru/La_2O_3 is proven over 80 hours. Therefore following articles are about La_2O_3-ZrO_2 mixed oxide support, which may lead to an understanding of how these supports work in reaction conditions.

In 2014, Tao *et al.* [56] studied CO_2 reforming of coke oven gas (58-60% H_2, 23-27% CH_4, and less than 3% CO_2) over Ni/La_2O_3-ZrO_2 catalysts. They have synthesized the catalysts by sol-gel technique and characterized by XRF, BET, XRD, H_2-TPR, TEM and TG-DSC. They have measured the effect of Ni loadings and calcination temperature of the catalysts. From their characterization results, all of the catalysts exhibited exceptional coking resistance. They have found that, 10 wt.% Ni/La_2O_3-ZrO_2 exhibits the best activity of over 95% CH_4 and CO_2 conversions at 800 °C and atmospheric pressure. Following this work in 2018, Tao *et al.* [57] published an article about enhanced activity of Ni-Mo_2C/La_2O_3-ZrO_2 bifunctional catalyst for DRM. In this article, they have synthesized catalysts *via* template method paired with incipient wetness impregnation and temperature-programmed carbonization. They have tested the catalyst in DRM at 700 to 900 °C under atmosperic pressure. Addition to their previous work, they have included Raman analysis to characterization. They have obtained Ni-Mo_2C particles with 3 nm diameter and La_2O_3-ZrO_2 supports shown a cubic lattice with sheet shape, which contains abundant oxygen vacancies. Interaction between these vacancies and Ni-Mo_2C particles reduces the apparent activation energy of CO_2, thus accelerating DRM reaction. They have found that, Ni-Mo_2C/La_2O_3-ZrO_2 (7.5 mol.% La_2O_3) shows the best activity of 94% CH_4 conversion and stability after 100 hours at 900 °C. This catalyst has improved BET surfrace area of 33.2 m^2/g, smaller crystallites, grain boundaries and oxidation-carbonization cycle of Ni-Mo_2C.

Angeli *et al.* [58] worked on catalyst development for SRM and model biogas at low temperature in 2016. In this article, they have reported the performance of Ni and Rh catalysts supported on La_2O_3-ZrO_2 and La_2O_3-CeO_2-ZrO_2 in a membrane reactor. They have determined the performance of the catalysts in different GHSV, temperature, steam to carbon ratio. They have found that, all catalysts were active in reforming at 400 to 550 °C and catalysts supported on La_2O_3-CeO_2-ZrO_2 has shown superiority and stability. They have explained this improvement with the presence of ceria, which contributes to reaction rate and the resistance to coke deposition. 10 wt.% Ni/La_2O_3-CeO_2-ZrO_2 exhibits very stable performance with 0.05 wt.% of carbon formed after 90 hours. From their TPO and TPH analysis, dominating type of carbon is highly reactive and can be removed by hydrogenation or oxidation at 500 °C.

In 2017, Goula *et al.* [59] studied biogas dry reforming over Ni supported on ZrO_2, La_2O_3-ZrO_2 and CeO_2-ZrO_2 in the temperature range of 500-800 °C and CH_4 to CO_2 of 1.5 to simulate biogas composition. They have found that, CeO_2 provides resistance to sintering by increasing the oxygen ion lability of support, which they thought to be the key factor for stability or improved Ni dispersion. When they analyzed deposited carbon after the reaction, filamentous tube like morphology occurs on Ni/ZrO_2 and Ni/La_2O_3-ZrO_2. On Ni/CeO_2-ZrO_2, they have detected small amount of carbon tube-like structures. Using Raman spectroscopy, they have found that Ni/ZrO_2 has the highest crystallinity, and therefore having the higher grapthitized carbon formed on catalyst. On the other hand, Ni/CeO_2-ZrO_2 had the lowest crystallinity. They have found that, Ni/La_2O_3-ZrO_2 and Ni/CeO_2-ZrO_2 have shown superior catalytic activity and stability than Ni/ZrO_2. They have explained this superiority with enhanced basicity, Ni dispersion and high oxygen vacancies of the mixed-oxide supports. They have reported that, basic elements like 2A group metals or lanthanides may enhance DRM by improving metal-support interaction which effects metal dispersion, and activating CO_2 by forming carbonates.

Finally, Cheng *et al.* [60] have investigated the effects of preparation technique and lanthana doping on Ni/La_2O_3-ZrO_2 catalysts for H_2 production by CO_2 reforming

of coke oven gas (58.5 mol% H_2, 31.2 mol% CH_4, 3.07 mol% CO_2, and 7.23 mol% CO). They have prepared 5 wt.% Ni/La_2O_3-ZrO_2 catalysts by homogeneous precipitation, template or sol-gel technique. These catalysts characterized by BET, XRD, TPR, TPH, TEM and TG-DSC. They have seen that, preparation technique affected the pore structure, characteristics of the catalysts and dispersion of active metal. They have found that, La_2O_3 doping increases the basicity and number of basic centers on the catalyst. They have seen that, carbon deposition on catalyst is a reversible process, thus can be eliminated. Their ideal and most active catalyst was, 5 wt.% Ni/La_2O_3-ZrO_2 with 8 wt.% La_2O_3 content. In 50 hour reaction, CH_4 and CO_2 conversions for this catalyst were 93.3% and 95.6%, respectively, where H_2 and CO selectivities were 93.8% and 98.1%, respectively.

3. EXPERIMENTAL WORK

3.1. Materials

3.1.1. Chemicals

Chemicals used in catalyst preparation are listed in Table 3.1. Al_2O_3 (Al), CaO (Ca), CeO_2 (Ce), La_2O_3 (La), ZrO_2 (Zr), Al_2O_3-ZrO_2 (AZ), CeO_2-ZrO_2 (CZ), La_2O_3-ZrO_2 (LZ), SiO_2-ZrO_2 (SZ) and WO_3-ZrO_2 (WZ) were used as supports and ruthenium nitrosyl nitrate were used as Ru-precursor. Deionized water with a conductivity less than 0.1 μS cm^{-1} is used to dilute the Ru-precursor and it was produced by Zeneer Water Purification System.

3.1.2. Liquids and Gases

The list of all liquid and gaseous feeds used in experimental system are given in Table 3.2 and Table 3.3, respectively. Only liquid feed and reactant in GDR is glycerol. Distilled water, ethanol and acetone in the Table 3.2 are used for cleaning purposes. For the gaseous feeds, CO_2 and N_2 were used in the reaction as reactant and inert gas, respectively. H_2 was used for reducing the catalysts. Ar and He were used as carrier gases of gas chromatographs (GC). Finally, CO, CH_4, C_2H_4, and C_2H_6 were used to calibrate GC's.

3.2. Experimental System

Experimental system utilized in this study consists of 3 main parts:

- Catalyst Preparation System: Catalysts prepared with incipient-to-wetness impregnation technique, which consists of an ultrasonic mixer, a vacuum pump, a Buchner flask, and a peristaltic pump.

Table 3.1. List of the chemicals used for catalyst preparation.

Chemical	**Formula**	**Vendor**	**MW (g/mol)**	**Purity**	**Use**
Aluminum oxide Alpha Phase	α-Al_2O_3 3/8" Pellets	Alfa Aesar	101.96	> 99%	Diluent
Aluminum oxide Gamma Phase	γ-Al_2O_3 1/8" Pellets	Alfa Aesar	101.96	> 99%	Support
Calcium oxide	CaO	Alfa Aesar	56.08	99.95%	Support
Ce (III) nitrate hexahydrate	$Ce(NO_3)_3{\cdot}6H_2O$	Sigma-Aldrich	434.22	99.99%	Support
Lanthanum (III) oxide	La_2O_3	Sigma-Aldrich	325.81	99.99%	Support
Zirconium oxide	ZrO_2	Alfa Aesar	123.22	> 99%	Support
Alumina-Zirconia	10 wt.% ZrO_2-Al_2O_3	Daiichi Kigenso	98.96	-	Support
Ceria-Zirconia	50 wt.% CeO_2-ZrO_2	Daiichi Kigenso	81.00	-	Support
Lanthana-Zirconia	9 wt.% La_2O_3-ZrO_2	Daiichi Kigenso	94.84	-	Support
Silica-Zirconia	10 wt.% SiO_2-ZrO_2	Daiichi Kigenso	69.40	-	Support
Tungsten-Zirconia	10 wt.% WO_3-ZrO_2	Daiichi Kigenso	87.98	-	Support
Ruthenium (III) nitrosyl nitrate solution	$Ru(NO)(NO_3)_x(OH)_y$ x+y=3	Sigma-Aldrich	318.10	Ru, 1.5 %	Active Metal
Deionized water	H_2O	-	18.02	-	Solvent

Table 3.2. List of liquids used in experiments.

Liquid	**Formula**	**MW (g/mol)**	**Vendor**	**Purity**	**Usage**
Glycerol	$C_3H_8O_3$	92.09	Merck	$> 99.5\%$ ACS Reagent	Reactant
Acetone	C_3H_6O	58.08	Labor Teknik	99.5%	Cleaning
Ethanol	C_2H_6O	46.07	Labor Teknik	96%	Cleaning
Water	H_2O	18.02	-	Distilled	Cleaning

Table 3.3. List of gases used in experiments.

Gas	**Formula**	**MW (g/mol)**	**Vendor**	**Purity**	**Usage**
Argon	Ar	39.95	Linde	99.99%	Carrier
Carbon Monoxide	CO	28.01	Linde	99.99%	Calibration
Carbon Dioxide	CO_2	44.01	Linde	99.99%	Reactant
Ethane	C_2H_6	30.07	Hat Grup	5% in He	Calibration
Ethylene	C_2H_4	28.05	Hat Grup	5% in He	Calibration
Helium	He	4.00	Linde	99.99%	Carrier
Hydrogen	H_2	2.01	Linde	99.99%	Reduction
Methane	CH_4	16.04	Linde	99.5%	Calibration
Nitrogen	N_2	28.01	Linde	99.99%	Inert

- Catalytic Reaction System: Reaction takes place in a quartz packed-bed reactor which placed inside a three-zone furnace to provide required temperatures, mass flow controllers to adjust gaseous feed flow, and a HPLC's pump section to provide very accurate liquid feed flow.
- Product Analysis System: Effluent of catalytic reaction system is analyzed by two gas chromatography devices with different columns to determine the composition of the product.

3.2.1. Catalyst Preparation System

In this study, catalysts were prepared by incipient-to-wetness impregnation technique. A simple illustration for this technique is given in Figure 3.1. Mixture is held in a Buchner flask, which put on Retsch UR1 ultrasonic mixer to provide continuous mixing throughout the process. Along with mixing, KNF diaphragm vacuum pump was used to remove air from the pores of the support. For drop-wise addition of active metal precursor to support, Masterflex peristaltic pump was used. Detailed synthesis process for each catalyst synthesized will be given in Section 3.3.

3.2.2. Catalytic Reaction System

The catalytic reaction system used in this work is divided into three major parts. These are, inlet section, reaction section and product analysis. Schematic of the system is given in Figure 3.2 and Figure 3.3 is the actual system that is used in this work.

3.2.2.1. Inlet Section. Inlet section of the catalytic reaction system consists of glycerol, which is fed into reactor using the precise pump of Shimadzu LC-20AT high-performance liquid chromatograph (unit 3 in Figure 3.2). Gaseous feeds fed into reactor from the cylinders of individual gases (specifications given in Table3.3), using Bronkhorst EL-FLOW Select mass flow controllers (MFC, unit 2 in Figure 3.2). These liquid and gaseous feeds are piped throughout the system using Swagelok tubes, unions and t-joints of sizes ranging from 1/16" to 1/4".

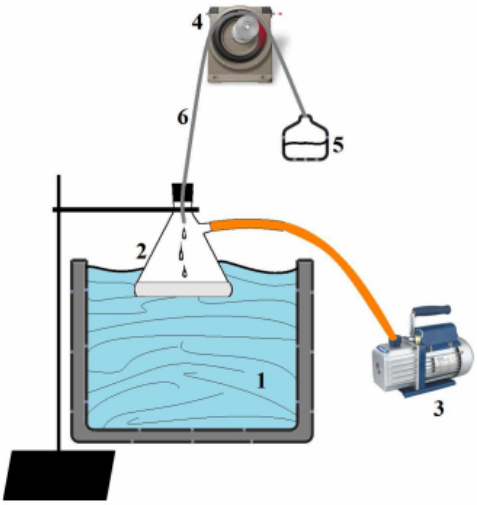

Figure 3.1. Illustration of impregnation system used in this work [61, 62]. 1. Ultrasonic Mixer, 2. Buchner Flask, 3. Vacuum Pump, 4. Peristaltic Pump, 5. Precursor Solution, 6. Tubing.

Using single-stage gas regulators (units 1a in Figure 3.2), outlet pressures of H_2, CO_2, and N_2 are reduced to 3 bar before feeding them into MFCs *via* 1/8" pipes. MFCs of individual gases are used to adjust volumetric flow rate before sending them into reactor. These MFCs might have a difference between their set points and actual flow rate. Thus, MFCs were calibrated before starting the reaction experiments, calibration charts of MFCs can be found in Appendix A. To eliminate back flow of the reactants, on-off valves were installed after each MFC. Exit of these on-off valves are united with 1/4" pipes to mix the gases, then reduced into 1/8" pipes *via* reducing union. Mixture of gases are sent to a 3-way valve which used to direct this mixture to reactor or GCs for feed gas analysis. 1/8" pipe that leads to reactor from this valve, is reduced to 1/16" before the injection into reactor.

Glycerol is fed from a 100 mL graduated cylinder to reactor *via* the pump of HPLC, using 1/16" pipes. Since the viscosity of glycerol is high, a heating line was wrapped around the 1/16" pipe that carries glycerol, and sealed with glass wool and aluminum foil to prevent heat loss. PID controller from TETRA is used to maintain

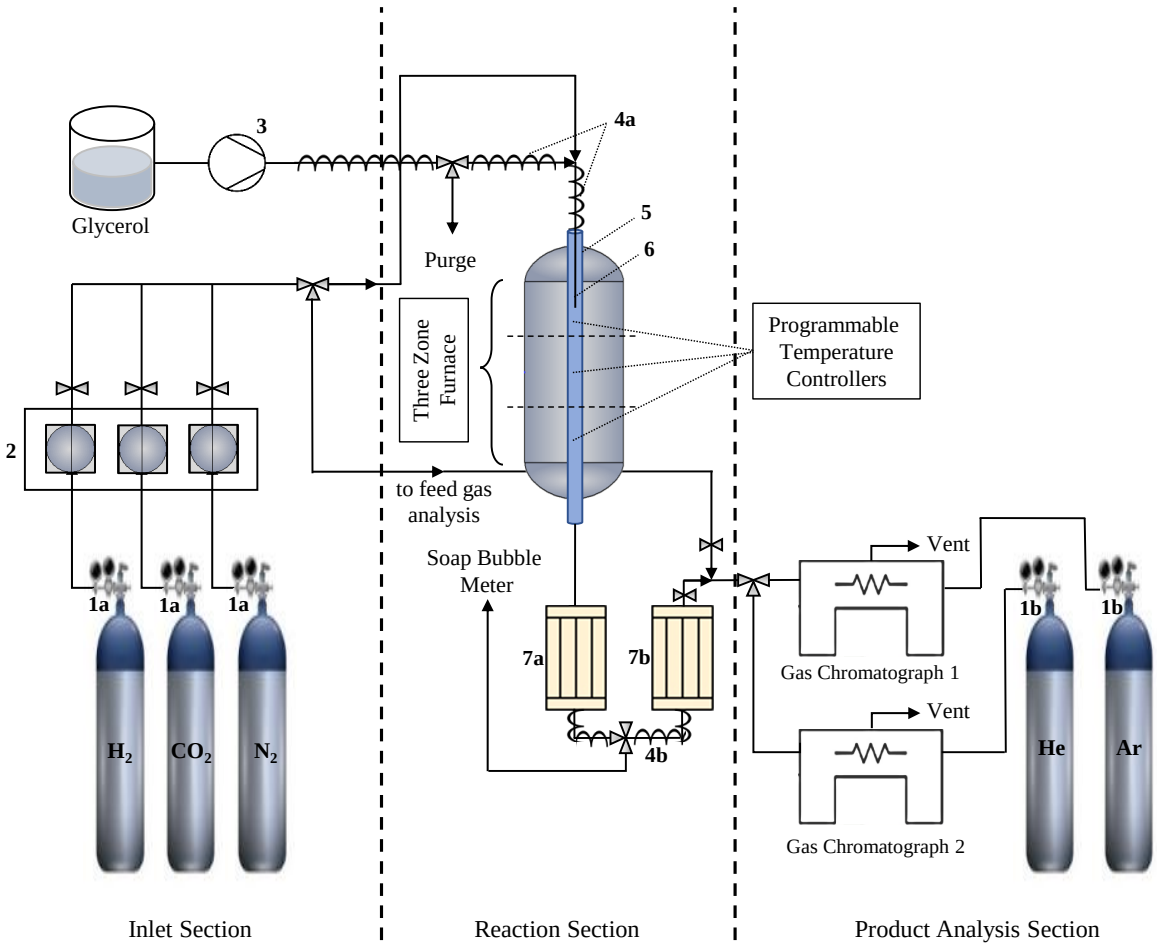

Figure 3.2. Schematic representation of the catalytic reaction system.

Figure 3.3. Actual catalytic reaction system that is used in this work.

constant 100 °C in this heating section to provide smoother glycerol flow. Before reaching reactor, an open-close valve was installed to establish a purge line for glycerol.

Just before the reactor, gaseous feed, and glycerol streams are united by a 1/16" t-joint. Then, reactant mixture injected to the reactor *via* a 1/16" pipe which elongates for 10 cm inside of quartz reactor to provide complete evaporation of glycerol. Three-zone furnace allows the tip of the injector to reach approximately 400 °C, which provides a homogeneous mixture of reactants at gas phase. This allows a constant CO_2 to glycerol ratio in the catalyst bed [61].

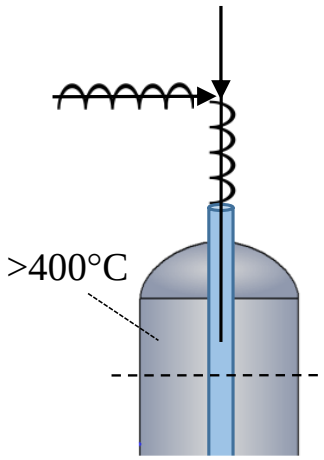

Figure 3.4. Illustration of reactor inlet and injector.

3.2.2.2. Reaction Section. Reaction section consists of a packed bed quartz reactor, which heated inside of PROTHERM PZF 12/50/500 three-zone furnace, and two cold traps inside of Dewar flasks.

Packed bed quartz reactor is a quartz cylinder with hourglass shape, which will be detailed in Section 3.4. Middle section of the quartz reactor aligns with the middle zone of furnace which is heated to the reaction temperature, this alignment can be seen in Figure 3.5. Rest of the three-zone furnace is kept specifically above 310 °C, to prevent condensation of glycerol throughout the reactor.

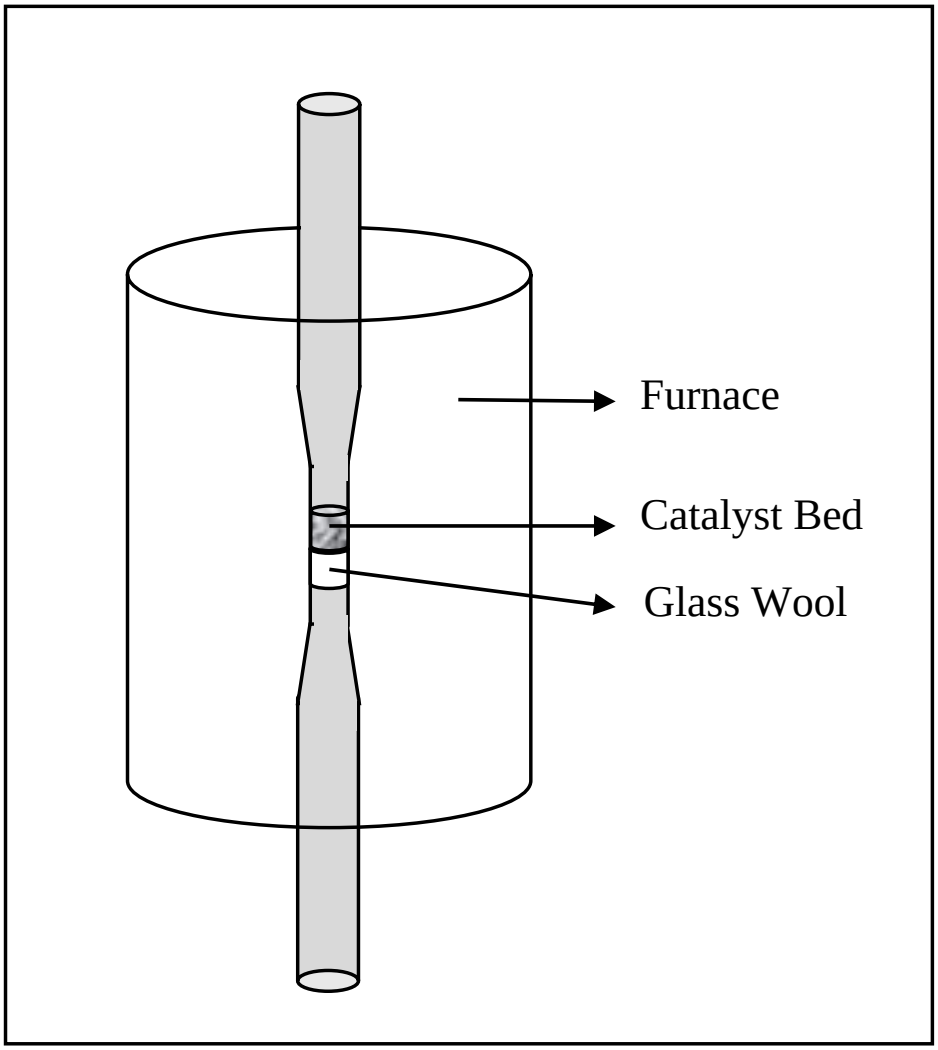

Figure 3.5. Illustration of a packed bed reactor.

Effluent of the reactor is sent to two sequential cold traps (units 7a and 7b in Figure 3.2), which contains ice to cool the vessels. Cold traps are used to condense water or any low boiling point hydrocarbons formed by side reactions. Exit of the initial cold trap (unit 7a in Figure 3.2) is routed by a 3-way valve, which can direct the stream to second cold trap (unit 7b in Figure 3.2) or soap bubble meter. Soap bubble meter is a flow meter, which used for determination of actual flow rate of any gaseous stream. Thus in the system, soap bubble meter is used for MFC calibration or leak check before any experiment. Soap bubble meter is connected to ventilation, which purges reactor effluent without proceeding to analysis section. Pipe between cold traps is wrapped with heating line in order to prevent any condensation, which may block the pipes. After the cold traps, exit stream of reactor leads to the product analysis system with liquid products removed.

3.2.2.3. Product Analysis Section. Product analysis section consists of two gas chromatographs and their carrier gases' cylinders. In this section, there are two inlets; first stream is coming directly from MFCs for feed gas analysis, and second stream comes from reaction section. These two inlets are unified by a 1/4" t-joint, then sent to a 3-way valve which directs incoming stream to septum outlet, or second 3-way valve. Second 3-way valve directs incoming stream to gas chromatograph 1 or gas chromatograph 2 (units GC-1 and GC-2 in Figure 3.2).

In product analysis section, composition of gaseous product stream, and feed stream are determined. In total, 7 product gases are determined in two different GCs. First GC, is a Shimadzu GC-2014 equipped with a thermal conductivity detector (TCD) and a permanent gases column. This GC uses Ar for carrier and gases are fed to GC's column *via* a manual sample loop. This GC detects H_2, N_2, CO, and CH_4 precisely. Second GC, is a Shimadzu GC-8A equipped also with a TCD, but a Porapak Q column was installed. This GC uses He for carrier gas and it has the identical sample loop with GC-1. This GC detects N_2, CO_2, C_2H_4 and C_2H_6. Calibration charts are presented in Appendix A.

Table 3.4. Operational specifications and parameters of gas chromatographs.

Parameter	**Shimadzu GC-2014 (GC-1)**	**Shimadzu 8-A (GC-2)**
Carrier gas	Argon	Helium
Carrier gas flow rate (NmL min^{-1})	25	30
Column material	Stainless steel	Stainless steel
Column packing material	Molecular Sieve 5A	Porapak Q
Column ID (mm)	2.1	2.1
Column length (m)	4.6	3
Column temperature (°C)	50	90
Detector type	Thermal conductivity	Thermal conductivity
Detector temperature (°C)	150	150
Detector current (mA)	50	120
Injector temperature (°C)	80	90
Sample loop volume (mL)	1.3	1.3

3.3. Catalyst Preparation

In this study ten different catalysts, namely RuAl, RuCa, RuCe, RuLa, RuZr, RuAZ, RuCZ, RuLZ, RuSZ and RuWZ were prepared. The preparation step includes, support preparation, incipient-to-wetness impregnation, and catalyst calcination.

3.3.1. Preparation of Support

3.3.1.1. Preparation of Al_2O_3. γ-Al_2O_3 in pellet form (specifications in Table 3.1) was pestled in a mortar and sieved to collect 45-60 mesh size (250-354 μm) particles. Then, collected support was calcined at 800 °C for 4 hours under air [61].

3.3.1.2. Preparation of CaO. CaO was purchased from Alfa Aesar below 80 mesh size, therefore pestling and sieving was bypassed to calcination at 800 °C for 4 hours under air.

3.3.1.3. Preparation of CeO_2. Cerium (III) nitrate was calcined at 600 °C for 4 hours under air. After precursor decomposes into CeO_2, obtained powder was sieved to 45-60 mesh size and calcined at 800 °C for 4 hours under air [61].

3.3.1.4. Preparation of La_2O_3. La_2O_3 was purchased from Sigma-Aldrich below 80 mesh size, therefore pestling and sieving was skipped to calcination at 800 °C for 4 hours under air.

3.3.1.5. Preparation of ZrO_2. ZrO_2 in pellet form was pestled and sieved to obtain 45-60 mesh size. Then, calcined at 800 °C for 4 hours under air [61].

3.3.1.6. Preparation of Mixed-oxide Supports. All mixed oxide supports (AZ, CZ, LZ, SZ, and WZ), were purchased from Daiichi Kigenso below 80 mesh size. Therefore, these mixed-oxide supports were only calcined at 800 °C for 4 hours under air.

3.3.2. Preparation of Active Catalysts

All of the supports mentioned in Section 3.3.1, have been impregnated with Ru-precursor to synthesize 1 wt% Ru-catalysts. Technique used to prepare catalysts was incipient-to-wetness impregnation for all the catalysts. Thus, similar procedure was applied with slight differences to synthesize all catalysts. Equipment used for this procedure is explained in Section 3.2.1.

3.3.2.1. Preparation of RuAl (Ru/Al_2O_3). 1 gram of 1 wt.% Ru/Al_2O_3 catalyst was prepared in one batch. First, 0.99 grams of Al_2O_3 was weighed and put into a Buchner flask. Then, this flask was mounted on catalysis preparation apparatus and put under vacuum for 30 minutes (this setup can be seen in Figure 3.1). Since the Ru-precursor used in this study is Ruthenium nitrosyl nitrate solution in dilute nitric acid (properties of this precursor is given in Table 3.1) which contains 1.5 wt.% of Ru, 0.667 grams of Ru-precursor ($\sim$ 0.623 mL, since the precursor is in liquid form and $\rho_{\text{precursor}}$ is 1.07 g/mL) is required for obtaining 0.01 grams of Ruthenium. This amount of Ru-precursor was taken with a micro-pipette, and diluted with 1 mL of deionized water in order to fulfill the incipient-to-wetness condition. After 30 minutes of vacuum, precursor solution was injected into support drop-wise with a speed of 0.04 m s^{-1} by the peristaltic pump. This addition formed a slurry which was mixed for 1.5 hours in ultrasonic mixer under vacuum to ensure good dispersion of active metal on the support. After this procedure, mixture was dried overnight at 110 °C and calcined under air at 800 °C for 4 hours [61].

3.3.2.2. Preparation of RuCa (Ru/CaO). 1 gram of 1 wt.% Ru/CaO was synthesized using using a very similar procedure to Ru/Al_2O_3, which explained in Section 3.3.2.1. Only difference between these procedures was, Ru-precursor was diluted with 0.1 mL of deionized water instead of 1 mL. This is due to smaller surface area of CaO than Al_2O_3 [61].

3.3.2.3. Preparation of RuCe (Ru/CeO_2). 1 gram of 1 wt.% Ru/CeO_2 was synthesized using using a very similar procedure to Ru/Al_2O_3, which explained in Section 3.3.2.1. Only difference between these procedures was, Ru-precursor was not diluted with any deionized water.

3.3.2.4. Preparation of RuLa (Ru/La_2O_3). 1 gram of 1 wt.% Ru/La_2O_3 was synthesized using using a very similar procedure to Ru/Al_2O_3, which explained in Section 3.3.2.1. Only difference between these procedures was, Ru-precursor was diluted with 0.4 mL of deionized water instead of 1 mL.

3.3.2.5. Preparation of RuZr (Ru/ZrO_2). 1 gram of 1 wt.% Ru/ZrO_2 was synthesized using using a very similar procedure to Ru/Al_2O_3, which explained in Section 3.3.2.1. Difference between these procedures was, Ru-precursor was not diluted with any water.

3.3.2.6. Preparation of RuAZ (Ru/Al_2O_3-ZrO_2). 1 gram of 1 wt.% Ru/Al_2O_3-ZrO_2 was synthesized using using a very similar procedure to Ru/Al_2O_3, which explained in Section 3.3.2.1. Difference between these procedures was, Ru-precursor was diluted with 1.15 mL of deionized water instead of 1 mL. This is due to higher surface area of Al_2O_3-ZrO_2 than Al_2O_3 [61].

3.3.2.7. Preparation of RuCZ (Ru/CeO_2-ZrO_2). 1 gram of 1 wt.% Ru/CeO_2-ZrO_2 was synthesized using using a very similar procedure to Ru/Al_2O_3, which explained in Section 3.3.2.1. Only difference between these procedures was, Ru-precursor was diluted with 0.35 mL of deionized water instead of 1 mL. This is due to smaller surface area of CeO_2-ZrO_2 than Al_2O_3 [61].

3.3.2.8. Preparation of RuLZ (Ru/La_2O_3-ZrO_2). 1 gram of 1 wt.% Ru/La_2O_3-ZrO_2 was synthesized similar to Ru/Al_2O_3, which explained in Section 3.3.2.1. Difference between these procedures was, Ru-precursor was diluted with 0.75 mL of deionized water.

3.3.2.9. Preparation of RuSZ (Ru/SiO_2-ZrO_2). 1 gram of 1 wt.% Ru/SiO_2-ZrO_2 was synthesized using using a very similar procedure to Ru/Al_2O_3, which explained in Section 3.3.2.1. Only difference between these procedures was, Ru-precursor was diluted with 0.7 mL of deionized water instead of 1 mL.

3.3.2.10. Preparation of RuWZ (Ru/WO_3-ZrO_2). 1 gram of 1 wt.% Ru/WO_3-ZrO_2 was synthesized using using a very similar procedure to Ru/Al_2O_3, which explained in Section 3.3.2.1. Only difference between these procedures was, Ru-precursor was diluted with 0.7 mL of deionized water instead of 1 mL.

3.3.3. Reduction of Catalysts

For heterogeneous catalysis, it is vital to reduce the metal oxides on the active metal sites to allow the catalyst to work at its maximum performance. In this study, this reduction was done at 800 °C, where catalyst brought to this temperature under inert N_2 flow. Then, at 800 °C, catalyst reduced under 40 NmL min^{-1} H_2 flow exactly for 2 hours before the reaction experiments. After the reduction, catalyst was cooled to reaction temperature under N_2 flow [63].

3.4. Reaction Experiments

In the reaction experiments, hourglass shaped quartz tubes with overall 80 cm in length, 2 cm inner diameter on wide parts, and 1 cm inner diameter in narrow part were used as reactors (represented in Figure 3.5). Before the experiments, middle of the quartz reactor is packed with 1 cm of quartz wool and 20 mg of catalyst with 700 mg of α-Al_2O_3 diluent in regular activity experiments. Catalyst and diluent used in the experiments was specifically pestled to 45-60 mesh size in order to ignore diffusion limitations. Diluent allows to adjust bed length to particle diameter ratio, which enables plug flow conditions [63]. In time on stream or residence time experiments, 150 mg of catalyst is packed without diluent in order to obtain pure spent samples for characterization purposes.

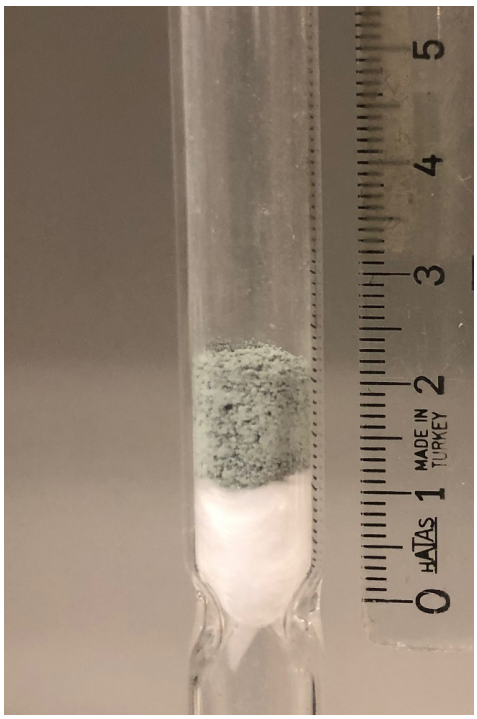

Figure 3.6. Packed middle part of the quartz reactor.

3.4.1. Activity Tests

In activity tests, effects of CO_2/G, temperature, and residence time on both CO_2 and glycerol conversions and product yields were investigated. For these experiments, total gas flow rate and volumetric flow rate of glycerol in gaseous phase was kept constant at 40 NmL min^{-1} and 4 NmL min^{-1}, respectively. Since glycerol flow rate is constant, CO_2 flow rate was adjusted for CO_2/G experiments, then N_2 flow rate was adjusted to complete 40 NmL min^{-1} total flow rate. For the effect of temperature, tests were done on a selected CO_2/G and only the temperature was changed in consecutive experiments. For the residence time, only the catalyst amount (thus the diluent amount) was changed on a specific temperature and CO_2/G. For catalyst screening experiments, reaction conditions of 750 °C, CO_2/G = 4, and residence time of 3.75 mg min NmL^{-1} was set. The CO_2/G of 4 was particularly selected due to the fact that it promotes formation of steam via RWGS, and thus generates an undesired scenario for the catalyst, as steam is an important sintering agent together with temperature. In

Table 3.5. Reaction parameters for catalytic tests.

Parameter	**Value**
Reaction Temperature (°C)	700, 750
Glycerol Flow Rate (NmL min^{-1})	4
CO_2 to Glycerol Ratio	1, 2, 3, 4
Catalyst Amount (mg)	20, 150
Total Flow Rate (NmL min^{-1})	40
Residence Time (mg min NmL^{-1})	0.5, 3.75

other words, the selected ratio represents a sort of worst-case conditions for the catalyst as mentioned in the previous studies [10, 11]. For the remainder of the tests, residence time was adjusted to 0.5 mg min NmL^{-1}. It is essential to change only the parameter is investigated while keeping other parameters constant. Investigated parameters are listed in Table 3.5. Detailed procedure on how did these tests were run is explained in Section 3.4.4.

3.4.2. Blank Tests

Blank tests were done to observe CO_2 and glycerol conversions without any catalyst presence. These experiments can also verify that quartz wool and α-Al_2O_3 diluent do not have any catalytic activity. Blank tests were done at different temperatures and CO_2 to glycerol ratios at constant total feed flow rate of 40 NmL min^{-1}.

3.4.3. Stability Tests

Stability experiments were done to observe the change of catalyst activity with time-on-stream. These tests were conducted for 72 hours at 750 °C, CO_2 to glycerol ratio of 3, and residence time of 3.75 mg min NmL^{-1}. These tests were run procedurally similar to activity experiments for the first 5 hours. However, after 5th hour, data was

taken with 2 hour intervals until the 69th hour, then it was taken with 1 hour intervals. If catalyst loses all its activity during the experiments, experiments were finalized.

3.4.4. Experimental Procedure

Experimental procedure followed is listed as:

- Quartz reactor is packed with quartz wool, catalyst, and diluent if necessary.
- Reactor is placed inside the furnace, and all connection parts are tightened.
- 40 NmL min^{-1} N_2 is fed to the reactor in order to start the leakage test. Leaks detected with soap bubble meter and soap bubbles applied to joint connections.
- Temperature controller of the furnace is set to 800 °C with $\sim$ 15 °C min^{-1} rate.
- 40 NmL min^{-1} flow rate of H_2 is fed to reactor and N_2 flow is closed to start the reduction for 2 hours. Heating lines are opened.
- GC-1 and GC-2 are set to operation parameters provided in Table 3.5. 30 minutes later, GC detectors are activated.
- When reduction is completed, H_2 flow is turned off and N_2 is fed to reactor with necessary flow rate for the reaction. Reactor is cooled down to reaction temperature.
- Dewar flasks are filled with ice. Pump was opened and glycerol is purged to fill the pipeline before reactor.
- When the experiment temperature is achieved, glycerol is directed to reactor. CO_2 is fed into the reactor with N_2. Reaction timer is started and effluent of the reactor is directed to GC side.
- First product analysis is made at the 30th minute of the experiment. Due to pipeline leading to GC-2 is longer, the analysis is first made with GC-2. Flow is directed to GC-1, and product gases are allowed to fill GC-1's sample loop for 2 minutes, then the analysis is made. After the GC-1 analysis, product stream is directed back to GC2.
- Rest of the data are taken every 45th minute until 5 hours, with the same procedure above.

- After the final product analysis, pump is closed. Furnace and heating lines are closed. Effluent of the reactor is directed to ventilation. Feed gases are directed to GCs, bypassing the reactor *via* a direct pipeline to GCs.
- After 15 minutes, feed gas analysis is done with GC-2. CO_2 flow is closed and N_2 is directed to reactor. Reactor is allowed to cool under N_2 flow. GCs are turned-off.

3.4.5. Measurement of Catalytic Activities

CO_2 conversion, glycerol conversion, product yields, selectivities and deactivation are the results of the experiments. These results are calculated using various formulas. Then calculated results leads to a conclusion about the parameter that investigated. Thus, accurate and precise calculation of results are vital in this study.

In glycerol dry reforming reaction, one of the main reactants is CO_2, and its conversion is calculated using Equation 3.1. Effluent flow rate of CO_2 is determined *via* GC-2 during the experiments, and inlet flow rate of CO_2 is determined in feed gas analysis, which is taken at the end of the every experiment.

$$x_{CO_2} = \frac{F_{CO_{2,in}} - F_{CO_{2,out}}}{F_{CO_{2,in}}} \tag{3.1}$$

As the name implies, other reactant in this reaction is glycerol. However, calculating glycerol conversion is not simple as CO_2 conversion. This is due to, steam and higher hydrocarbons that may be produced along the reaction (see Section 2.1). These products are in liquid phase in room temperature, thus they are liquefied in cold traps. Therefore, only the glycerol conversion to gaseous products can be calculated from GC results. For the rest of the study, term "glycerol conversion" is used for glycerol conversion to gaseous products. To calculate glycerol conversion, atomic balance around hydrogen was used since only hydrogen source in the reactants is glycerol. Thus, every product that contains hydrogen must be originated from glycerol [61]. These products

are; H_2, CH_4, C_2H_4, and C_2H_6. Equation 3.2 shows the glycerol conversion calculated from hydrogen balance. H_2 and CH_4 flows were determined from the GC-1, and C_2H_4 and C_2H_6 flows were determined from GC-2.

$$x_G = \frac{2F_{H_2} + 4F_{CH_4} + 4F_{C_2H_4} + 6F_{C_2H_6}}{8F_{G,in}} \times 100 \tag{3.2}$$

When there are multiple reactions occur in the process, yield and selectivity are important indicators of catalytic activity. Yield (Y_i) of a product is based on moles of glycerol fed and, calculated using Equation 3.3. Selectivity (S_i) of a product is based on moles of glycerol converted, and calculated using Equation 3.4.

$$Y_i = \frac{F_{i,out}}{F_{G,in}} \tag{3.3}$$

$$S_i = \frac{F_{i,out}}{x_G F_{G,in}} \tag{3.4}$$

4. RESULTS AND DISCUSSION

4.1. Catalysts with Single Oxide Supports

4.1.1. Catalyst Screening

In this section, activities of RuAl, RuCa, RuCe, RuLa, and RuZr at 750 °C and $CO_2/G = 4$ will be investigated. Then, catalysts which potentially exhibit activity towards GDR will be selected. Effect of temperature, CO_2/G, and residence time will be investigated on these selected catalysts. Lastly, stability experiments will be done with most promising catalyst. The experimental findings will be compared with their pertinent theoretical limits calculated by means of thermodynamic analysis.

4.1.1.1. Thermodynamic Analysis. For determination of the thermodynamic limits of the reaction at experiment parameters, CHEMCAD 7.1.4 software was used. A Gibbs free energy reactor was simulated at 750 °C and $CO_2/G = 4$. Components in the simulation was selected by the possible reaction routes and reactions which explained in Section 2.1. These components are: C(s), CO, CO_2, CH_4, C_2H_4, C_2H_6, C_2H_4O (acetaldehyde), C_2H_6O (ethanol), C_3H_6O (acetol, allyl alcohol, and propionaldehyde), C_3H_4O (acrolein), $C_3H_8O_3$ (glycerol), H_2, H_2O, and N_2.

Results of this simulation are tabulated in Table 4.1, and Table 4.2 in the form of product yield and selectivity, CO_2 conversion, and glycerol conversion. No glycerol, acetol, allyl alcohol, propionaldehyde, acrolein, acetaldehyde, ethanol, and solid carbon was predicted in the product stream. Glycerol conversion to both liquid and gaseous products was found 100%, as no glycerol yield was obtained at reactor effluent stream. This finding is also in alignment with the literature. However, H_2O was produced, thus glycerol conversion to gaseous products are lower than 100%.

Table 4.1. Thermodynamic product yields at 750 °C.

T (°C)	$\mathbf{Y_{H_2}}$	$\mathbf{Y_{CO}}$	$\mathbf{Y_{CO_2}}$	$\mathbf{Y_{CH_4}}$	$\mathbf{Y_{H_2O}}$	$\mathbf{H_2/CO}$	$\mathbf{x_{CO_2}}$ (%)	$\mathbf{x_G}$ (%)
750	2.67	4.30	2.70	0.01	1.32	0.62	32.7	67.1

Table 4.2. Thermodynamic product selectivity values at 750 °C.

T (°C)	$\mathbf{S_{H_2}}$	$\mathbf{S_{CO}}$	$\mathbf{S_{CO_2}}$	$\mathbf{S_{CH_4}}$	$\mathbf{S_{H_2O}}$
750	3.98	6.42	4.03	0.01	1.96

4.1.1.2. Activity Tests. In Figure 4.1, CO_2 conversions of RuAl, RuCa, RuCe, RuLa, RuZr, and blank test in GDR at 750 °C, CO_2/G = 4, and residence time of 3.75 mg min NmL^{-1} are provided. When the effect of single oxide supported catalysts on CO_2 are compared, Al_2O_3 and CaO gives the least amount of conversion with 13.4% and 13.1%, respectively. Although these supports exhibits lower CO_2 conversion than others, it is clear that presence of any Ru-based catalyst accelerates this reaction when compared with the blank test. In the middle of the spectrum, RuCe and RuLa shows 17.9% and 18.1% CO_2 conversions, respectively. Both of these catalysts were used for DRM in the literature and found active in this reaction [42, 43]. However, in GDR they have shown mediocre conversions. Finally, RuZr shows the highest activity by far with 28.4%, where it exceeds the second most active catalyst by 10% conversion difference. Also, RuZr delivers $\sim$ 87% of equilibrium conversion, which is equal to 32.7% under the current reaction conditions. This significant activity difference can be possibly be attributed to the strong metal-support interaction between Ru and ZrO_2 which reported by Whang *et al.* [48]. Activity-wise, it is clear that this interaction is key to activate Ru in GDR.

In Figure 4.2, Glycerol conversions of RuAl, RuCa, RuCe, RuLa, and RuZr in GDR at 750 °C, CO_2/G = 4, and residence time of 3.75 mg min NmL^{-1} are provided. Due to nature of how the glycerol to gaseous products conversion are calculated, sev-

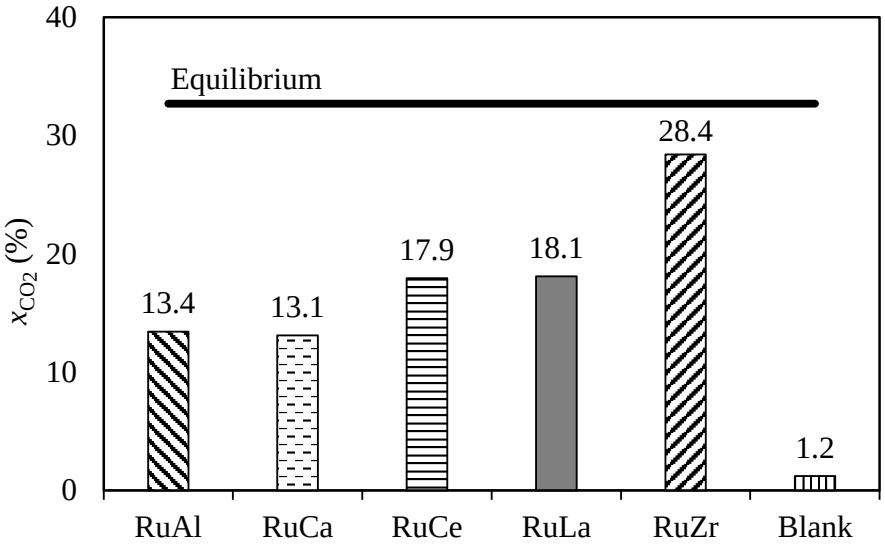

Figure 4.1. Carbon dioxide conversions over Ru supported on single oxide supports (T=750 °C, CO_2/G = 4, and τ = 3.75 mg min NmL^{-1}).

eral catalysts have passed the equilibrium conversion. For the sake of the comparison, these excesses were counted as at thermodynamic limit. Every catalyst have been tested increases glycerol conversion at least by 20% when compared with blank test. RuAl, RuCa, and RuLa have hit the thermodynamic limit, where RuZr achieved approximately 98% of the equilibrium conversion.

Several catalysts have shown good CO_2 and glycerol conversions. However, due to reaction mechanism, glycerol can be converted to various undesirable products (see Section 2.1). Therefore, a yield and selectivity comparison may provide a better understanding of which catalyst produces more desirable products (*i.e.* H_2 and CO) to conclude catalyst screening. In Table 4.3, gaseous product yields of RuAl, RuCa, RuCe, RuLa, RuZr, and blank test are provided. Amongst these catalysts, RuAl, RuCa, and RuLa give glycerol conversions at thermodynamic limit. However, it is seen that, these catalysts produced high amounts of CH_4 which boost their glycerol conversions since x_G increases significantly with 4 hydrogen atoms of CH_4. When compared with RuZr, these catalysts yield 30.6%, 36.7%, and 19% less H_2 than RuZr, respectively. Also, when these catalysts compared with RuCe, their glycerol conversion is approximately

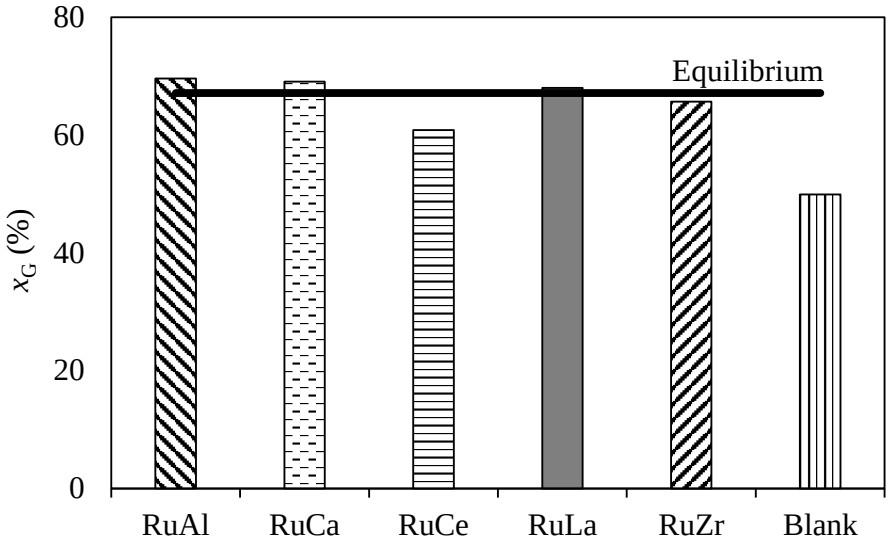

Figure 4.2. Glycerol conversions over Ru supported on single oxide supports in screening test (T=750 °C, CO_2/G = 4, and τ = 3.75 mg min NmL^{-1}).

9% higher. However, RuCe yielded more H_2 and CO, and less CH_4 than RuAl, RuCa, and RuLa. Since the goal of GDR is producing syngas, RuZr is the best catalyst amongst compared with 2.42 moles of H_2, and 3.98 moles of CO produced by one mol of glycerol fed. In all the catalysts tested, H_2/CO ratio is below 1, which is found suitable for Fischer-Tropsch synthesis in the literature [12].

Table 4.3. Product yields over single oxide supported catalysts in screening experiments (T = 750 °C, CO_2/G = 4, and τ = 3.75 mg min NmL^{-1}).

Catalyst	$\mathbf{Y_{H_2}}$	$\mathbf{Y_{CO}}$	$\mathbf{Y_{CH_4}}$	$\mathbf{Y_{C_2H_4}}$	$\mathbf{Y_{C_2H_6}}$	$\mathbf{H_2/CO}$	$\boldsymbol{x_{CO_2}}$	$\boldsymbol{x_G}$
RuAl	1.68	2.98	0.54	0	0.01	0.56	13.4	69.6
RuCa	1.53	2.82	0.56	0.01	0.03	0.54	13.1	69.1
RuCe	1.96	3.12	0.22	0	0.01	0.63	17.9	60.8
RuLa	1.75	3.30	0.45	0	0.02	0.53	18.1	68.0
RuZr	2.42	3.98	0.10	0	0	0.61	28.4	65.7
Blank	0.55	1.30	0.46	0.20	0.04	0.43	1.2	49.9

In Table 4.4 product selectivities of single oxide supported catalysts are provided. Similar trend continues with the product yields due to minimal glycerol conversion difference between catalysts. While RuZr is the most selective catalyst to both H_2 and CO, RuCa exhibits the worst selectivity to H_2 and CO amongst the catalysts tested. With comparison to blank test, presence of a catalyst in the reaction reduces product selectivities towards higher hydrocarbons. Therefore, presence of a good catalyst increases both CO_2 and glycerol conversions in the favor of H_2 and CO selectivity. Additionally, RuZr creates an edge over the rest of the catalysts tested by converting CH_4, C_2H_4, and C_2H_6 to increase H_2 and CO selectivity.

Table 4.4. Product selectivities over single oxide supported catalysts in screening test (T = 750 °C, CO_2/G = 4, and τ = 3.75 mg min NmL^{-1}).

Catalyst	$\mathbf{S_{H_2}}$	$\mathbf{S_{CO}}$	$\mathbf{S_{CH_4}}$	$\mathbf{S_{C_2H_4}}$	$\mathbf{S_{C_2H_6}}$
RuAl	2.41	4.29	0.77	0	0.02
RuCa	2.21	4.08	0.81	0.02	0.04
RuCe	3.22	5.13	0.36	0	0.01
RuLa	2.57	4.86	0.67	0	0.03
RuZr	3.68	6.06	0.16	0	0
Blank	1.11	2.61	0.93	0.41	0.07

In Figures 4.3 and 4.4 H_2 and CO yield comparisons amongst single oxide supported catalysts can be seen, respectively. RuZr yields in the most H_2 and CO, thus reaching approximately 90% and 92.5% of the thermodynamic yields of these products. RuCa have yielded the lowest of H_2 and CO yields amongst catalytsts tested with the values of 1.53 and 2.82, respectively. However, these values are still higher than blank tests. So presence of a catalyst is essential for this reaction.

From the screening tests at 750 °C, CO_2 to glycerol ratio of 4, and residence time of 3.75 mg min NmL^{-1}, only RuZr shows promise as an active and selective GDR catalyst for syngas production. Thus, in the following sections effect of reaction parameters on RuZr will be tested thoroughly.

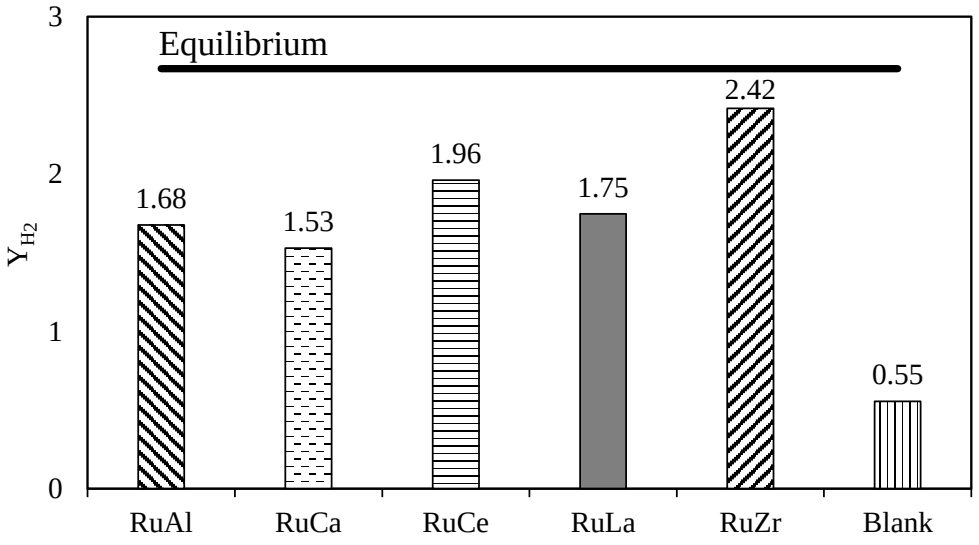

Figure 4.3. H_2 yields over single oxide supported catalysts in screening experiments (T=750 °C, CO_2/G = 4, and τ = 3.75 mg min NmL^{-1}).

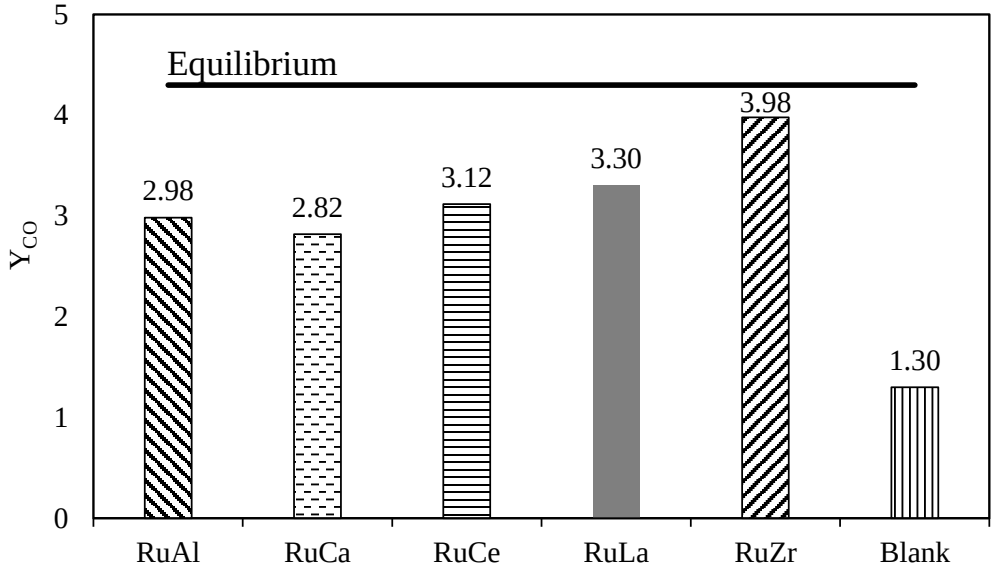

Figure 4.4. CO yields over single oxide supported catalysts in screening experiments (T=750 °C, CO_2/G = 4, and τ = 3.75 mg min NmL^{-1}).

4.1.2. Effect of CO_2/G

Molar amount of CO_2 in feed stream is known to have an effect on the product yield from the literature [7, 10, 11]. In this section, CO_2/G is adjusted between 1 to 4, by changing CO_2 volumetric flow rate. Glycerol feed and total flow rate are kept constant as 4 and 40 NmL min^{-1}, respectively, by means of adjusting via the flow rate of N_2, the balance gas. Similar to previous section (see Section 4.1.1.1), a thermodynamic analysis is made for CO_2/G.

4.1.2.1. Thermodynamic Analysis. Thermodynamic analysis is made to determine equilibrium conversions and product yields for CO_2/G = 1 to 4, *via* CHEMCAD software. Details of the methodology for the simulation are explained in Section 4.1.1.1. Temperature of the reactor is kept constant to 750 °C. In the Tables 4.5 and 4.6, product yields and selectivities at equilibrium are provided.

Table 4.5. Thermodynamic product yields at CO_2/G (T=750 °C).

CO_2/G	Y_{H_2}	Y_{CO}	Y_{CO_2}	Y_{CH_4}	Y_{H_2O}	H_2/CO	x_{CO_2} (%)	x_G (%)
1	3.49	3.40	0.57	0.03	0.46	1.02	43.0	88.6
2	3.17	3.78	1.22	0.01	0.80	0.84	39.3	80.0
3	2.90	4.07	1.93	0.01	1.08	0.71	35.7	73.0
4	2.67	4.30	2.70	0.01	1.32	0.62	32.7	67.1

Increasing the CO_2 ratio in the feed reduces both CO_2 and glycerol conversions. With increasing CO_2 to glycerol ratio, yield of H_2 decreases while CO yield increases. Although H_2 yield decreases, increased ratio promotes syngas selectivity. When CO_2 amount increases in the process, RWGS starts to dominate and therefore decreases H_2/CO ratio. This relation was also reported by Wang *et al.* [24]. Thus, the thermodynamic analysis done in this study is in alignment with the literature. In the literature, relation between CH_4 formation leading to coking was explained [17]. Increasing CO_2/G reduces CH_4 formation, thus preventing solid carbon formation.

Table 4.6. Thermodynamic product selectivities at CO_2/G (T=750 °C).

CO_2/G	S_{H_2}	S_{CO}	S_{CO_2}	S_{CH_4}	S_{H_2O}
1	3.94	3.84	0.64	0.03	0.52
2	3.97	4.72	1.52	0.02	1.00
3	3.98	5.57	2.65	0.01	1.48
4	3.98	6.42	4.03	0.01	1.96

4.1.2.2. Activity Tests. In the activity tests, effect of CO_2/G is investigated over RuLa and RuZr are presented in Figure 4.5. Highest CO_2 conversions are delivered at CO_2/G = 3 on both RuZr and RuLa by 31.8% and 20%, respectively. Although thermodynamics states increased CO_2 conversion with decreasing CO_2/G, both of the catalysts exhibits their maximum CO_2 conversion at the ratio of 3. In the past, there are several studies that states ratio 1 is the optimum condition for GDR [5,31,35,36]. However, in recent studies, increasing ratio exhibited better CO_2 conversions [10, 11, 38]. Clearly, same conclusion can be reached in this work.

The trend observed in Figure 4.5 can be explained with the increased extent of DRM reaction. CH_4 yield in the product stream decreases with increasing CO_2/G which reported in Table 4.7. When CO_2/G = 1, extent of DRM decreases due to lower amounts of CO_2 present in the reactor. Therefore, CO_2 conversion decreases and CH_4 yield increases. Moreover, increasing CO_2 in the feed causes increase in RWGS leading to more H_2O formation, thus allowing steam reforming reactions to occur simultaneously with dry reforming reactions. This combined reforming may also factor in for the CH_4 consumption in the reactor.

In Figure 4.6, glycerol conversions of RuLa and RuZr at different CO_2 to glycerol ratios are presented. For both of the catalysts, glycerol conversion decreases with increasing CO_2/G, which is in alignment with thermodynamics. In all of the CO_2 to glycerol ratios tested, both of the catalysts exhibits very high conversions. RuZr hits

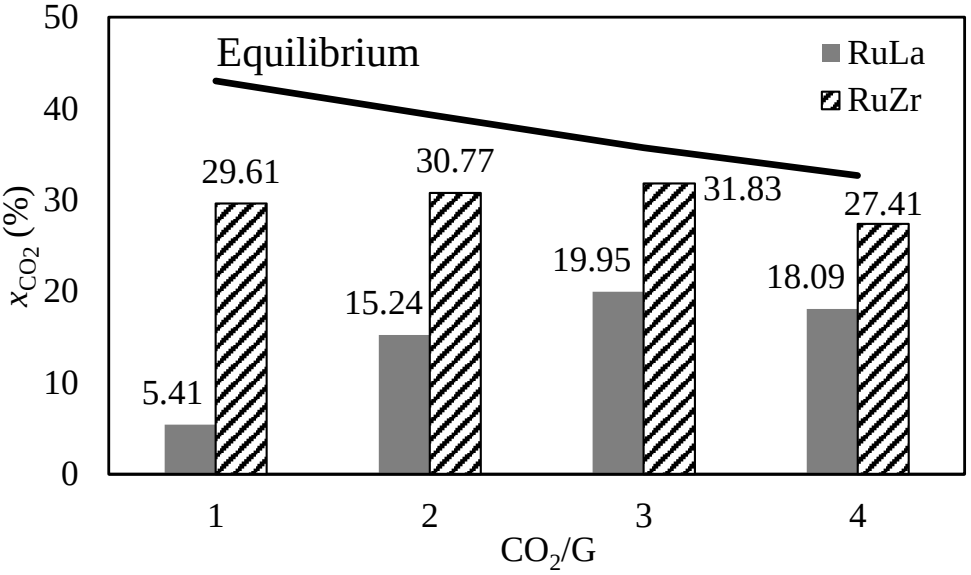

Figure 4.5. CO_2 conversions of RuLa and RuZr at CO_2 to glycerol ratios (T=750 °C).

the thermodynamic limit at CO_2 to glycerol ratios of 1,2 and 3, where in ratio 4 it yielded over 93% of the equilibrium conversion. RuLa hits the thermodynamic limit at ratio 4, where it exhibits 97% of the equilibrium conversion for the rest of the ratios tested.

In Table 4.7 product yields of RuLa and RuZr at different CO_2/G are presented. From the thermodynamic analysis in Section 4.1.2.1, an decreasing trend for H_2 yield with increasing CO_2/G is expected. Experimental results are proving this analysis, with H_2 yield of RuLa decreasing from 2.40 to 1.75, and from 3.24 to 2.35 for RuZr. However, this relation is proportional for CO yields, where CO yield of RuLa increases with ratio from 2.68 to 3.30, and 3.28 to 3.86 for RuZr. Therefore, as the ratio increases, H_2/CO ratio decreases. For RuZr H_2/CO ratio decreases from 0.99 to 0.61 with increasing CO_2 to glycerol ratio, whereas for RuLa H_2/CO ratio decreases from 0.90 to 0.53. Therefore, quality of syngas can be adjusted with changing the CO_2 to glycerol ratio.

In Table 4.8 product selectivities of RuLa and RuZr are presented. Although both of the catalysts exhibits very good glycerol conversions, it is essential to convert

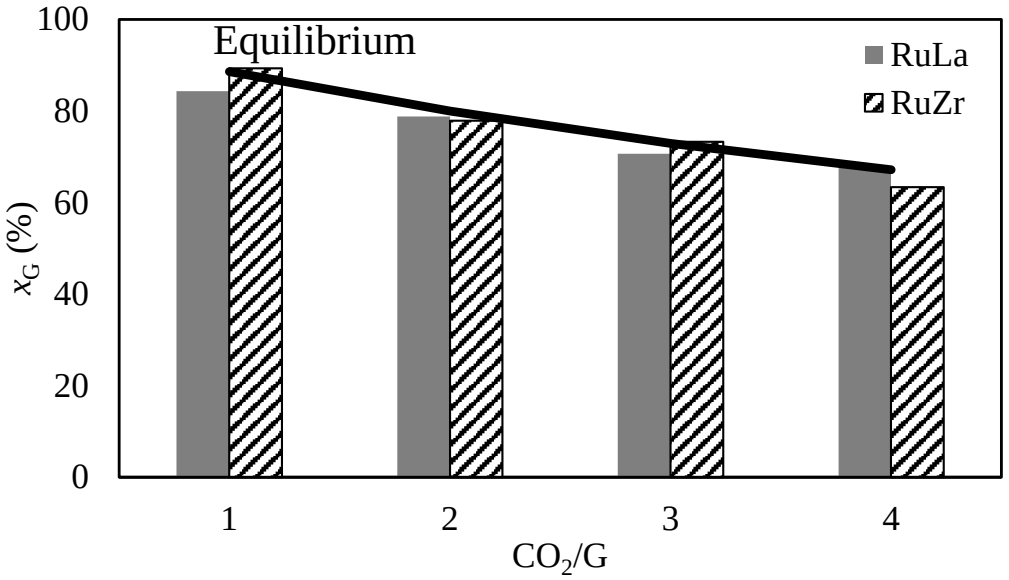

Figure 4.6. Glycerol conversions of RuLa and RuZr over CO_2/G (T=750 °C).

the reactants to desired products, which are H_2 and CO. Therefore, selectivity towards these products are very important when determining the better catalyst. In every ratio tested, RuZr exhibits its superiority over RuLa for H_2 and CO selectivity. Also, RuZr exhibits lower selectivity towards undesirable products in every ratio tested.

In summary, RuZr exhibits better activity and selectivity than RuLa in every CO_2/G, and CO_2/G = 3 is found to be the most promising one. RuZr hits the thermodynamic limit for glycerol conversion and 89.2% of CO_2 equilibrium conversion (second closest is ratio 4 with 84% CO_2 conversion). Also at CO_2/G = 3, RuZr yields 95% and 97% of the H_2 and CO thermodynamic yields, respectively. Furthermore, RuZr exhibits highest H_2 and lowest CH_4 selectivities in ratio 3. Since RuZr works very well in this conditions, CO_2 to glycerol ratio of 3 selected as default conditions for this catalyst and for the rest of the present study.

Table 4.7. Product yields over RuLa and RuZr over CO_2/G (T = 750 °C).

	$\mathbf{CO_2/G}$	$\mathbf{Y_{H_2}}$	$\mathbf{Y_{CO}}$	$\mathbf{Y_{CH_4}}$	$\mathbf{Y_{C_2H_4}}$	$\mathbf{Y_{C_2H_6}}$	$\mathbf{H_2/CO}$	$\boldsymbol{x}_{\mathbf{CO_2}}$	$\boldsymbol{x}_{\mathbf{G}}$
RuLa	1	2.40	2.68	0.46	0	0.02	0.90	5.41	84.34
	2	1.95	2.81	0.56	0	0.03	0.69	15.24	78.83
	3	1.68	2.97	0.53	0	0.02	0.56	19.95	70.62
	4	1.75	3.30	0.45	0	0.02	0.53	18.09	67.99
RuZr	1	3.24	3.28	0.16	0	0	0.99	29.61	89.29
	2	2.89	3.61	0.11	0	0	0.80	30.77	77.86
	3	2.76	3.97	0.08	0	0	0.70	31.83	73.27
	4	2.35	3.86	0.09	0	0	0.61	27.41	63.32

Table 4.8. Product selectivities over RuLa and RuZr over CO_2/G (T = 750 °C).

	$\mathbf{CO_2/G}$	$\mathbf{S_{H_2}}$	$\mathbf{S_{CO}}$	$\mathbf{S_{CH_4}}$	$\mathbf{S_{C_2H_4}}$	$\mathbf{S_{C_2H_6}}$
RuLa	1	2.85	3.17	0.54	0	0.02
	2	2.47	3.56	0.71	0	0.04
	3	2.37	4.21	0.76	0	0.04
	4	2.57	4.86	0.67	0	0.03
RuZr	1	3.63	3.68	0.18	0	0
	2	3.71	4.64	0.15	0	0
	3	3.77	5.41	0.11	0	0
	4	3.72	6.10	0.14	0	0

4.1.3. Effect of Reaction Temperature

Reaction temperature is an important parameter in which it determines the reaction rates in GDR by kinetics, and limits by thermodynamics. Since GDR is an highly endothermic reaction, temperature carries a crucial role on kinetics. For RuZr and RuLa, effect of temperature is investigated at 700 and 750 °C. Chronologically, effect of temperature for RuLZ (see Section 4.2.2) is investigated before the effect of CO_2/G. Thus, temperature analysis for RuLZ is done at CO_2/G = 4. Therefore, thermodynamic analysis for the reaction temperature is done for 650, 700 and 750 °C for both of CO_2/G = 3 and 4, in order to determine CO_2 and glycerol conversions, product yields and product selectivities at equilibrium.

4.1.3.1. Thermodynamic Analysis. Thermodynamic analysis is made to determine equilibrium conversions and product yields for reaction temperatures of 650 to 750 °C, *via* CHEMCAD software. Details of the methodology for the simulation are explained in Section 4.1.1.1. CO_2/G ratios are kept constant to 3 and 4 while the reaction temperatures tested individually for these ratios. In the Tables 4.9 and 4.10, product yields and selectivities at equilibrium are provided.

From the thermodynamic analysis, H_2 and CO yields increase with increasing temperature. However, CO yield increases more than H_2. This is due to increasing rate of RWGS with increased temperature, since RWGS is an endothermic reaction. More CO is produced while H_2 is consumed by RWGS. From this effect, H_2/CO ratio decreases from 0.75 to 0.71 when the temperature increased. When the reaction temperature increases, CO_2 conversion increases. Increase in temperature enhances the rate of DRM to remove CH_4, and hinders the rate of Boudouard reaction for solid carbon removal, making higher temperatures a necessity to increase the activity and maintain the stability over the course of reaction. However, glycerol conversion sets its peak at 700 °C. When this thermodynamic analysis is compared with experimental analyses done by other researchers, it is safe to say that this analysis is in alignment with the literature [17, 24].

Table 4.9. Thermodynamic product yields at different reaction temperatures tested (CO_2/G = 3 and 4).

	T (°C)	$\mathbf{Y_{H_2}}$	$\mathbf{Y_{CO}}$	$\mathbf{Y_{CO_2}}$	$\mathbf{Y_{CH_4}}$	$\mathbf{Y_{H_2O}}$	$\mathbf{H_2/CO}$	$\boldsymbol{x_{CO_2}}$	$\boldsymbol{x_G}$
$\mathbf{CO_2/G = 3}$	650	2.77	3.29	2.37	0.12	0.99	0.84	21.21	75.31
	700	2.95	3.91	2.06	0.03	0.98	0.75	31.54	75.40
	750	2.90	4.07	1.93	0.01	1.08	0.71	35.71	72.94
$\mathbf{CO_2/G = 4}$	650	2.71	3.85	3.05	0.11	1.07	0.70	23.9	73.2
	700	2.75	4.15	2.84	0.02	1.20	0.66	29.2	70.1
	750	2.67	4.30	2.70	0.01	1.32	0.62	32.7	67.1

Table 4.10. Thermodynamic product selectivities at different reaction temperatures (CO_2/G = 3 and 4).

	T (°C)	$\mathbf{S_{H_2}}$	$\mathbf{S_{CO}}$	$\mathbf{S_{CO_2}}$	$\mathbf{S_{CH_4}}$	$\mathbf{S_{H_2O}}$
$\mathbf{CO_2/G = 3}$	650	3.68	4.37	3.15	0.16	1.31
	700	3.91	5.19	2.73	0.05	1.30
	750	3.98	5.58	2.65	0.01	1.48
$\mathbf{CO_2/G = 4}$	650	3.70	5.26	4.17	0.15	1.46
	700	3.93	5.92	4.05	0.04	1.71
	750	3.98	6.42	4.03	0.01	1.96

4.1.3.2. Activity Tests. In Figure 4.7 CO_2 conversions of RuLa and RuZr at 700 and 750 °C are presented. For RuZr, increase in CO_2 conversion with temperature can be clearly seen. One possibility of this result is the carbon deposition on RuZr at lower temperature which hinders CO_2 conversion significantly. On the other hand, RuLa exhibits very interesting results, in which the activity drop between 700 and 750 °C is only 0.65%. In the literature, Carrara *et al.* [42] found that Ru-La complex is excellent for paraffin decomposition, thus showing excellent stability over the course of DRM reaction. Therefore, this might be a reason of why RuLa does not lose its activity at reduced temperature.

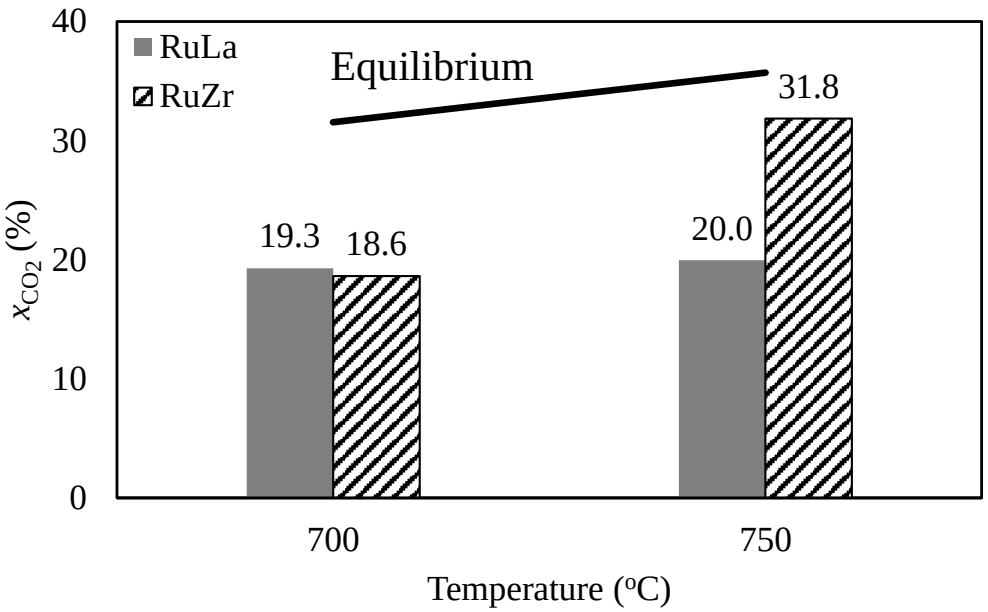

Figure 4.7. CO_2 conversions of RuLa and RuZr at 700 and 750 °C (CO_2/G = 3).

In Figure 4.8 glycerol conversions of RuLa and RuZr at 700 and 750 °C are given. Similar to Section 4.1.2.2, both of the catalysts hits or comes very close to the thermodynamic limit. RuZr hits the thermodynamic limit in both 700 and 750 °C with 76.3% and 73.3 %, respectively. Whereas RuLa exhibits 73.6 % and 70.6% glycerol conversions at 700 and 750 °C, respectively. These conversions are 97.6% and 96.8% of the thermodynamic limits in increasing temperature order, respectively. Although CO_2 conversions of both catalysts increases with increasing temperatures,

glycerol conversion of catalysts tested decreases. These results are parallel with the thermodynamic analysis made in Section 4.1.3.1.

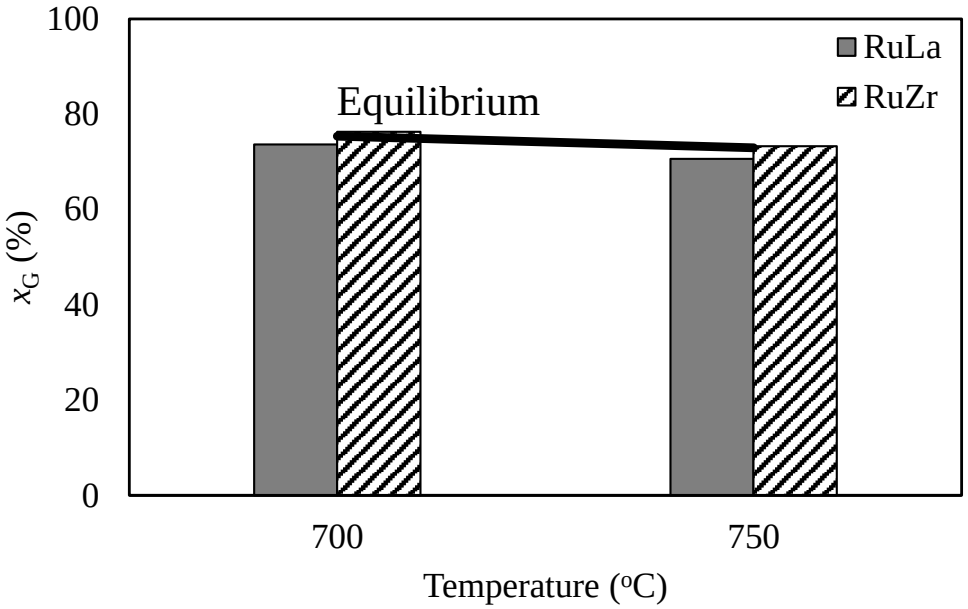

Figure 4.8. Glycerol conversions of RuLa and RuZr at 700 and 750 °C (CO_2/G = 3).

In Table 4.11, product yields, H_2/CO ratios, and conversions of RuLa and RuZr for 700 and 750 °C are given. Yields of H_2 and CO increases for both of the catalyst tested with increasing temperature. For RuLa, when the increase in H_2 yield is more significant with 1.68 to 1.90, CO yield increases with bare minimum of 2.97 to 2.98. This might be explained with, comparative rate increase of reforming reactions being higher than the rate increase of RWGS. Therefore, H_2/CO ratio of RuLa increases from 0.56 to 0.64. This conclusion can also be backed up with the decrease of CH_4 yield. With increasing temperature, CH_4 yield of RuLa decreases from 0.53 to 0.47, which may be the indication of increased DRM rate, which results in increased H_2 yield. For RuZr, with increasing temperature both of the H_2 and CO yields increased from 2.22 to 3.16, and 2.76 to 3.97, respectively. While H_2 and CO yield increases, CH_4 yield decreases from 0.38 to 0.08. The reason behind this inversely proportional relation, might cause from increasing activity of DRM, similar to RuLa. However, H_2/CO ratio of RuZr remains the same for the 700 and 750 °C, with the value of 0.7. This might

Table 4.11. Product yields of RuLa and RuZr at 700 and 750 °C (CO_2/G = 4).

	T (°C)	$\mathbf{Y_{H_2}}$	$\mathbf{Y_{CO}}$	$\mathbf{Y_{CH_4}}$	$\mathbf{Y_{C_2H_4}}$	$\mathbf{Y_{C_2H_6}}$	$\mathbf{H_2/CO}$	$\boldsymbol{x_{CO_2}}$	$\boldsymbol{x_G}$
RuLa	700	1.68	2.97	0.53	0	0.02	0.56	19.29	73.63
	750	1.90	2.98	0.47	0	0.03	0.64	19.95	70.62
RuZr	700	2.22	3.16	0.38	0	0.02	0.70	18.62	76.29
	750	2.76	3.97	0.08	0	0	0.70	31.83	73.27

cause from the rate increase of RWGS being comparatively small when compared to the rate of DRM at the temperatures tested.

In Table 4.12 product selectivities of RuLa and RuZr at 700 and 750 °C are presented. For both of the catalysts, selectivities of the desired products H_2 and CO increases with temperature. Meanwhile, for RuZr, selectivities of undesired CH_4 and C_2H_6 decreases with increasing temperature. However, for RuLa, when CH_4 selectivity decreases with temperature increase, C_2H_6 selectivity increases slightly. When the catalysts compared, RuZr is more selective to desired products at both 700 and 750 °C. At 700 °C, RuZr exhibits only the 74.5 and 79.7% of the thermodynamic selectivities of H_2 and CO, respectively. However, at 750 °C, selectivities of H_2 and CO increases to 94.8 and 97% of the thermodynamic selectivity, respectively.

The effect of the reaction temperature is investigated in this section. Increasing reaction temperature creates a very slight effect on activity and product selectivity of RuLa. However for RuZr, working at reaction temperature of 750 °C improves both catalytic activity and product selectivity. Therefore, working at 750 °C with RuZr is desirable, since this catalyst has proven its dominance over RuLa in both activity and selectivity for syngas synthesis by GDR.

Table 4.12. Product selectivities of RuLa and RuZr at 700 and 750 °C (CO_2/G = 4).

	T (°C)	$\mathbf{S_{H_2}}$	$\mathbf{S_{CO}}$	$\mathbf{S_{CH_4}}$	$\mathbf{S_{C_2H_4}}$	$\mathbf{S_{C_2H_6}}$
RuLa	700	2.28	4.04	0.73	0	0.03
	750	2.69	4.22	0.67	0	0.05
RuZr	700	2.91	4.14	0.50	0	0.03
	750	3.77	5.41	0.11	0	0

4.1.4. Effect of Residence Time

Residence time is an important parameter which determines the extent of occurring reactions in a reactor. In this section, effect of residence time is investigated over RuLa and RuZr by adjusting the amount of catalyst packed inside the reactor. Therefore, 20 and 150 mg of RuLa and RuZr which corresponds to 0.5 and 3.75 mg_{cat} min NmL^{-1} are packed and tested in experiment at 750 °C and CO_2/G = 3.

Effect of residence time on CO_2 conversions of RuLa and RuZr can bee seen in Figure 4.9. CO_2 conversions of both RuLa and RuZr increases as expected. However, since RuZr is already very close to equilibrium conversion, CO_2 conversion of RuZr is increased by only 0.7% with additional 130 mg of catalyst addition. However for RuLa, increasing catalyst weight increases CO_2 conversion by 12%. This difference between RuZr and RuLa might be caused from the dispersion of Ru-nanoparticles. From the literature, it is known that Ru dispersion on ZrO_2 is increased due to the strong metal-support interaction between them [48]. However, observing such large difference between 20 mg and 150 mg experiments for RuLa might be caused from the reduced dispersion of Ru-nanoparticles on La_2O_3, which may be an indication of weaker metal-support interaction between Ru and La_2O_3.

In Figure 4.10, effect of residence time on glycerol conversions of RuLa and RuZr are presented. With increasing catalyst weight, glycerol conversion of RuLa increases where glycerol conversion of RuZr decreases. This might be caused from the higher CH_4

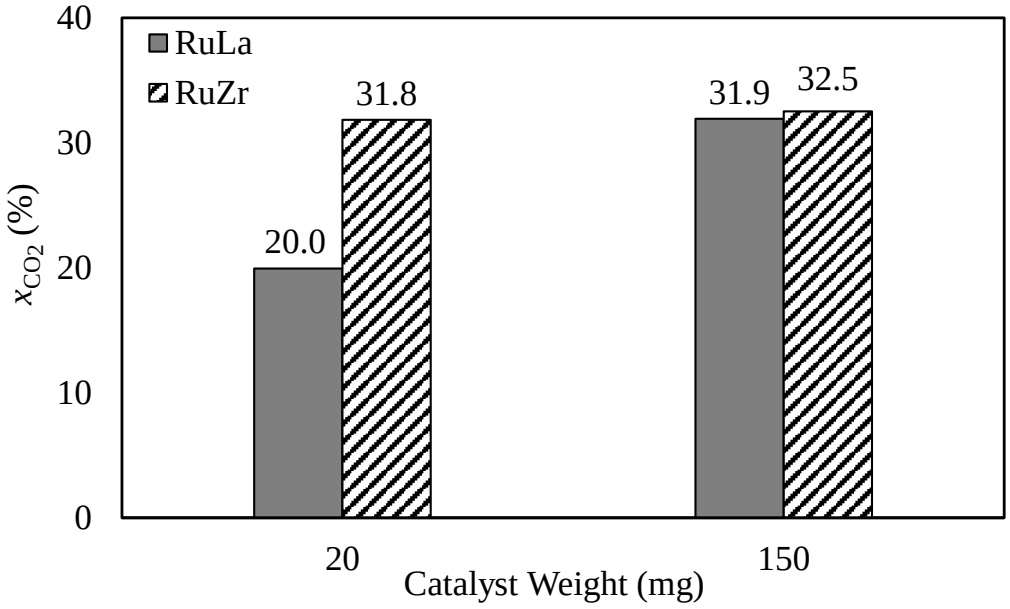

Figure 4.9. Effect of residence time on CO_2 conversions (T = 750 °C, CO_2/G = 3).

selectivity of RuLa, thus increasing glycerol conversion to gaseous products with the increasing activity. However, glycerol conversion of RuZr decreases from thermodynamic limit to 70.8%. This might be explained with the stability of RuZr, increased amounts of catalyst might deactivate slower due to increased extent of reverse Boudouard reaction. Therefore products that increase glycerol conversion such as CH_4 will form less, therefore reducing overall glycerol conversion at the end of the experiment.

From the residence time analysis, increasing the residence time of RuLa improves its activity significantly, however requires almost 7.5 times more catalyst to provide these results. Therefore using this catalyst might not be economically feasible. For RuZr, increasing the residence time improves the activity very less which is an indicator of its active nature induced by the possible presence of well-dispersed Ru-nanoparticles.

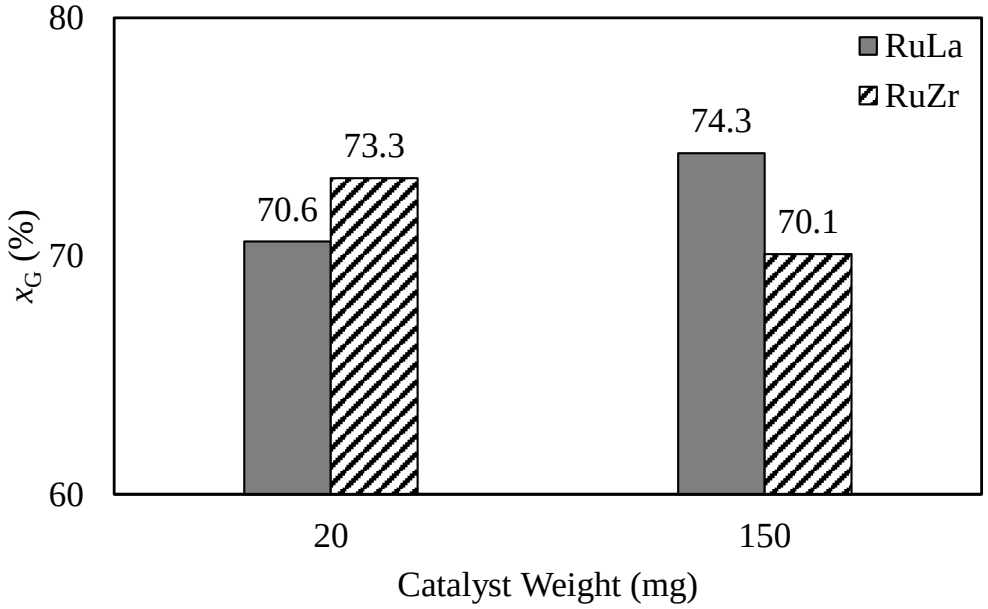

Figure 4.10. Effect of τ on glycerol conversions (T = 750 °C, CO_2/G = 3).

4.2. Catalysts with Binary Oxide Supports

4.2.1. Catalyst Screening

Although RuZr has shown good activity and product selectivity in Section 4.1. There are still room for improvement in activity and stability of the catalyst. Therefore, five ZrO_2 based binary oxide supported catalysts are synthesized and tested in catalyst screening similar to Section 4.1.1. These catalysts are, RuAZ, RuCZ, RuLZ, RuSZ and RuWZ. Thermodynamic analysis of catalyst screening experiment conditions is done in Section 4.1.1.1.

4.2.1.1. Activity Tests. In Figure 4.11, CO_2 conversions of binary oxide supported catalysts are provided. The results show that CO_2 conversion is very responsive to the second oxide in the support. From the Section 4.1.1, RuZr has exhibited 28.4% CO_2 conversion. However, apart from RuLZ, every other binary oxide catalyst have yielded worse CO_2 conversions than RuZr. Although in literature Ru supported on

ceria-zirconia had shown good activity for DRM and GSR, RuCZ (50 wt.% CeO_2) has exhibited worse CO_2 conversion than both of RuCe and RuZr in GDR [44,52]. Addition of zirconia to alumina in RuAZ (10 wt.% ZrO_2, 90 wt.% Al_2O_3), had improved CO_2 conversion by only 0.7 %. Whang *et al.* [48] have found RuSZ to be very active for DRM. However RuSZ has shown CO_2 conversion of only 7.6%. Addition of tungsten oxide completely inhibits the activity of zirconia, thus losing activity during the reaction completely. Finally, there is one candidate that performs at thermodynamic limit of CO_2 conversion, which is RuLZ. Addition of 9 wt.% La_2O_3 to ZrO_2 have increased the CO_2 conversion by approximately 4.5%. In literature the enhanced activity of LZ is explained with enhanced basicity, high active metal dispersion, and increased oxygen vacancies [59, 60].

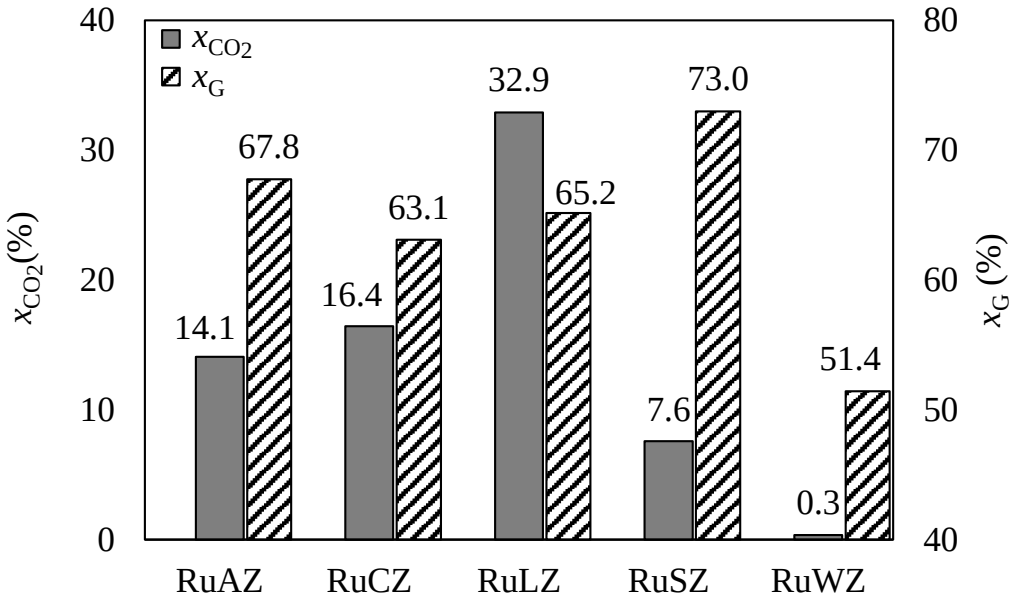

Figure 4.11. CO_2 and glycerol conversions over Ru supported on binary-oxide supports (T=750 °C, CO_2/G = 4, and τ = 3.75 mg min NmL^{-1}).

Also in Figure 4.11, glycerol conversions of RuAZ, RuCZ, RuLZ, RuSZ, and RuWZ at 750°C, CO_2/G = 4, and residence time of 3.75 mg min NmL^{-1} are given. Reason behind the slightly higher glycerol conversions than thermodynamic limit are explained in Section 4.1.1.2. For the glycerol conversion, RuAZ and RuSZ have hit the

thermodynamic limit, where RuCZ and RuLZ have reached 94% and 97% of the equilibrium conversion. However, since the activity of RuWZ dies during the experiment, its glycerol conversion is 51.4%, which is only 1% higher than blank test.

In Table 4.13 product yields, H_2/CO ratios, and conversions of the binary oxide supported catalysts are listed. RuLZ have yielded the most H_2 and CO among the catalysts tested, with the values of 2.61 and 4.28, respectively. H_2 and CO yields of RuLZ correspond to the 97.6 and 99.6% of the pertinent thermodynamic limits, respectively. Other catalysts have yielded less H_2 and CO yield than RuLZ, closest H_2 yield is achieved by RuSZ by 1.90, and closest CO yield is achieved by RuCZ with 2.91. Difference between RuLZ and the rest is apparently the CH_4 and C_2H_6 yields. RuLZ might create this difference by employing more CO_2 to convert CH_4 by DRM, since RuLZ exhibits more CO_2 conversion and yields no CH_4. Moreover, the catalyst most likely demonstrated high activity towards RWGS, which generated H_2O sufficient to steam reform the C_1-C_2 hydrocarbons to H_2 and CO. Comparison of H_2 and CO yields can be seen in Figures 4.12 and 4.13. When the H_2/CO ratios are compared, RuSZ have exhibited maximum ratio among the catalysts tested with the value of 0.67. Glycerol conversion anomaly of RuSZ can be explained by its yields, which exhibits higher H_2 than other catalysts (except RuLZ) and yields the most amount of CH_4. Therefore, these hydrogen species boost the glycerol conversion of RuSZ, which calculated by hydrogen balance. Rest of the catalysts have exhibited H_2/CO between 0.61 to 0.53.

In Table 4.14, product selectivities for screened catalysts are given. For the syngas selectivity, RuLZ leads the tested catalysts by a large margin. H_2 and CO selectivities of RuLZ are at the thermodynamic limit with the values of 4 and 6.57, respectively. Also, RuLZ is not selective to any of the gaseous undesired products, with the yields of CH_4, C_2H_4 and C_2H_6 being equal to zero. However, rest of the catalysts tested have exhibited very low syngas selectivities and high CH_4 selectivities which is a result of inactivity of the catalysts.

Table 4.13. Product yields over binary oxide supported catalysts in screening experiments (T = 750 °C, CO_2/G = 4, and τ = 3.75 mg min NmL^{-1}).

Catalyst	$\mathbf{Y_{H_2}}$	$\mathbf{Y_{CO}}$	$\mathbf{Y_{CH_4}}$	$\mathbf{Y_{C_2H_4}}$	$\mathbf{Y_{C_2H_6}}$	$\mathbf{H_2/CO}$	$\boldsymbol{x_{CO_2}}$	$\boldsymbol{x_G}$
RuAZ	1.68	2.89	0.50	0.00	0.01	0.58	14.1	67.8
RuCZ	1.53	2.91	0.47	0.00	0.02	0.53	16.4	63.1
RuLZ	2.61	4.28	0.00	0.00	0.00	0.61	32.9	65.2
RuSZ	1.90	2.86	0.52	0.00	0.01	0.67	7.6	73.0
RuWZ	0.54	1.41	0.46	0.21	0.05	0.38	0.3	51.4

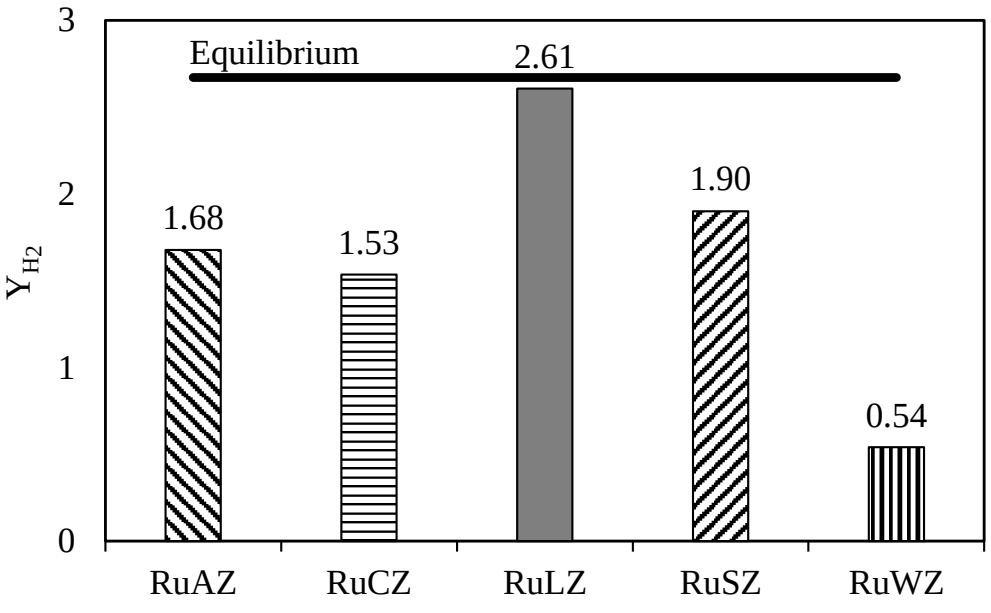

Figure 4.12. H_2 yields over binary oxide supported catalysts in screening experiments (T=750 °C, CO_2/G = 4, and τ = 3.75 mg min NmL^{-1}).

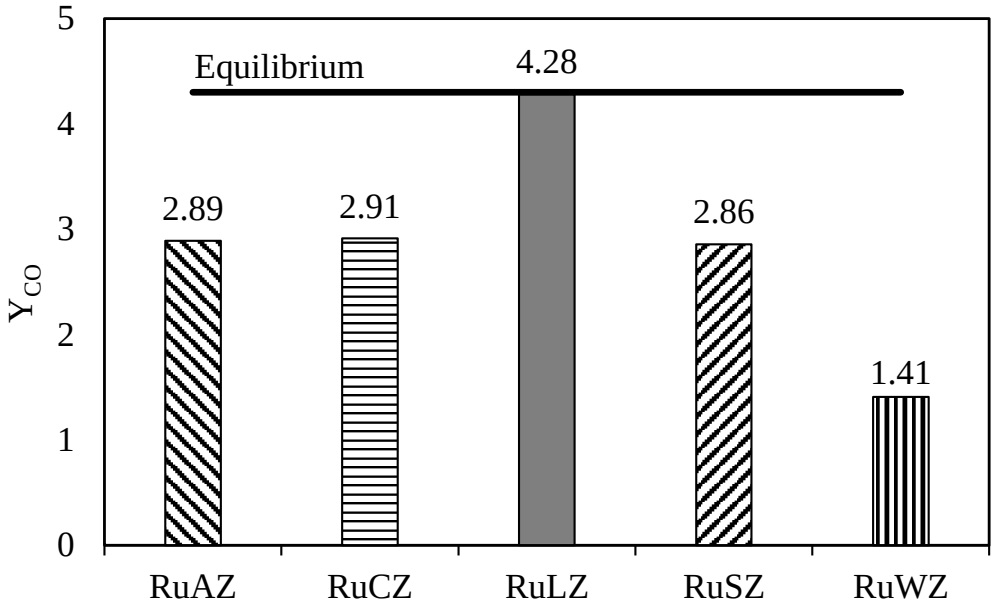

Figure 4.13. CO yields over binary oxide supported catalysts in screening experiments (T=750 °C, CO_2/G = 4, and τ = 3.75 mg min NmL^{-1}).

Table 4.14. Product selectivities over binary oxide supported catalysts in screening experiments (T = 750 °C, CO_2/G = 4, and τ = 3.75 mg min NmL^{-1}).

Catalyst	$\mathbf{S_{H_2}}$	$\mathbf{S_{CO}}$	$\mathbf{S_{CH_4}}$	$\mathbf{S_{C_2H_4}}$	$\mathbf{S_{C_2H_6}}$
RuAZ	2.47	4.26	0.74	0	0.02
RuCZ	2.43	4.61	0.74	0	0.03
RuLZ	4.00	6.57	0	0	0
RuSZ	2.60	3.91	0.72	0	0.02
RuWZ	1.05	2.74	0.90	0.42	0.11

From the catalyst screening, it is clear that amongst the binary oxides tested, addition of La_2O_3 to ZrO_2 support enhances the catalytic activity and selectivity of the single oxide RuZr. Rest of the binary oxide supports have reduced the activity and selectivity of the ZrO_2 significantly. Therefore, effect of reaction parameters will be investigated for only RuLZ in the following sections. It is, however, worth noting that the binary oxides CZ, AZ, SZ and WZ require further investigation, as the relative amounts of the oxides in the support have clear impacts on the catalytic activity. The supports tested here were investigated with only one composition (per support) dictated by the supplier. This is a clear room for improvement, which will be carried out in future studies.

4.2.2. Effect of Reaction Temperature

Similar to Section 4.1.3, effect of reaction temperature on CO_2 and glycerol conversions, product yields and product selectivities is investigated over RuLZ, with reaction temperatures from 650 to 750 °C. For specified reaction conditions, a thermodynamic analysis is made in Section 4.1.3.1. Therefore, this section will start directly from activity tests.

4.2.2.1. Activity Tests. Carbon dioxide conversions of RuLZ at 650 to 750 °C are given in Figure 4.14. Although thermodynamics allows higher CO_2 conversions, in experiment at 650 °C no significant activity is seen. However when the reaction temperature is increased from 650 to 700 °C, CO_2 conversion increased significantly to 25.3, which is the 86.8% of the equilibrium conversion. This sharp increase might be explained with the severe carbon formation on the catalyst at 650 °C which inhibits the catalytic activity, since Boudouard reaction is favored at lower temperatures. From 700 to 750 °C, CO_2 conversion increases from 25.3 to 29.5, which is the 90% of the equilibrium conversion.

Glycerol conversions of RuLZ at 650 to 750 °C are given in Figure 4.15. From 650 to 700 °C, glycerol conversion of RuLZ increased from 51.8 to 66.8%. Although

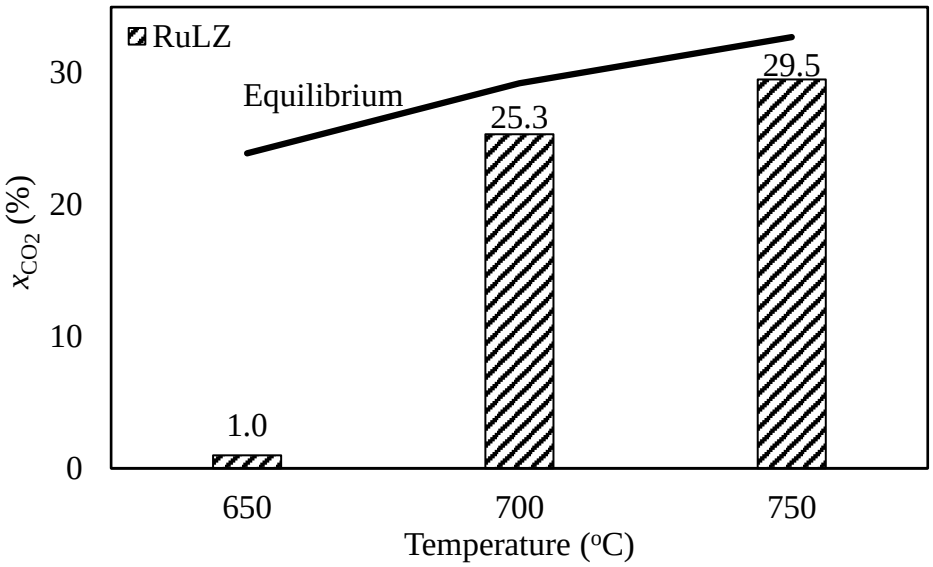

Figure 4.14. CO_2 conversions over RuLZ at reaction temperatures from 650 to 750 °C (CO_2/G = 4, and τ = 0.5 mg min NmL^{-1}).

increasing temperature improves glycerol conversion from 650 to 700 °C, maximum glycerol conversion is achieved at 700 °C 66.8%. Thermodynamically, this can be explained *via* increased rate of RWGS. Due to the endothermic nature of RWGS, amount of water produced increases, which leads to a decrease in H_2 content in gaseous phase at elevated temperatures, thus decreasing glycerol conversion.

In Table 4.15, product yields, H_2/CO ratios, CO_2 and glycerol conversions of RuLZ at 650 to 750 °C are presented. From 650 to 700 °C H_2 yield increases with the values of 0.88 to 2.47. However, from 700 to 750 °C, yield of H_2 decreases from 2.47 to 2.38. This is due to increased rate of RWGS. Since higher temperatures favor RWGS, more H_2 are consumed to form H_2O and CO. Thus, yield of CO increases from 3.9 to 4.07 between 700 and 750 °C. This increase also lowers the H_2/CO ratio from 0.63 to 0.59. Increasing temperature reduces CH_4 yield from 0.36 to 0.1 at 700 °C. This might be explained with the increasing rate of dry reforming reactions due to their endothermic nature, and activation of steam reforming reactions by the H_2O generation caused by RWGS.

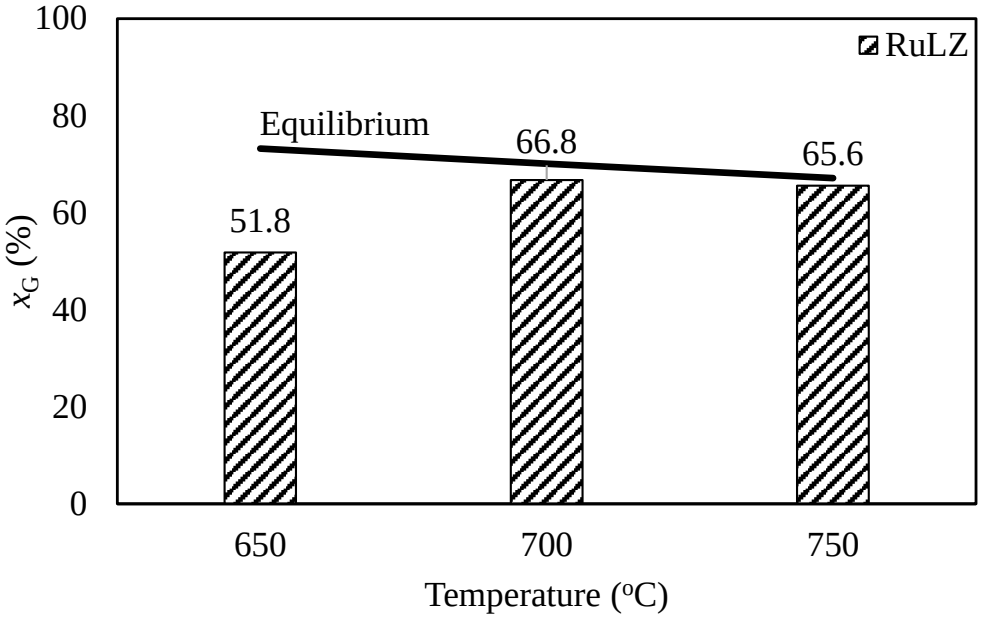

Figure 4.15. Glycerol conversions over RuLZ at temperatures from 650 to 750 ºC (CO_2/G = 4, and τ = 0.5 mg min NmL^{-1}).

Table 4.15. Product yields over RuLZ at reaction temperatures from 650 to 750 ºC (CO_2/G = 4, and τ = 0.5 mg min NmL^{-1}).

T (ºC)	$\mathbf{Y_{H_2}}$	$\mathbf{Y_{CO}}$	$\mathbf{Y_{CH_4}}$	$\mathbf{Y_{C_2H_4}}$	$\mathbf{Y_{C_2H_6}}$	$\mathbf{H_2/CO}$	$\boldsymbol{x}_{\mathbf{CO_2}}$	$\boldsymbol{x}_{\mathbf{G}}$
650	0.88	1.63	0.36	0.15	0.06	0.54	0.99	51.81
700	2.47	3.90	0.10	0	0	0.63	25.34	66.76
750	2.38	4.07	0.12	0	0	0.59	29.51	65.59

Table 4.16. Product selectivities over RuLZ at reaction temperatures from 650 to 750 °C (CO_2/G = 4, and τ = 0.5 mg min NmL^{-1}).

T (°C)	$\mathbf{S_{H_2}}$	$\mathbf{S_{CO}}$	$\mathbf{S_{CH_4}}$	$\mathbf{S_{C_2H_4}}$	$\mathbf{S_{C_2H_6}}$
650	1.69	3.14	0.69	0.30	0.11
700	3.70	5.85	0.15	0	0
750	3.63	6.20	0.19	0	0

In Table 4.16, product selectivities of RuLZ at the reaction temperatures are presented. Due to inactivity of RuLZ at 650 °C, selectivities of H_2 and CO are lower than 700 and 750 °C while undesired product selectivities are higher at 650 °C. At this temperature RuLZ exhibits very high selectivity towards CH_4, C_2H_4 and C_2H_6, which are the indicators of inactivity. However, at 700 °C both C_2H_4 and C_2H_6 selectivities are inhibited, where CH_4 selectivity is reduced to 0.1. RuLZ exhibits the highest H_2 selectivity at 700 °C with 2.47, where the highest CO selectivity is observed at 750 °C with 4.07.

From the reaction temperature analysis, it is clear that working below 700 °C is irrational due to reduced activity and yields of undesirable products. However, this temperature analysis has proven that working at 700 °C could be an option due to high activity and high selectivity towards H_2 production.

4.2.3. Effect of CO_2/G

Similar to Section 4.1.2, effect of CO_2/G on catalyst activity, product yield and selectivity is investigated. Reaction conditions are kept exactly the same as Section 4.1.2. Among the binary oxide supported catalysts, only the RuLZ demonstrated a promising performance. Therefore, this section investigates effect of CO_2/G on GDR over RuLZ catalyst. Since the reaction conditions are the same, no additional thermodynamic analysis is required. Initial thermodynamic analysis done for the CO_2 to glycerol ratios scanned can be found in Section 4.1.2.1.

4.2.3.1. Activity Tests. In this section, effect of CO_2 to glycerol ratio on CO_2 and glycerol conversions, H_2 and CO yields and selectivities was investigated over RuLZ. Effect of CO_2 to glycerol ratio on CO_2 conversion is given in Figure 4.16. RuLZ exhibits over 29% CO_2 conversion in every CO_2/G tested. Maximum CO_2 conversion of 32.4% is observed at CO_2/G = 2. RuLZ achieves approximately 90% of the equilibrium conversion at CO_2/G = 3 and 4, whereas in ratios 1 and 2, these values are 74.2 and 82.5% of the equilibrium conversion, respectively. This might be caused from increased carbon formation at lower ratios, since the decrease in the CO_2 amount in the reactor favors the Boudouard reaction in the favor of the solid carbon formation.

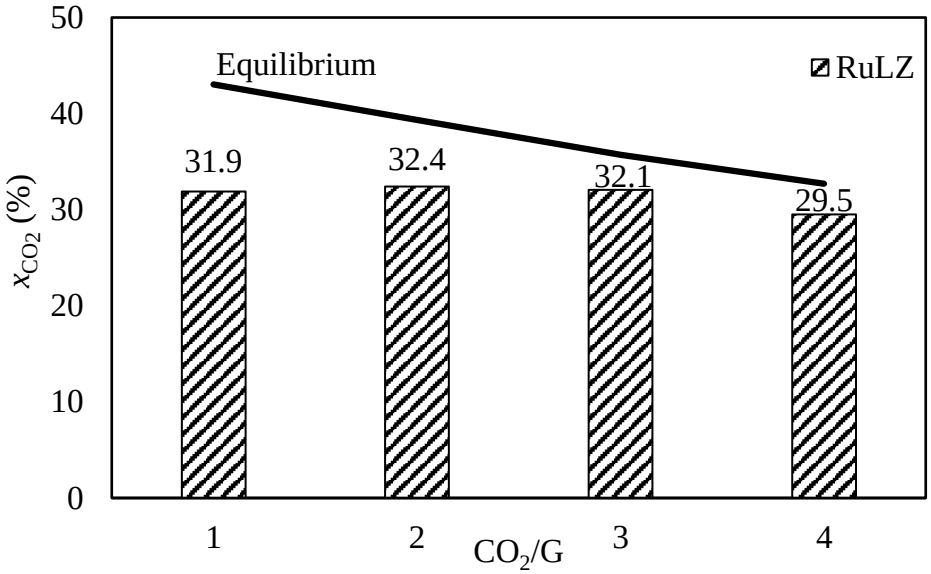

Figure 4.16. Carbon dioxide conversions over RuLZ at different CO_2 to glycerol ratios (T=750 °C, and τ = 0.5 mg min NmL^{-1}).

In Figure 4.17, glycerol conversions of RuLZ at different CO_2 to glycerol ratios are given. In every CO_2/G tested, RuLZ have reached above 97.6% of the equilibrium conversion. With increasing ratios, glycerol conversion of RuLZ have decreased from 88.2 to 65.6%. This decrease is in alignment with the thermodynamic limit of glycerol conversion. In ratio 3, glycerol conversion of RuLZ have hit the thermodynamic limit with 73%.

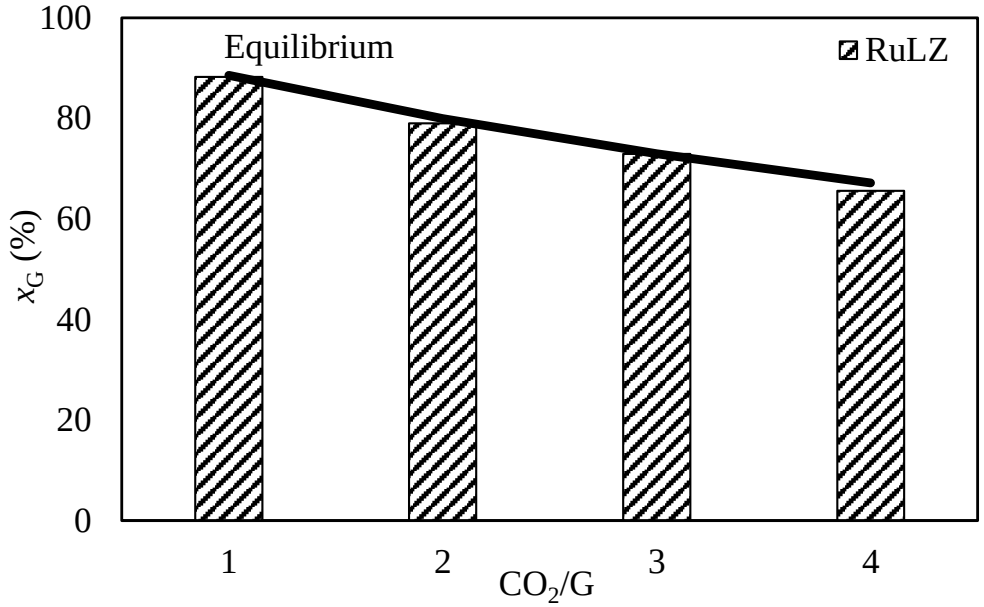

Figure 4.17. Glycerol conversions over RuLZ at different CO_2 to glycerol ratios (T=750 °C, and τ = 0.5 mg min NmL^{-1}).

Product yields, H_2/CO ratios, CO_2 conversions and glycerol conversions of RuLZ at all of the CO_2 to glycerol ratios tested are given in Table 4.17. With increasing CO_2/G, yield of H_2 decreases from 3.43 to 2.38, whereas yield of CO increases from 3.31 to 4.07. These results follow the thermodynamic trend, where H_2 yield decreases from 98.2 to 89.1% of thermodynamic limit by increasing CO_2/G. This decrease is much smaller for CO yield, which decreases from 97.3 to 94.6% of the thermodynamic limit. By increasing CO_2/G, H_2/CO ratio decreased from 1.04 to 0.59. Product selectivities of RuLZ at different feed ratios are given in Table 4.18. Selectivity of H_2 decreases from 3.89 to 3.63, where the selectivity of CO increases from 3.75 to 6.20 upon enriching the feed with CO_2. Also, selectivity of CH_4 increases from 0.06 to 0.19 with increasing the CO_2/G.

From the CO_2/G analysis, RuLZ have exhibited the best CO_2 and glycerol conversion by 90 and 100% of the thermodynamic limit at CO_2/G = 3. However, when the product yields are investigated, H_2 yield and H_2/CO are higher at CO_2/G = 2. This creates a dilemma to select an optimum feed ratio for GDR over RuLZ.

Table 4.17. Product yields over RuLZ at different CO_2/G (T = 750 °C).

CO_2/G	Y_{H_2}	Y_{CO}	Y_{CH_4}	$Y_{C_2H_4}$	$Y_{C_2H_6}$	H_2/CO	x_{CO_2}	x_G
1	3.43	3.31	0.05	0	0	1.04	31.90	88.20
2	3.08	3.69	0.04	0	0	0.83	32.42	79.03
3	2.66	3.92	0.13	0	0	0.68	32.08	72.96
4	2.38	4.07	0.12	0	0	0.59	29.51	65.59

Table 4.18. Product selectivities over RuLZ at different CO_2/G (T = 750 °C).

CO_2/G	S_{H_2}	S_{CO}	S_{CH_4}	$S_{C_2H_4}$	$S_{C_2H_6}$
1	3.89	3.75	0.06	0	0
2	3.89	4.67	0.05	0	0
3	3.65	5.37	0.17	0	0
4	3.63	6.20	0.19	0	0

To address this dilemma, two additional tests are made. In these tests, time on stream is elongated to 24 hours, and the residence time increased to 3.75 mg min NmL^{-1}. The purpose of this comparison is to observe the behaviour of the catalyst along its time on stream. From the results of these experiments, at CO_2/G = 2, RuLZ has lost 13.2% of its activity, which started with 39.3% (thermodynamic limit) and ended the experiment with 34.1% CO_2 conversion. Whereas, at CO_2/G = 3, RuLZ have started the experiment with 34.3% and ended at 31.3%. This result leads to 8.75% deactivation. CO_2 conversion results of this experiment are presented in Figure 4.18. Therefore, for the following parametric analyses and stability tests, CO_2/G = 3 is selected as the default.

4.2.4. Effect of Residence Time

Similar to Section 4.1.4, effect of residence time is investigated for RuLZ. In Figure 4.19, CO_2 and glycerol conversions of RuLZ at 20 and 150 mg experiments are

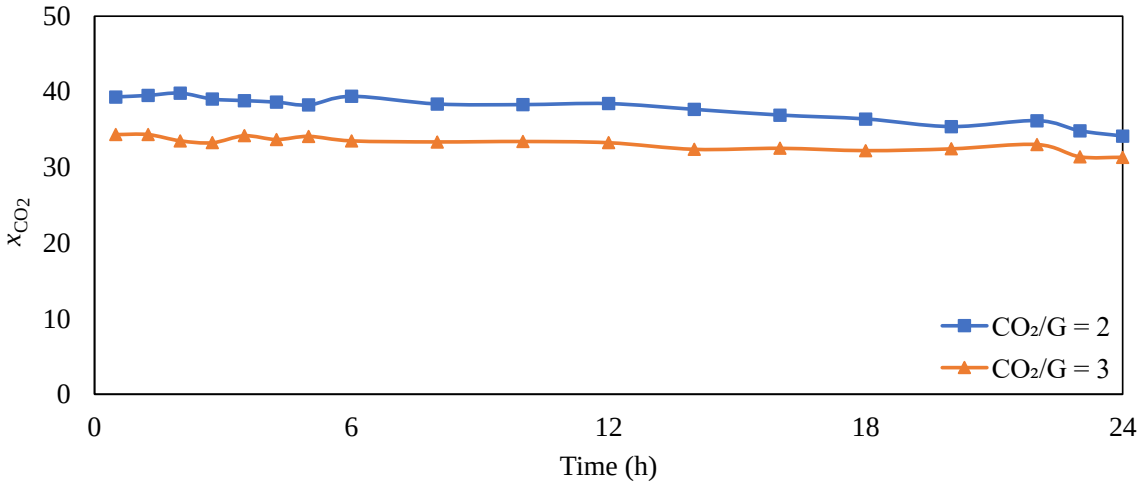

Figure 4.18. CO_2 conversions over RuLZ at CO_2/G = 2 and 3 in 24 hours ToS experiment (T=750 °C, and τ = 3.75 mg min NmL^{-1}).

presented. When the catalyst amount is increased, CO_2 conversion of RuLZ increases from 32.1 to 34.5%, which is approximately 97% of the equilibrium conversion. As expected, glycerol conversion of RuLZ decreases from 73 to 71.9%. This might be due to increased extent of RWGS and reverse Boudouard reaction which decreases H_2 yield and removal of carbonaceous products improves the stability of the catalyst. Therefore in the long term, reducing CH_4 yield which increases the glycerol conversion.

Similar to RuZr in Section 4.1.4, increasing residence time by 7.5 times effects CO_2 conversion by only 2.5%. The small increase in CO_2 conversion is an indication of superior activity of the RuLZ.

4.2.5. Catalyst Stability

There are two possible deactivation mechanisms for GDR. These are active metal sintering and coke deposition. Several studies have found that, if the carbon deposited on the surface are whisker, encapsulating or filamentous type carbon, they are reversible, and can be easily removed *via* oxidation [8,31,34,38]. Sintering occurs at high temperatures reached in this work, and becomes effective when H_2O is more available

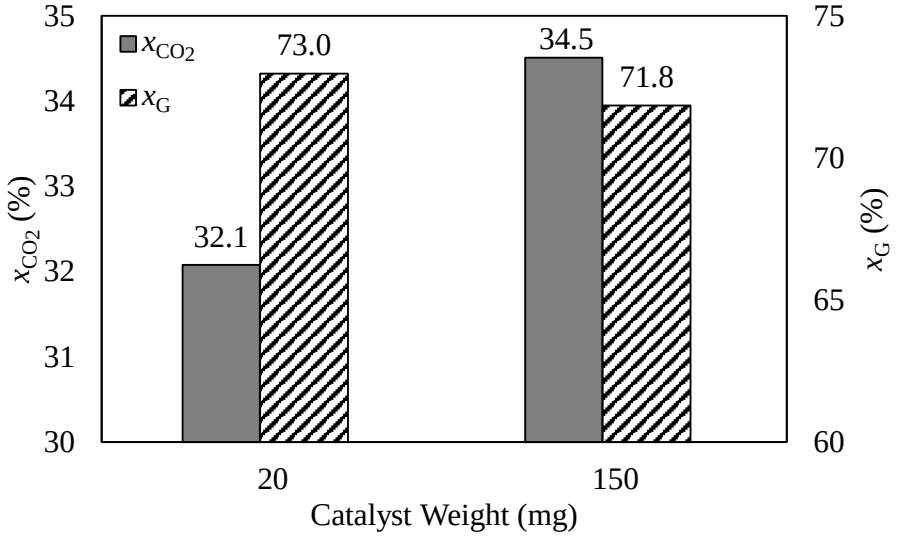

Figure 4.19. Effect of residence time on CO_2 and glycerol conversions of RuLZ (T=750 °C and CO_2/G = 3).

in the system, which formed through RWGS. Although it is impossible to determine the exact reason of deactivation without characterization, there is a hypothetical cut-off where increasing CO_2/G ratio increases H_2O yield which may increase sintering, also increasing feed ratio favors the inverse Boudouard reaction to remove solid carbon.

In the previous sections, ten catalysts in total are screened, and effect of reaction parameters are investigated over promising catalysts. For single oxide supports ZrO_2, and for the binary oxide supports 9 wt.% La_2O_3-ZrO_2 is exhibited the best activity and selectivity towards desired products. In this section, effect of lanthana on the stablity of zirconia supported Ru catalysts will be investigated. Stability of the catalysts will be investigated at the reaction temperature of 750 °C, CO_2/G = 3, and residence time of 3.75 mg min NmL^{-1}. These reaction parameters are determined by the results of the parametric investigation done in previous sections. Catalyst amount of 150 mg is used without any diluent. In order to understand the effect of La_2O_3 addition to ZrO_2 support, RuLa, RuZr and RuLZ are tested in stability experiments. These experiments are carried out for 72 hours.

In Figure 4.20, CO_2 conversions of RuLa, RuZr and RuLZ throughout the stability experiments can be seen. RuZr have started at thermodynamic limit, but deactivated over the course of the experiment. At the end of the experiment, RuZr have lost 28% of its activity from 35% to 23.7%. However, at the last 3 hours of the experiment, RuZr have continued to deactivate. Therefore, if the experiment is elongated, this deactivation would be much higher. RuLa have exhibited better activity, where it started with 33% CO_2 conversion, and after 72 hours it deactivated by 20%, which it ended the experiment with 26% CO_2 conversion. For RuLZ, initial activity is slightly lower than RuZr with 34.4% CO_2 conversion. However at the end of the experiment, RuLZ have deactivated only 13%, in which it finished the experiment with 29.3% CO_2 conversion.

From these results, it can be seen that, presence of La_2O_3 improves the stability of Ru/ZrO_2. Reason behind this improved stability might cause from the increased lattice oxygen availability and higher basicity with the addition of La_2O_3 to LZ, which may help to oxidize more solid carbon on the surface than ZrO_2. Therefore, allowing catalyst to preserve its activity for a longer time.

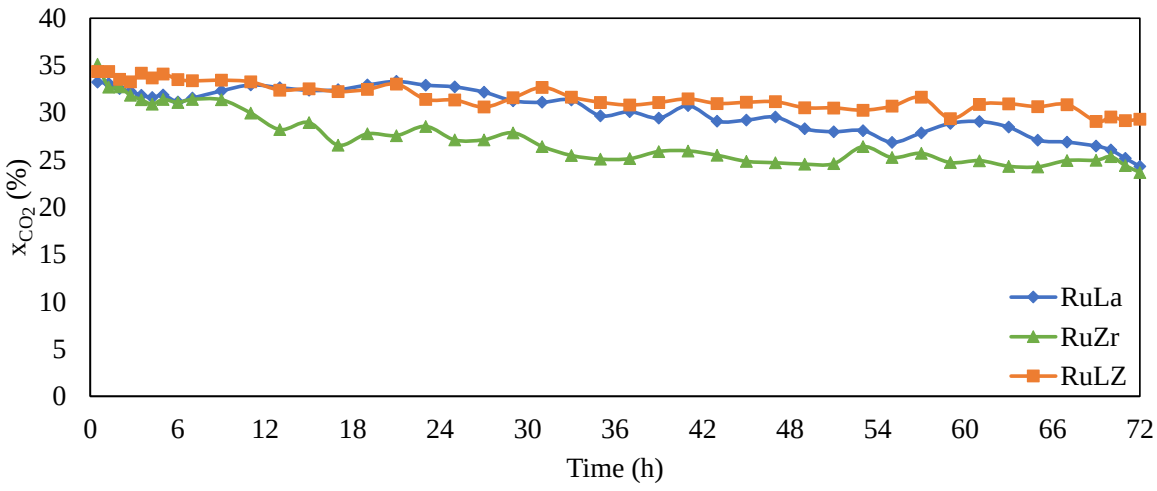

Figure 4.20. CO_2 conversions of RuLa, RuZr and RuLZ in stability experiments (T=750 °C, $CO_2/G = 3$ and $\tau = 3.75$ mg min NmL^{-1}).

In Figure 4.21, glycerol conversions of RuLa, RuZr and RuLZ in stability experiments are given. Due to how glycerol conversion is calculated, results may fluctuate. Contrary to CO_2, glycerol conversion has a tendency to increase due to activity loss. When RWGS rate decreases, amount of H_2 consumed decreases by this reaction. Since water is trapped in cold traps, decrease of RWGS rate increases glycerol conversion to gaseous products. Glycerol conversion of RuZr have increased from approximately 72 to 75%. For RuLa, glycerol conversion have increased from 73% to 75% after 72 hours. However, glycerol conversion of RuLZ remained at 76% throughout the experiment.

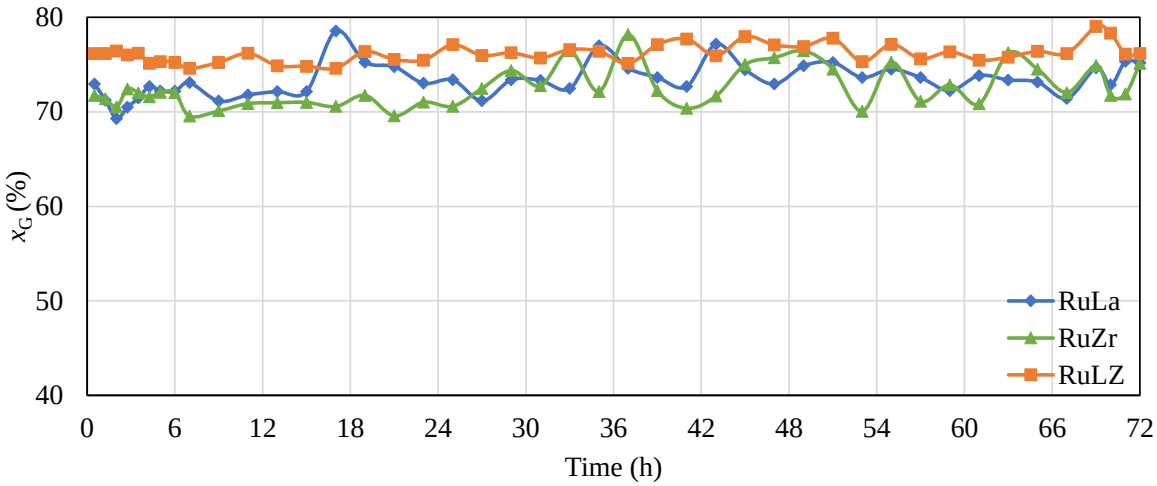

Figure 4.21. Glycerol conversions of RuLa, RuZr and RuLZ in stability experiments (T=750 °C, CO_2/G = 3 and τ = 3.75 mg min NmL^{-1}).

In Table 4.19, product yields, H_2/CO ratios, CO_2 conversions and glycerol conversions of RuLa, RuZr and RuLZ in stability experiments are given. These values are tabulated with approximately 12 hours intervals for the sake of simplicity. RuLa have deactivated approximately 20% over 72 hours, and therefore yields of H_2 and CO are decreased from 2.84 and 3.96 to 2.40 and 3.61, respectively. Additionally, yield of CH_4 have increased from 0.04 to 0.29 in 72 hours. At the end of the experiments, trace amounts of C_2H_6 is detected, which is a sign of deactivation. H_2/CO ratio is decreased from 0.72 to 0.66 after 72 hours. Due to its significant deactivation over time, H_2 and CO yield of RuZr decreases from 2.83 and 3.99 to 2.4 and 3.57, respectively. Meanwhile, due to deactivation CH_4 yield increases 0.02 to 0.3 over time. No C_2 species

yield observed in 72 hours. However, due to rate of deactivation, these products might be observed if the experiment continued. H_2/CO ratio is decreased from 0.71 to 0.67. This might be due to deactivation of reforming reactions affected more than RWGS and reverse Boudouard reactions. RuLZ yields more H_2 and CO than RuZr with the initial values of 3.02 and 4.21, respectively. Also H_2 and CO yields of RuLZ decreases less than RuZr, with the final values of 2.91 and 3.94, respectively. Due to its superior stability, CH_4 yield increases from 0.01 to 0.07.

Product selectivities of RuLa, RuZr and RuLZ are given in Table 4.20. Due to the difference in glycerol conversion, initial product selectivities of RuLa, RuZr and RuLZ are very similar and nearly at thermodynamic limit. However, RuLa and RuZr deactivates more rapidly than RuLZ, and these catalysts ends the experiments with H_2 selectivities of 3.19 and 3.20, respectively. Also after 72 hours CO selectivities of these catalysts 4.81 and 4.76, respectively. Where, RuLZ ends the experiment with 3.82 and 5.18 H_2 and CO selectivities, respectively. Catalysts are not selective to higher hydrocarbons, C_2 selectivities remain at near zero during the reaction. Due to deactivation, selectivity of CH_4 increases from 0.05 to 0.39 for RuLa and 0.03 to 0.40 for RuZr, where it increases only from 0.02 to 0.09 for RuLZ.

Table 4.19. Product yields of RuLa, RuZr and RuLZ catalysts in stability experiments (T = 750 °C, CO_2/G = 3, and τ = 3.75 mg min NmL^{-1}).

	t (h)	$\mathbf{Y_{H_2}}$	$\mathbf{Y_{CO}}$	$\mathbf{Y_{CH_4}}$	$\mathbf{Y_{C_2H_4}}$	$\mathbf{Y_{C_2H_6}}$	$\mathbf{H_2/CO}$	$\boldsymbol{x_{CO_2}}$	$\boldsymbol{x_G}$
RuLa	0.5	2.84	3.96	0.04	0	0	0.72	33.23	72.95
	13	2.78	3.99	0.05	0	0	0.70	33.72	72.14
	25	2.78	3.96	0.08	0	0	0.70	32.73	73.02
	37	2.72	3.89	0.13	0	0	0.70	30.11	74.60
	49	2.62	3.81	0.18	0	0	0.69	28.30	74.85
	61	2.48	3.68	0.23	0	0.01	0.67	29.07	73.84
	72	2.40	3.61	0.29	0	0.01	0.66	26.05	75.19
RuZr	0.5	2.83	3.99	0.02	0	0	0.71	35.13	71.73
	13	2.54	3.74	0.15	0	0	0.68	28.21	70.96
	25	2.40	3.61	0.21	0	0	0.66	27.11	70.58
	37	2.55	3.75	0.29	0	0	0.68	25.14	78.17
	49	2.47	3.65	0.29	0	0	0.68	24.56	76.44
	61	2.29	3.48	0.27	0	0	0.66	24.93	70.83
	72	2.40	3.57	0.30	0	0	0.67	23.69	75.11
RuLZ	0.5	3.02	4.21	0.01	0	0	0.72	34.35	76.15
	13	2.97	4.09	0.01	0	0	0.73	32.39	74.87
	25	3.05	4.16	0.01	0	0	0.73	31.34	77.09
	37	2.98	4.07	0.01	0	0	0.73	30.80	75.11
	49	3.03	4.10	0.02	0	0	0.74	30.52	76.91
	61	2.96	4.00	0.03	0	0	0.74	30.88	75.45
	72	2.91	3.94	0.07	0	0	0.74	29.31	76.15

Table 4.20. Product selectivities of RuLa, RuZr and RuLZ in stability experiments (T = 750 °C, CO_2/G = 3, and τ = 3.75 mg min NmL^{-1}).

	Time (h)	$\mathbf{S_{H_2}}$	$\mathbf{S_{CO}}$	$\mathbf{S_{CH_4}}$	$\mathbf{S_{C_2H_4}}$	$\mathbf{S_{C_2H_6}}$
RuLa	0.5	3.90	5.43	0.05	0	0
	13	3.86	5.53	0.07	0	0
	25	3.80	5.43	0.11	0	0
	37	3.64	5.22	0.17	0	0
	49	3.50	5.09	0.24	0	0.01
	61	3.35	4.98	0.31	0	0.01
	72	3.19	4.81	0.39	0	0.01
RuZr	0.5	3.95	5.56	0.03	0	0
	13	3.58	5.28	0.21	0	0
	25	3.39	5.12	0.30	0	0
	37	3.26	4.79	0.37	0	0
	49	3.23	4.78	0.39	0	0
	61	3.23	4.91	0.38	0	0
	72	3.20	4.76	0.40	0	0
RuLZ	0.5	3.96	5.53	0.02	0	0
	13	3.97	5.47	0.02	0	0
	25	3.96	5.40	0.02	0	0
	37	3.96	5.41	0.02	0	0
	49	3.95	5.34	0.03	0	0
	61	3.92	5.30	0.04	0	0
	72	3.82	5.18	0.09	0	0

5. CONCLUSION

The goal of this study was to develop an active and stable Ru-based catalyst for glycerol dry reforming, and to investigate the effects of reaction parameters on catalyst activity, product selectivity and catalyst stability. Investigated parameters were reaction temperature, CO_2 to glycerol ratio in feed, and residence time. Effect of these parameters on CO_2 and glycerol conversion, H_2 and CO yield, and deactivation rate was investigated. By the time of this thesis written, characterizations of investigated catalysts are being made. Therefore, results of the experiments was discussed with the characterization result knowledge in the literature.

5.1. Conclusions from Ru Catalysts Supported on Single Oxides

At the start of the project, Ru-based catalysts have been used for glycerol dry reforming or similar processes were scanned in literature. Although there are many Ru-based catalysts used for DRM and GSR, there is only one article about GDR, which written by Tavanarad *et al.* in 2018 [9]. From the literature survey, promising single oxide supports were selected. These were, Al_2O_3 (Al), CaO (Ca), CeO_2 (Ce), La_2O_3 (La), and ZrO_2 (Zr).

These catalysts were synthesized with 1 wt.% Ru and tested in catalyst screening (see Section 4.1. From the initial results, RuZr have exhibited very good activity amongst others. From the literature, strong metal-support interaction between Ru and ZrO_2 was known. Thus, screening results have exhibited this relation, and set the direction of the research to ZrO_2 based supports.

When reaction parameters was investigated over RuZr, reaction temperature decreased the activity of RuZr significantly. CO_2 to glycerol ratio was found to be effective to adjust H_2/CO ratio of the syngas produced. Residence time was found to be is not very effective since RuZr is already highly active at lowest amount of residence time.

From the parametric analysis, optimum parameters for RuZr was 750 °C, CO_2/G = 3, and residence time of 0.5 mg min NmL^{-1}. In these conditions, RuZr have exhibited 31.8% CO_2 conversion, 73% glycerol conversion, approximately 95 and 97% of the thermodynamic H_2 and CO selectivity, respectively. Produced syngas had H_2/CO ratio of 0.7.

5.2. Conclusions from Ru Catalysts Supported on Binary Oxides

At the end of the 5 hours activity experiments, deactivation in RuZr was observed. Thus, an improvement was needed to RuZr. For this reason, ZrO_2 based binary oxide catalyst supports was acquired from Daiichi Kigenso. These supports were, Al_2O_3-ZrO_2 (AZ), CeO_2-ZrO_2 (CZ), La_2O_3-ZrO_2 (LZ), SiO_2-ZrO_2 (SZ) and WO_3-ZrO_2 (WZ). From a similar screening experiment series, RuLZ was the only binary oxide supported catalyst which improved the activity and selectivity of RuZr (see Section 4.2).

Effect of reaction parameters were also investigated for RuLZ and finally RuLZ was compared with RuLa and RuZr at stability experiments. When reaction parameters was investigated over RuLZ, reaction temperature decreased the activity of RuLZ, however at 700 °C RuLZ was still very active when compared with thermodynamic limit. Using different CO_2/G values, syngas with H_2/CO ratio ranging from 0.6 to 1 can be obtained.

Optimum conditions for RuLZ were, 750 °C, CO_2/G = 3, and residence time of 0.5 mg min NmL^{-1}, which is the same conditions with RuZr. In these conditions RuLZ have exhibited 32.1% CO_2 conversion, 73% glycerol conversion, 92 and 96% of the thermodynamic H_2 and CO selectivity, respectively. Produced syngas had H_2/CO ratio of 0.7. However, RuLZ have shown the most important improvement at catalyst stability, which after 72 hours RuLZ have only deactivated 13%, where RuLa and RuZr were deactivated over 20 and 28%, respectively.

5.3. Recommendations

- Characterizations must focus on the interactions between Ru and La-Zr, to find out; the dispersion of Ru over the support and verify the metal-support interaction, coking type on the surface of the catalyst and effect of LZ on the removal of it. The basicity of LZ, which is believed to make it more active than Zr or La, should be confirmed by characterization studies.
- Metal loading of Ru can be investigated to improve cost and performance.
- La_2O_3 amount in ZrO_2 can be manipulated to improve catalytic performance.
- The binary oxides CZ, AZ, SZ and WZ require further investigation, as the relative amounts of the oxides in the support have clear impacts on the catalytic activity. The supports tested here were investigated with only one composition (per support) dictated by the supplier. This is a clear room for improvement, which will be carried out in future studies.
- Yttria-stabilized-zirconia could be an interesting support selection due to coke formation reduction of yttria.
- Lower amounts of Ce in CZ or La-Ce-Zr ternary oxide support could improve catalyst stability due to oxygen vacancies on ceria domains which inhibits carbon formation
- Ru-Ni bimetallic catalysts can be investigated to improve cost and performance.

REFERENCES

1. Van Gerpen, J., "Biodiesel processing and production", *Fuel processing technology*, Vol. 86, No. 10, pp. 1097–1107, 2005.

2. European Eurodiesel Board, *Statistics*, 2016, `http://www.ebb-eu.org/stats.php`, accessed at July 2019.

3. Meher, L. C., D. V. Sagar and S. Naik, "Technical aspects of biodiesel production by transesterification—a review", *Renewable and sustainable energy reviews*, Vol. 10, No. 3, pp. 248–268, 2006.

4. Cintas, P., S. Tagliapietra, E. C. Gaudino, G. Palmisano and G. Cravotto, "Glycerol: a solvent and a building block of choice for microwave and ultrasound irradiation procedures", *Green Chemistry*, Vol. 16, No. 3, pp. 1056–1065, 2014.

5. Lee, H. C., K. W. Siew, J. Gimbun and C. K. Cheng, "Synthesis and characterisation of cement clinker-supported nickel catalyst for glycerol dry reforming", *Chemical Engineering Journal*, Vol. 255, pp. 245–256, 2014.

6. Siew, K. W., H. C. Lee, M. R. Khan, J. Gimbun and C. K. Cheng, "CO2 reforming of glycerol over La-Ni/Al2O3 catalyst: A longevity evaluative study", *Journal of Energy Chemistry*, Vol. 24, No. 3, pp. 366–373, 2015.

7. Arif, N. N. M., D.-V. N. Vo, M. T. Azizan and S. Z. Abidin, "Carbon dioxide dry reforming of glycerol for hydrogen production using Ni/ZrO2 and Ni/CaO as catalysts", *Bulletin of Chemical Reaction Engineering & Catalysis*, Vol. 11, No. 2, pp. 200–209, 2016.

8. Harun, N., S. Z. Abidin, O. U. Osazuwa, Y. H. Taufiq-Yap and M. T. Azizan, "Hydrogen production from glycerol dry reforming over Ag-promoted Ni/Al2O3", *International Journal of Hydrogen Energy*, Vol. 44, No. 1, pp. 213–225, 2019.

9. Tavanarad, M., F. Meshkani and M. Rezaei, "Synthesis and Application of Noble Metal Nanocatalysts Supported on MgAl 2 O 4 in Glycerol Dry Reforming Reaction", *Catalysis Letters*, Vol. 148, No. 1, pp. 164–172, 2018.

10. Bulutoglu, P. S., Z. Say, S. Bac, E. Ozensoy and A. K. Avci, "Dry reforming of glycerol over Rh-based ceria and zirconia catalysts: New insights on catalyst activity and stability", *Applied Catalysis A: General*, Vol. 564, pp. 157–171, 2018.

11. Bac, S., Z. Say, Y. Kocak, K. E. Ercan, M. Harfouche, E. Ozensoy and A. K. Avci, "Exceptionally active and stable catalysts for CO2 reforming of glycerol to syngas", *Applied Catalysis B: Environmental*, p. 117808, 2019.

12. Rostrupnielsen, J. and J. B. Hansen, "CO2-reforming of methane over transition metals", *Journal of Catalysis*, Vol. 144, No. 1, pp. 38–49, 1993.

13. Rostrup-Nielsen, J. R., "Production of synthesis gas", *Catalysis today*, Vol. 18, No. 4, pp. 305–324, 1993.

14. Schulz, H., "Short history and present trends of Fischer–Tropsch synthesis", *Applied Catalysis A: General*, Vol. 186, No. 1-2, pp. 3–12, 1999.

15. Wilhelm, D., D. Simbeck, A. Karp and R. Dickenson, "Syngas production for gas-to-liquids applications: technologies, issues and outlook", *Fuel processing technology*, Vol. 71, No. 1-3, pp. 139–148, 2001.

16. Shah, Y. T. and T. H. Gardner, "Dry reforming of hydrocarbon feedstocks", *Catalysis Reviews*, Vol. 56, No. 4, pp. 476–536, 2014.

17. Freitas, A. C. and R. Guirardello, "Comparison of several glycerol reforming methods for hydrogen and syngas production using Gibbs energy minimization", *International Journal of Hydrogen Energy*, Vol. 39, No. 31, pp. 17969–17984, 2014.

18. Lin, Y.-C., "Catalytic valorization of glycerol to hydrogen and syngas", *interna-*

tional journal of hydrogen energy, Vol. 38, No. 6, pp. 2678–2700, 2013.

19. Liu, B. and J. Greeley, "Decomposition pathways of glycerol via C–H, O–H, and C–C bond scission on Pt (111): A density functional theory study", *The Journal of Physical Chemistry C*, Vol. 115, No. 40, pp. 19702–19709, 2011.

20. Valliyappan, T., N. Bakhshi and A. Dalai, "Pyrolysis of glycerol for the production of hydrogen or syn gas", *Bioresource Technology*, Vol. 99, No. 10, pp. 4476–4483, 2008.

21. Shekhar, R. and M. A. Barteau, "Decarbonylation and hydrogenation reactions of allyl alcohol and acrolein on Pd (110)", *Surface science*, Vol. 319, No. 3, pp. 298–314, 1994.

22. Wang, Z., X.-M. Cao, J. Zhu and P. Hu, "Activity and coke formation of nickel and nickel carbide in dry reforming: a deactivation scheme from density functional theory", *Journal of catalysis*, Vol. 311, pp. 469–480, 2014.

23. Wang, S., Q. Wang, X. Song and J. Chen, "Dry autothermal reforming of glycerol with in situ hydrogen separation via thermodynamic evaluation", *International Journal of Hydrogen Energy*, Vol. 42, No. 2, pp. 838–847, 2017.

24. Wang, X., M. Li, M. Wang, H. Wang, S. Li, S. Wang and X. Ma, "Thermodynamic analysis of glycerol dry reforming for hydrogen and synthesis gas production", *Fuel*, Vol. 88, No. 11, pp. 2148–2153, 2009.

25. Kale, G. R. and B. D. Kulkarni, "Thermodynamic analysis of dry autothermal reforming of glycerol", *Fuel Processing Technology*, Vol. 91, No. 5, pp. 520–530, 2010.

26. Balat, M. and H. Balat, "Progress in biodiesel processing", *Applied energy*, Vol. 87, No. 6, pp. 1815–1835, 2010.

27. Zakaria, Z., M. Jusoh, A. Johari, M. Zaini and F. Kasim, "Thermodynamic analysis of hydrogen production from ethanol-glycerol mixture through dry reforming", *Energy Procedia*, Vol. 61, pp. 2391–2394, 2014.

28. Saimon, N. N., M. Jusoh, M. Kamaruddin, A. Arsad and Z. Y. Zakaria, "Thermodynamic Analysis of Hydrogen Production from Methanol-Ethanol-Glycerol Mixture through Dry Reforming", *Chemical Engineering Transactions*, Vol. 56, pp. 967–972, 2017.

29. Fernández, Y., A. Arenillas, J. M. Bermúdez and J. Menéndez, "Comparative study of conventional and microwave-assisted pyrolysis, steam and dry reforming of glycerol for syngas production, using a carbonaceous catalyst", *Journal of Analytical and Applied Pyrolysis*, Vol. 88, No. 2, pp. 155–159, 2010.

30. Lee, H. C., K. W. Siew, J. Gimbun and C. K. Cheng, "Application of Cement Clinker as Ni-Catalyst Support for Glycerol Dry Reforming", *Bulletin of Chemical Reaction Engineering & Catalysis*, Vol. 8, No. 2, p. 137, 2013.

31. Lee, H. C., K. W. Siew, M. R. Khan, S. Y. Chin, J. Gimbun and C. K. Cheng, "Catalytic performance of cement clinker supported nickel catalyst in glycerol dry reforming", *Journal of Energy Chemistry*, Vol. 23, No. 5, pp. 645–656, 2014.

32. Siew, K. W., H. C. Lee, J. Gimbun and C. K. Cheng, "Production of CO-rich hydrogen gas from glycerol dry reforming over La-promoted Ni/Al2O3 catalyst", *international journal of hydrogen energy*, Vol. 39, No. 13, pp. 6927–6936, 2014.

33. Siew, K. W., H. C. Lee, J. Gimbun and C. K. Cheng, "Characterization of La-promoted Ni/Al2O3 catalysts for hydrogen production from glycerol dry reforming", *Journal of Energy Chemistry*, Vol. 23, No. 1, pp. 15–21, 2014.

34. Siew, K. W., H. C. Lee, J. Gimbun, S. Y. Chin, M. R. Khan, Y. H. Taufiq-Yap and C. K. Cheng, "Syngas production from glycerol-dry (CO2) reforming over La-promoted Ni/Al2O3 catalyst", *Renewable energy*, Vol. 74, pp. 441–447, 2015.

35. Mohd Arif, N. N., N. Harun, N. M. Yunus, D.-V. N. Vo, M. T. Azizan and S. Zainal Abidin, "Reforming of glycerol for hydrogen production over Ni based catalysts: Effect of support type", *Energy Sources, Part A: Recovery, Utilization, and Environmental Effects*, Vol. 39, No. 7, pp. 657–663, 2017.

36. Harun, N., J. Gimbun, M. T. Azizan and S. Z. Abidin, "Characterization of Ag-promoted Ni/SiO2 catalysts for syngas production via carbon dioxide (CO2) dry reforming of glycerol", *Bulletin of Chemical Reaction Engineering & Catalysis*, Vol. 11, No. 2, pp. 220–229, 2016.

37. Harun, N., S. Z. Abidin, N. N. M. Arif, N. A. M. Razali, M. T. Azizan *et al.*, "Characterization of Ni catalyst supported on α-Al2O3 and SiO2 for Syngas Production via Dry Reforming of Glycerol", *Malaysian Journal of Catalysis*, Vol. 3, No. 2, 2017.

38. Tavanarad, M., F. Meshkani and M. Rezaei, "Production of syngas via glycerol dry reforming on Ni catalysts supported on mesoporous nanocrystalline Al2O3", *Journal of CO2 Utilization*, Vol. 24, pp. 298–305, 2018.

39. Ferreira-Aparicio, P., C. Marquez-Alvarez, I. Rodrıguez-Ramos, Y. Schuurman, A. Guerrero-Ruiz and C. Mirodatos, "A transient kinetic study of the carbon dioxide reforming of methane over supported Ru catalysts", *Journal of Catalysis*, Vol. 184, No. 1, pp. 202–212, 1999.

40. Ferreira-Aparicio, P., I. Rodrıguez-Ramos, J. Anderson and A. Guerrero-Ruiz, "Mechanistic aspects of the dry reforming of methane over ruthenium catalysts", *Applied Catalysis A: General*, Vol. 202, No. 2, pp. 183–196, 2000.

41. Schuurman, Y., C. Mirodatos, P. Ferreira-Aparicio, I. Rodriguez-Ramos and A. Guerrero-Ruiz, "Bifunctional pathways in the carbon dioxide reforming of methane over MgO-promoted Ru/C catalysts", *Catalysis letters*, Vol. 66, No. 1-2, pp. 33–37, 2000.

42. Carrara, C., J. Munera, E. A. Lombardo and L. M. Cornaglia, "Kinetic and stability studies of Ru/La 2 O 3 used in the dry reforming of methane", *Topics in Catalysis*, Vol. 51, No. 1-4, pp. 98–106, 2008.

43. Safariamin, M., L. H. Tidahy, E. Abi-Aad, S. Siffert and A. Aboukaïs, "Dry reforming of methane in the presence of ruthenium-based catalysts", *Comptes Rendus Chimie*, Vol. 12, No. 6-7, pp. 748–753, 2009.

44. Chen, J., C. Yao, Y. Zhao and P. Jia, "Synthesis gas production from dry reforming of methane over Ce0. 75Zr0. 25O2-supported Ru catalysts", *International journal of hydrogen energy*, Vol. 35, No. 4, pp. 1630–1642, 2010.

45. Kehres, J., J. G. Jakobsen, J. W. Andreasen, J. B. Wagner, H. Liu, A. Molenbroek, J. Sehested, I. Chorkendorff and T. Vegge, "Dynamical properties of a Ru/MgAl2O4 catalyst during reduction and dry methane reforming", *The Journal of Physical Chemistry C*, Vol. 116, No. 40, pp. 21407–21415, 2012.

46. Derk, A. R., G. M. Moore, S. Sharma, E. W. McFarland and H. Metiu, "Catalytic dry reforming of methane on ruthenium-doped ceria and ruthenium supported on ceria", *Topics in Catalysis*, Vol. 57, No. 1-4, pp. 118–124, 2014.

47. Gennequin, C., S. Hany, H. L. Tidahy, S. Aouad, J. Estephane, A. Aboukaïs and E. Abi-Aad, "Influence of the presence of ruthenium on the activity and stability of Co–Mg–Al-based catalysts in CO 2 reforming of methane for syngas production", *Environmental Science and Pollution Research*, Vol. 23, No. 22, pp. 22744–22760, 2016.

48. Whang, H. S., M. S. Choi, J. Lim, C. Kim, I. Heo, T.-S. Chang and H. Lee, "Enhanced activity and durability of Ru catalyst dispersed on zirconia for dry reforming of methane", *Catalysis Today*, Vol. 293, pp. 122–128, 2017.

49. Gallo, A., C. Pirovano, M. Marelli, R. Psaro and V. Dal Santo, "Hydrogen Production by Glycerol Steam Reforming with Ru-based Catalysts: A Study on Sn

Doping", *Chemical Vapor Deposition*, Vol. 16, No. 10-12, pp. 305–310, 2010.

50. Gallo, A., C. Pirovano, P. Ferrini, M. Marelli, R. Psaro, S. Santangelo, G. Faggio and V. Dal Santo, "Influence of reaction parameters on the activity of ruthenium based catalysts for glycerol steam reforming", *Applied Catalysis B: Environmental*, Vol. 121, pp. 40–49, 2012.

51. Sundari, R. and P. D. Vaidya, "Reaction kinetics of glycerol steam reforming using a Ru/Al2O3 catalyst", *Energy & Fuels*, Vol. 26, No. 7, pp. 4195–4204, 2012.

52. Kim, J. and D. Lee, "Glycerol steam reforming on supported Ru-based catalysts for hydrogen production for fuel cells", *International Journal of Hydrogen Energy*, Vol. 38, No. 27, pp. 11853–11862, 2013.

53. Gallegos-Suárez, E., A. Guerrero-Ruiz and I. Rodríguez-Ramos, "Efficient hydrogen production from glycerol by steam reforming with carbon supported ruthenium catalysts", *Carbon*, Vol. 96, pp. 578–587, 2016.

54. Kousi, K., D. Kondarides, X. Verykios and C. Papadopoulou, "Glycerol steam reforming over modified Ru/Al2O3 catalysts", *Applied Catalysis A: General*, Vol. 542, pp. 201–211, 2017.

55. Dahdah, E., S. Aouad, C. Gennequin, J. Estephane, B. Nsouli, A. Aboukaïs and E. Abi-Aad, "Glycerol steam reforming over Ru-Mg-Al hydrotalcite-derived mixed oxides: Role of the preparation method in catalytic activity", *International Journal of Hydrogen Energy*, Vol. 43, No. 43, pp. 19864–19872, 2018.

56. Tao, W., H. Cheng, W. Yao, X. Lu, Q. Zhu, G. Li and Z. Zhou, "Syngas production by CO2 reforming of coke oven gas over Ni/La2O3–ZrO2 catalysts", *international journal of hydrogen energy*, Vol. 39, No. 32, pp. 18650–18658, 2014.

57. Tao, Q., Z. Wang, B. Jayasundera, C. Guo, Y. Gan, L. Zhang, Z. Lu, H. Tan and C. Yan, "Enhanced catalytic activity of Ni–Mo 2 C/La 2 O 3–ZrO 2 bifunctional

catalyst for dry reforming of methane", *Journal of materials science*, Vol. 53, No. 20, pp. 14559–14572, 2018.

58. Angeli, S. D., L. Turchetti, G. Monteleone and A. A. Lemonidou, "Catalyst development for steam reforming of methane and model biogas at low temperature", *Applied Catalysis B: Environmental*, Vol. 181, pp. 34–46, 2016.

59. Goula, M., N. Charisiou, G. Siakavelas, L. Tzounis, I. Tsiaoussis, P. Panagiotopoulou, G. Goula and I. Yentekakis, "Syngas production via the biogas dry reforming reaction over Ni supported on zirconia modified with CeO2 or La2O3 catalysts", *international journal of hydrogen energy*, Vol. 42, No. 19, pp. 13724–13740, 2017.

60. Cheng, H., G. Li, H. Zhao, X. Lu, Q. Xu and W. Tao, "Effects of preparation technique and lanthana doping on Ni/La2O3-ZrO2 catalysts for hydrogen production by CO2 reforming of coke oven gas", *Catalysis Today*, Vol. 318, pp. 23–31, 2018.

61. Bulutoglu, P. S., *Parametric investigation of catalytic dry reforming of glycerol to synthesis gas*, Master's Thesis, Boğaziçi University, Turkey, 2017.

62. Karakaya, M., *Experimental and quantitative analysis of multiphase catalytic reactions under microfluidic conditions and geometries*, Ph.D. Thesis, Bogazici University, Turkey, 2014.

63. Simsek, E., M. Karakaya, A. K. Avci *et al.*, "Oxidative steam reforming of methane to synthesis gas in microchannel reactors", *International Jjournal of Hydrogen Energy*, Vol. 38, No. 2, pp. 870–878, 2013.

APPENDIX A: CALIBRATION OF MASS FLOW CONTROLLERS

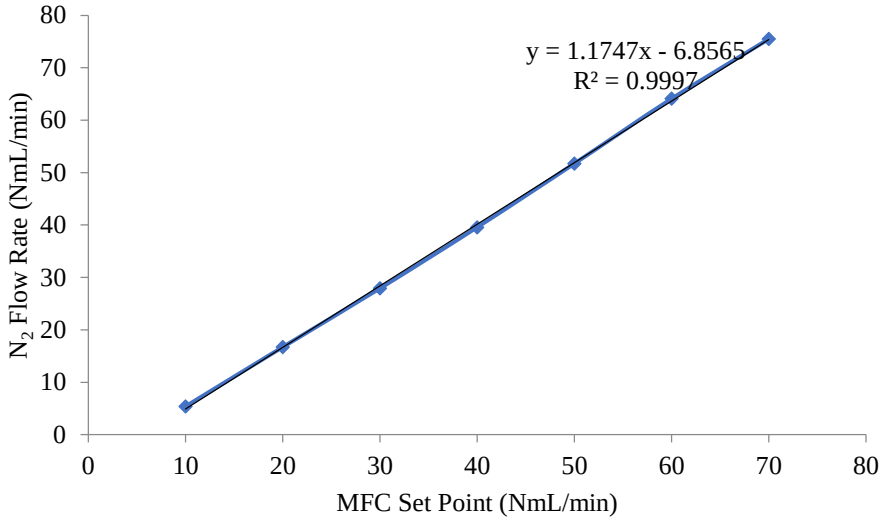

Figure A.1. Calibration curve of N_2 MFC.

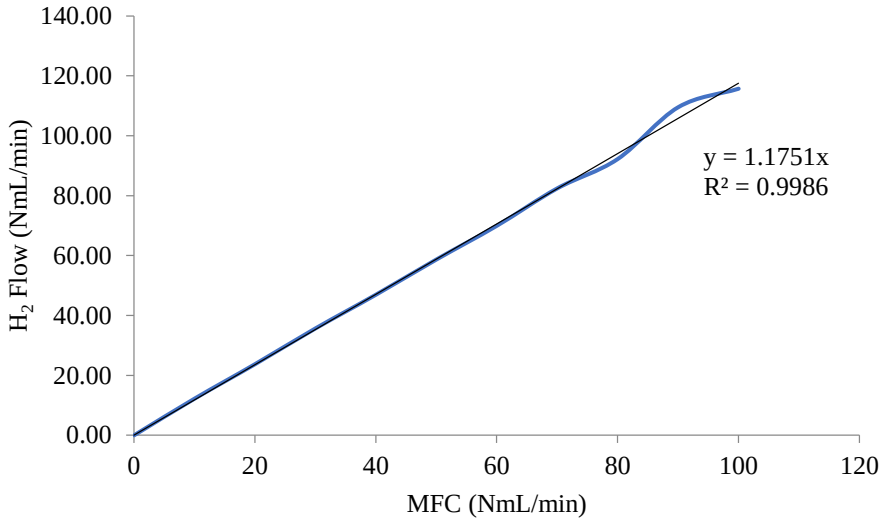

Figure A.2. Calibration curve of H_2 MFC.

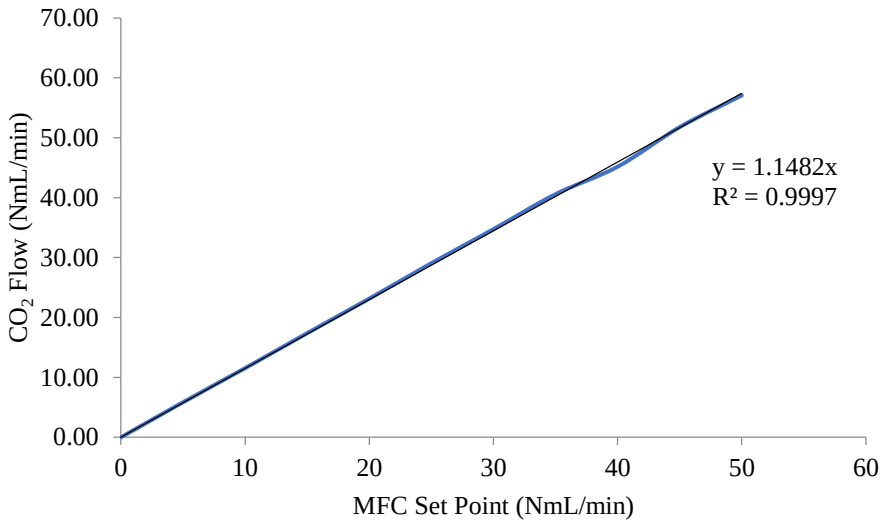

Figure A.3. Calibration curve of CO_2 MFC.

APPENDIX B: CALIBRATION OF GAS CHROMATOGRAPHS

B.1. Shimadzu GC-2014 Calibration Curves

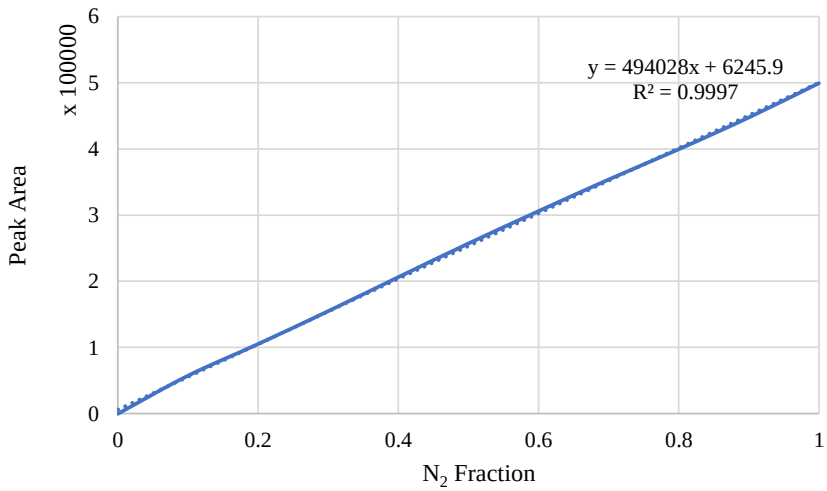

Figure B.1. N_2 calibration curve of GC-1.

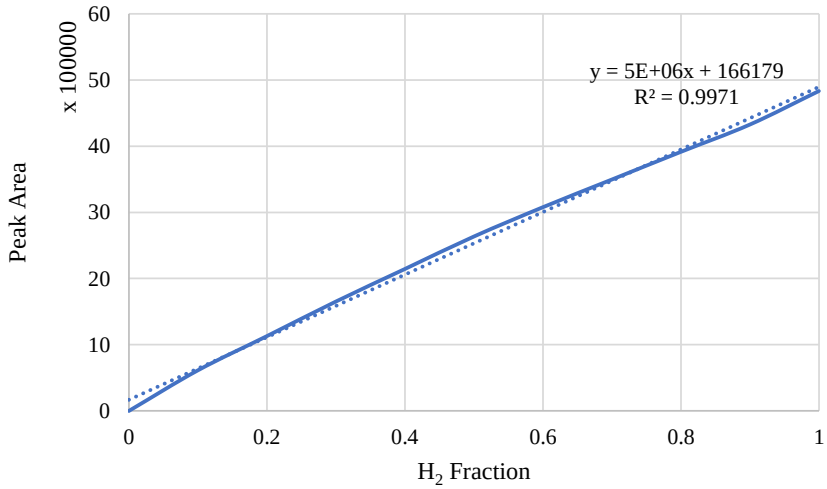

Figure B.2. H_2 calibration curve of GC-1.

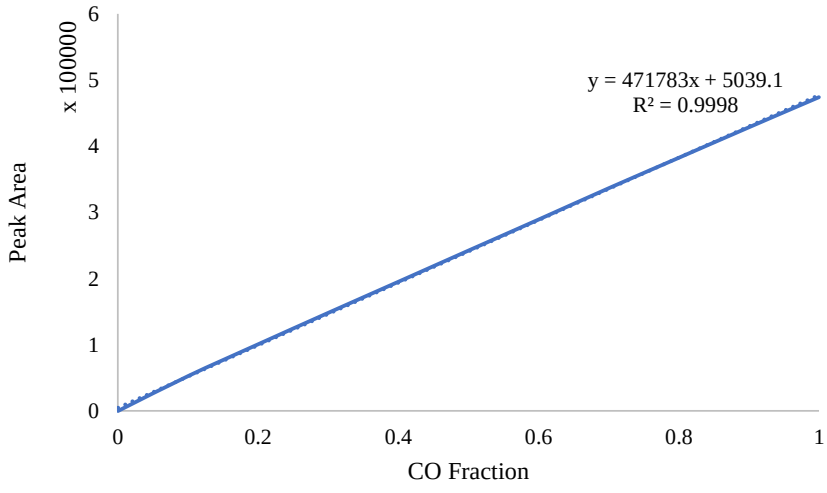

Figure B.3. CO calibration curve of GC-1.

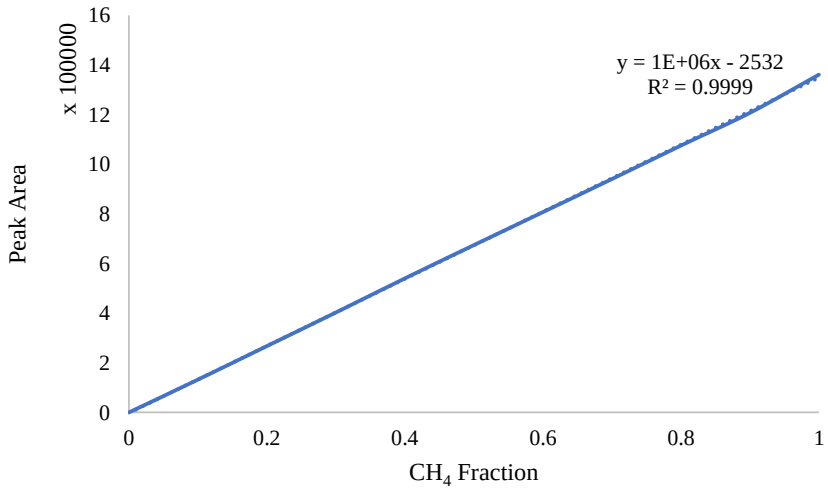

Figure B.4. CH_4 calibration curve of GC-1.

B.2. Shimadzu GC-8A Calibration Curves

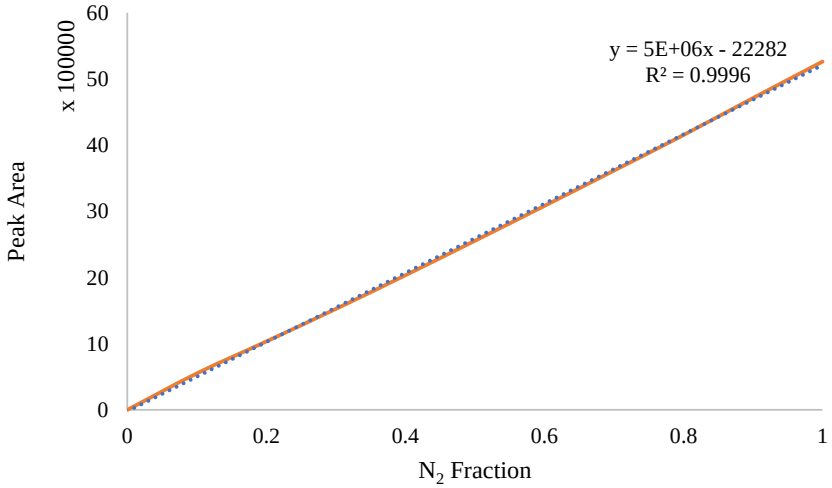

Figure B.5. N_2 calibration curve of GC-2.

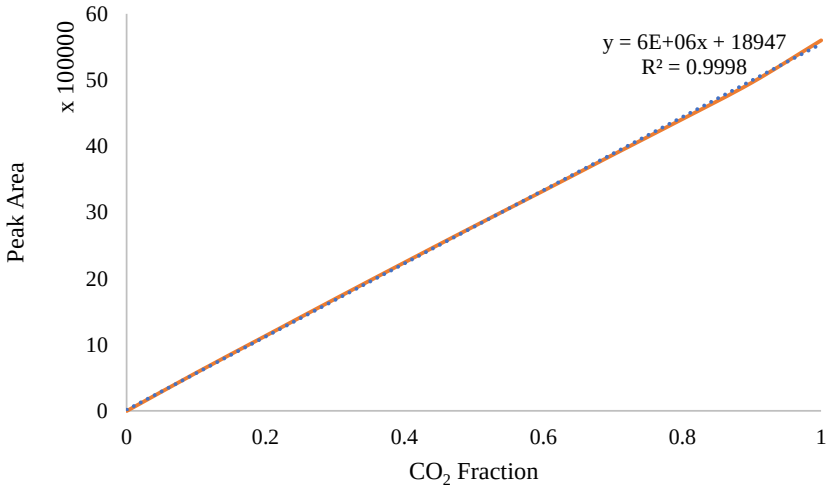

Figure B.6. CO_2 calibration curve of GC-2.

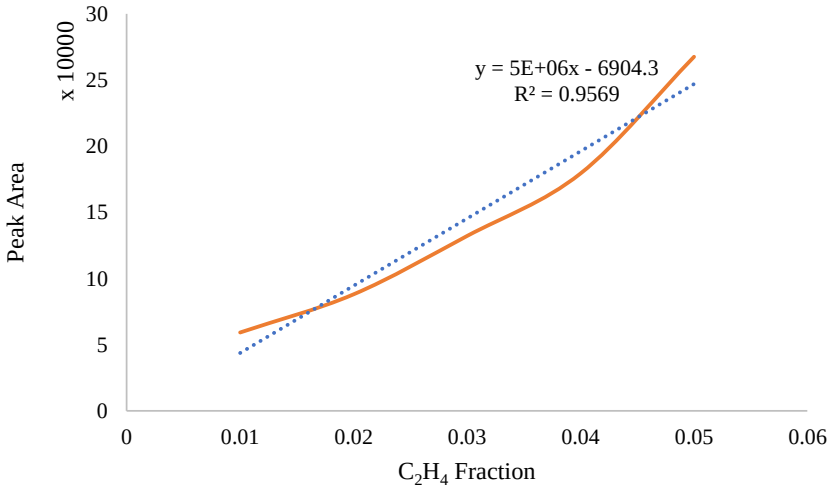

Figure B.7. C_2H_4 calibration curve of GC-2.

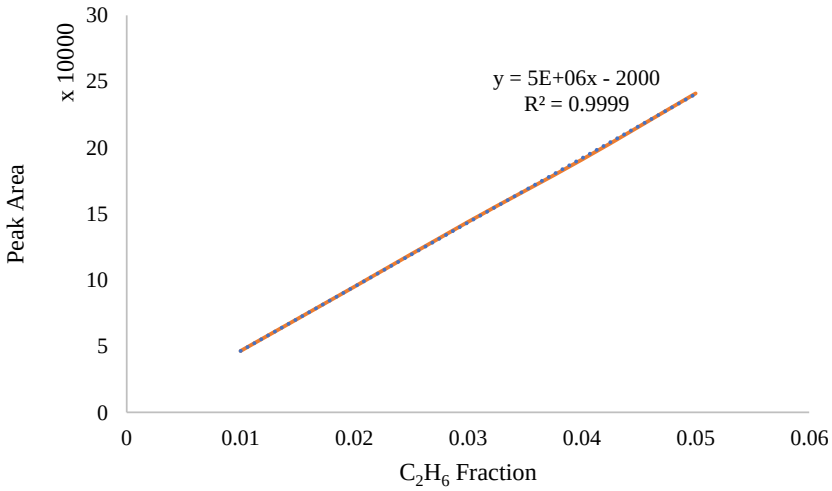

Figure B.8. C_2H_6 calibration curve of GC-2.